Winter 2018

Value Added Products From Lignin and Biomass Derivatives

Chen Li
Old Dominion University, lichen20028@odu.edu

VALUE ADDED PRODUCTS FROM LIGNIN AND BIOMASS DERIVATIVES

by

Chen Li
B.S. June 2007, Zhengzhou University
M.E. January 2010, University of Science and Technology Beijing

A Dissertation Submitted to the Faculty of
Old Dominion University in Partial Fulfillment of the
Requirements for the Degree of

DOCTOR OF PHILOSOPHY

ENVIRONMENTAL ENGINEERING

OLD DOMINION UNIVERSITY
December 2018

Approved by:

Sandeep Kumar (Director)

Ben Stuart (Member)

Mujde Erten-Unal (Member)

Xiaoyu Zhang (Member)

ABSTRACT

VALUE ADDED PRODUCTS FROM LIGNIN AND BIOMASS DERIVATIVES

Chen Li
Old Dominion University, 2018
Director: Dr. Sandeep Kumar

Pyrolysis is one of the traditional lignin and biomass utilization methods. The liquid products bio-oil and solid products bio-char are the main value-added products from lignin pyrolysis. Due to the narrow application and low quality, using the pyrolysis method to produce bio-oil and bio-char cannot bring sufficient economic benefits. In this dissertation, two methods were investigated to improve the quality of lignin bio-products.

Instead of direct pyrolysis, chemical activation (pyrolysis) was introduced in this dissertation. Compared to bio-char, the lignin chemical activation product lignin-activated-carbon has better economic value. With the best activation conditions, the lignin-activated-carbon produced a surface area of around 1117 m^2/g, and the yield percentage could reach around 50%. Compared to commercial activated carbon, lignin-activated-carbon had a similar Iodine Number., Methylene Blue Number, BET Surface area, and better yield percentage. The use of $ZnCl_2$ activated for the carbon method proved to be one of the best ways of utilizing lignin biomass residue.

Bio-oil produced from lignin is a very complex mixture of several organic compounds. However, furfural and acetone are two significant compounds present in bio-oil produced from lignin. An electrochemical hydrogenation method was investigated to upgrade oil and obtain more valuable products, such as isopropanol, Tetrahydrofurfuryl alcohol, and 2-Methyltetrahydrofuran. A novel electrochemical hydrogenation reactor, polymer electrolyte

membrane fuel cell was used in the experiment and results show that target products could be produced in a mild process condition (low temperature and atmospheric pressure) with high current efficiency and high selectivity. The degradation of membranes due to the contamination of the polymer electrolyte membrane fuel cell, the mitigation methods and the effective working hours of the polymer electrolyte membrane fuel cell were investigated.

This thesis is dedicated to the proposition that the harder you work, the luckier you get.

ACKNOWLEDGMENTS

Right now is the time for me to recall my Ph.D. study journey in Old Dominion University. There are many people who have contributed to the successful completion of this dissertation. First I would like to thank my advisor, Dr. Sandeep Kumar, without his insightful directions on my academic area, I could not have finished this dissertation. His cleverness, wisdom, and personality have huge effects on me as I learned how to be a successful academician in the future.

Particularly I am very grateful to my committee- Dr. Xiaoyu Zhang, with his incredible patience and guidance on my scientific research and manuscript revision, His guidance has enhanced my ability a lot on scientific writing and critical thinking. Furthermore, I extend many, many thanks to my other committee members for their patience and suggestions for my research and editing of this dissertation. The untiring efforts of my major advisor deserve special recognition. Without all the knowledge and techniques I have learned from you, I could not finish this dissertation.

I would also like to acknowledge the help and support from my research group members: Ali Teymouri, Caleb Talbot, Adams Kameron, Alexander Asiedu, Ashani Samaratunga, who have made our group as a home for study, for work and for living here as an international student far away from his own country. And I also appreciate the technical assistance from Drs. Can Zhou, Qiang Tang, and Yazdanshenas Elias who help with the experiment set up.

Most importantly, I would like to thank my family, it is your love, understanding, and support encourage me to overcome the difficulties through the Ph.D. study journey, and made the process full of warmth and happiness.

NOMENCLATURE

AC	Activated Carbon
C_o	Initial concentrations, (mg/L)
C_e	Equilibrium concentrations, (mg/L)
EA	Elemental analysis
ECH	Electrochemical hydrogenation
FA	Furfuryl alcohol
FM	2(3H)-Furanon, 5-methyl-
FTIR	Fourier transform infrared
GV	Gamma-Valerolactone
MB	Methylene Blue
MEA	The membrane electrode assembly
MPK	2-Pentanone
MTHF	2-Methyltetrahydrofuran
PEM	Polymer electrolyte membrane
PEMFC	Polymer electrolyte membrane fuel cell
Qe	Adsorbed amount of unit AC, (mg/g)
q_t	The adsorption amount with regard to adsorption time, (mg/g)
SEM	Scanning electron microscopy
slpm	Standard liter per minute
THFA	Tetrahydrofurfuryl alcohol
TGA	Thermo-gravimetric analyses
UHS	Un-hydrolyzed solid

XRD	X-Ray Diffraction analyses
V	Volume, (ml)

TABLE OF CONTENTS

Page

Chapter

LIST OF TABLES

Table Page

LIST OF FIGURES

Figure Page

Figure Page

CHAPTER 1

INTRODUCTION

Lignin, a valuable resource for chemicals and energy, is a main component of wood, together with cellulose and hemicellulose. It is the second largest source of organic raw material [1], constituting about 4-35 wt% of most biomass, 16-25 wt% of hardwoods and 23-35 wt% of softwoods [2]. As the most abundant natural aromatic polymer [3], lignin has a highly branched three-dimensional phenolic structure (Fig.1) including three main phenylpropane units, namely p-coumaril, coniferyl and sinapyl. Softwood lignin contains relatively few sinapyl units and consists mainly of guaiacyl structures, while hardwood lignin contains guaiacylsyringyl structures.

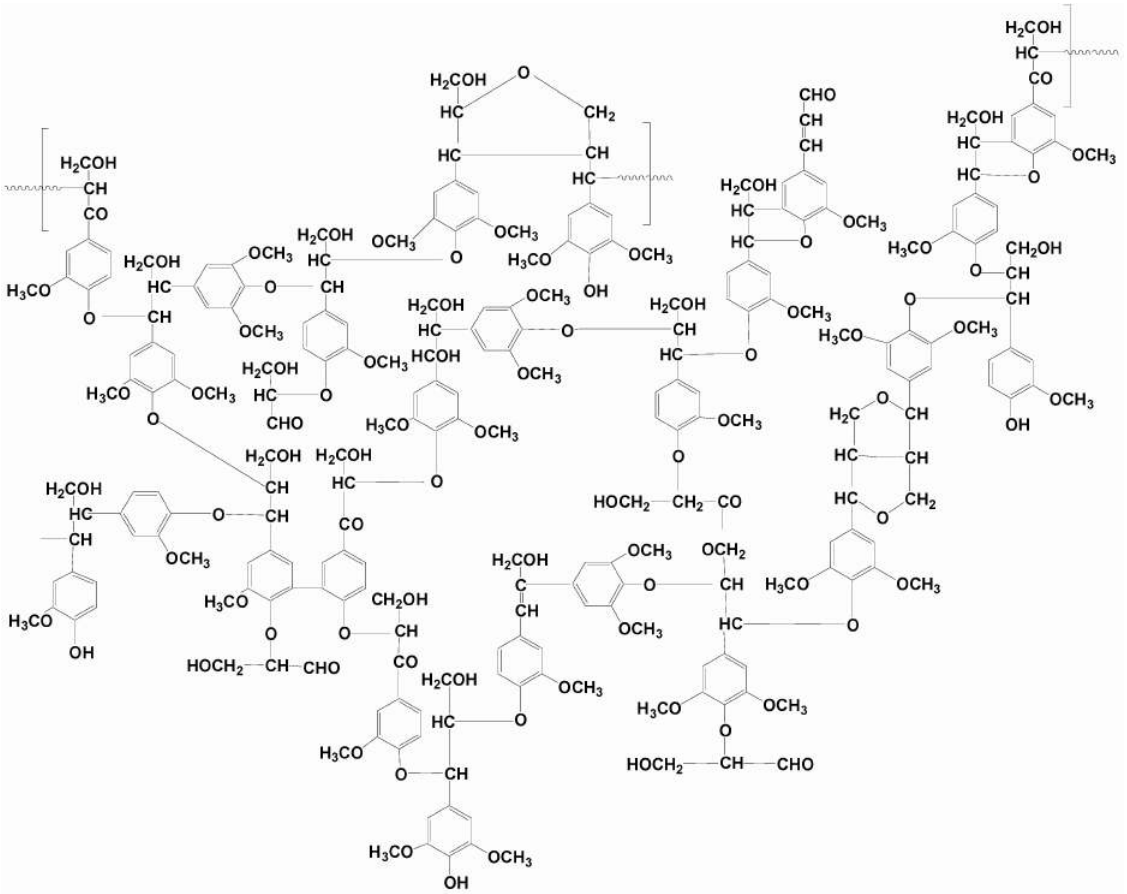

Figure 1. Partial structure of hardwood lignin[4]

As a by-product of the paper industry, lignin is most often used by paper mills as a fuel for the recovery of its energy content. However, due to the very large generated quantities, lignin is increasingly considered as a potential source of chemicals, and studies of its thermal degradation receive much interest. [4]

The structure of lignin suggests that it can be a valuable source of chemicals, particularly phenolics. However, lignin depolymerization with selective bond cleavage is the major challenge for converting it into value-added chemicals. Pyrolysis (thermolysis), gasification, hydrogenolysis, chemical oxidation, and hydrolysis under supercritical conditions are the major thermochemical methods studied with regard to lignin depolymerization. Pyrolytic oil and syngases are the primary products obtained from pyrolysis and gasification.

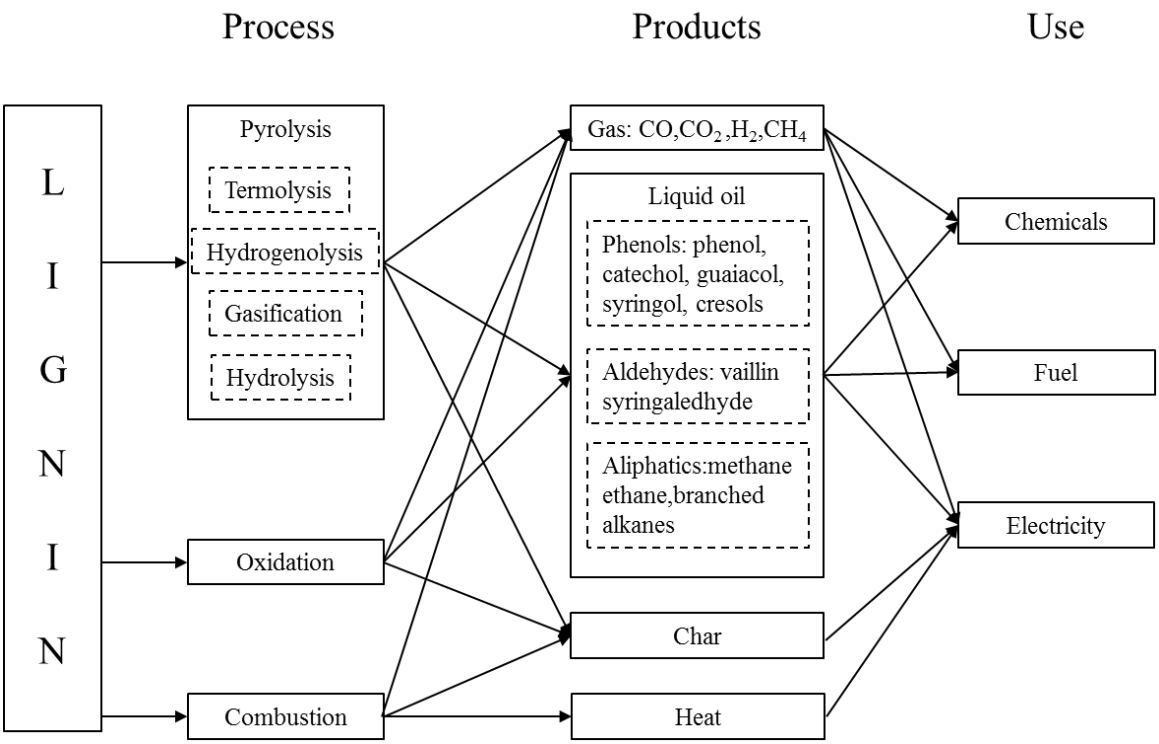

Figure 2. Major Thermochemical lignin conversion processes and their potential products

Lignin bio-oil, lignin bio-char (activated carbon), and lignin depolymerization production are several value-added products from lignin. The objectives of this study are to develop value-added bioproducts from production processes.

1.1 Activated Carbon Production from Lignin Biomass

Activated carbons (ACs) are well known for their high adsorption ability due to their porous structure and large internal surface area, ranging from 500 to 2000 m^2/g. These are used in the engineering field as adsorbents for removing inorganic environmental pollutants [5-8] and organic compounds [9-11] from both gas and liquid phases. Therefore, it will be beneficial to develop a production process of ACs from renewable feedstock, which is economical and efficient.

Recently, there has been an abundance of research efforts in developing processes to produce ACs from biomass waste, which contains a high amount of organic constituents such as cellulose, hemicellulose, and lignin [12]. ACs were produced in environmentally friendly ways and economically [13] by thermal conversion processes of pyrolysis and gasification for various biomass wastes such as apricot stone shells [14, 15], bean pods [16], olive stones [17, 18], sugar cane, bagasse, rice, straw, rice hull and pecan shells [19].

ACs production mainly has two steps. The first occurs through carbonization of the biomass under 800℃, followed by either physical or chemical activation of the carbonized product [13]. Compared to a physical activation procedure, chemical activation occurs at a lower temperature and has a better quality of porous structure ACs and lower energy costs [20]. Widely used chemical reagents such as $ZnCl_2$, NaOH, H_3PO_4, and metal chemicals (e.g., KOH and K_2CO_3) are reported in the literature as raw precursors of lignocellulosic materials as well as coals [21-25]. Chemical activation is a commonly used method for AC production. The summary of biomass feedstock chemical activation for AC production is shown in Table 7 (Seen in appendices). High surface area (700~2000 m^2/g) activated carbon is expected when the biomass waste is used as feedstock and chemical activation is the production method.

1.2 Lignin Bio-oil Derivatives and Upgrading Method

Bio-oil, the liquid product from fast pyrolysis of biomass, is a promising sustainable material for transportation fuel production. However, the raw bio-oil is not ready for end users because of several disadvantages: (1) High water content; (2) High viscosity; (3) High ash content; (4) High oxygen content and low heating value; (5) High corrosiveness. The typical bio-oil composition is shown in Table 1 and Table 2.

Table 1. Bio-oil from rice husk [26].

Composition	Wt%	Composition	Wt%
Formic acid	7.69	H_2O(wt%)	25.2
Hydroxybutyric	2.31	pH	2.8
Fufural	5.00	Density(kg/m^3)	1190
Benzoic acid	1.15	Viscosity(mm^2/s)	128
2-Cyclopentane-1-one	1.42	LHV(MJ/kg)	17.42
4H-Pyran-4-one	2.15	C(wt%)	41.7
Acetophenone	1.00	H(wt%)	7.7
2-hydroxyl	1.85	O(wt%)	50.3
3,5-dimethyl-4-hydroxyl	1.92	N(wt%)	0.3

Table 2. Bio-oil from wood [27].

Composition	Wt%	Composition	Wt%
Acetic acid	15.33	Other ketones	6.77
Acetone	5.29	Other aldehydes	8.75
1-hydroxy-2-propanone	14.97	Phenols	8.20
Hydroxyacetaldehyde	10.58	Ethers	0.94
Methanol	4.59	Other Alcohols	6.86
Levoglucosan	3.94	Others	1.33
Other acids and esters	10.84		

Due to the presence of unsaturated oxygenates such as aldehydes, ketones, carboxylic acids, acetone, furfural, and phenols, for long-term storage and any further upgrading, bio-oil must first be stabilized in order to minimize downstream coke formation, catalyst deactivation and carbon loss to the gas phase. A central goal of pyrolysis lignin and upgrading lignin bio-oil is to convert

the oxygen-rich, hydrogen-poor, high-molecular-weight lignin into hydrocarbons that are compatible with today's petroleum-derived fuels or directly used as a high-quality combustion fuel. popular bio-oil upgrade methods and comparison are shown in Table 8 (Seen in appendices) [28].

Most popular oil upgrade methods like hydrotreating and hydrocracking usually use supported nickel catalyst, and the reaction is carried out at a high temperature (500°C) with a hydrogen gas pressure in the range of 100–1000psig.

1.3 Electrochemical Hydrogenation Method

Electrochemical hydrogenation (ECH) is considered as an energy saving and environmentally friendly method to upgrade organics, by integrating both the catalytic and the electrochemical methods. The ECH reaction mechanism of organics is suggested as the following equations (1-5) [29-34].

Anode side:

1. Hydrogen or water lost electrons and generate protons;

   H_2 -> $2(H^+) + 2e^-$; H_2O -> $1/2O_2 + 2(H^+) + 2e^-$

Cathode side:

2. Protons react with electrons and generate $M(H)_{ads}$ (M are an adsorption sites);

   $(H^+) + e- + M$ -> $M\ (H)_{ads} + H_2O$

3. Organic molecules Y=Z are adsorbed by adsorption sites M;

   $Y = Z + M$ -> $M(Y=Z)_{ads}$

4. $M(H)_{ads}$ react with the adsorbed organic molecules;

   $M(Y=Z)_{ads} + 2M(H)_{abs}$ -> $M(YH-ZH)_{abs} + 2M$

5. Hydrogenated products are generated;

$M(YH\text{-}ZH)_{abs}$ -> YH-ZH + M

6. H_2 molecules are reproduced;

$2M(H)_{ads}$ -> H_2 (gas) +2M $M(H)_{ads}$ + (H+) + e- -> H_2 (gas) +M

In the anode, either hydrogen pumping or water electrolysis lead to the generation of electrons and protons (H^+) (eq. 1). In the cathode, chemisorbed hydrogen M $(H)_{ads}$ is generated in *situ* on the electrocatalyst surface and reacts with the adsorbed organics (eq. 2). Note that hydrogenation also competes with hydrogen gas evolution (eq. 6), which has a negative influence on the current efficiency and H_2 utilization. ECH allows the reactions (eq.s 3, 4, and 5) to happen at low temperatures and ambient pressure. Compared to conventional hydrogenation methods, the overall ECH process takes place in a mild operating condition (i.e. low temperature and atmospheric pressure) and only uses electrical energy. Therefore, intense thermal energy input is not required in ECH. All of the protons used by ECH are supplied by either water or H_2, which eliminates the need for any reducing agent. ECH can be conducted onsite using fuel cell stacks and renewable power sources to produce hydrogen enriched compounds. This will avoid or minimize the storage and transportation of corrosive and hazardous chemicals.

ECH has been widely investigated to upgrade unsaturated compounds to corresponding saturated chemicals, like soybean oil [35], bio-oil [36], edible oil [37, 38], levulinic acid [39-41], aromatic compounds [34, 42-51], lactic acid [52], lignin [53], furfural [54-60], acetaldehyde [61], ethanol [61], acetylene [62], , cyclohexane [30] and glucose [63]. In all those cases, reactions take place under mild conditions with temperatures below 100 ℃, atmospheric pressure, and no reducing chemicals. The current efficiency is defined as the efficiency of electrogenerated H_2 addition to unsaturated bonds, and maximum report in those cases is up to 45% [35, 37, 38, 62]. ECH efficiency is determined by the capabilities of catalysts, which is

directly related to all the processes described in equations 1-6. Compared to nickel (Ni), copper (Cu) and lead (Pb), activated carbon fibers supported platinum (Pt) demonstrated the best catalytic activities for upgrading various organics, such as furfural [60] and acetaldehyde [61]. The electrochemical conversion efficiency is affected by many factors, such as the nature of electrodes [64], current density [65], temperature [48, 62, 66, 67], solvent compositions [30, 33, 67], solution pH [30, 43, 54, 66, 68], and chemical potential [35, 36, 66].

H-type cell was commonly used [31, 36, 42, 44, 45, 49, 53-55, 59, 60, 65, 68]. A typical H-type cell consists of two electrode chambers, between which a cation exchange membrane is sandwiched. Compared to the traditional homogenous electrolyte single chamber cell [39, 40, 46, 52, 54, 61], the basic anolyte and the acidic/neutral catholyte H-type cells [42, 54, 66] are proved to improve proton transmission efficiency.

The typical H-type cell is shown in Figure 3, and the typical single chamber cell is shown in Figure 4.

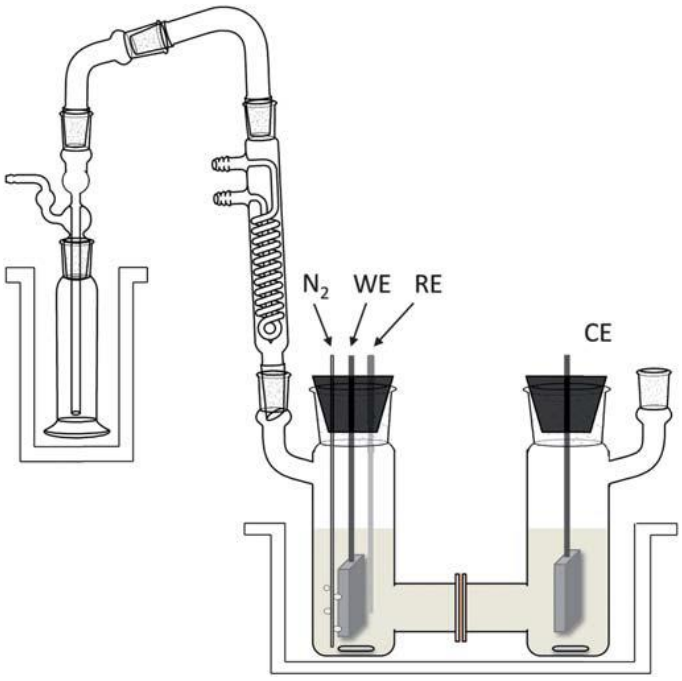

Figure 3. Electrochemical set-up with a divided H-cell, reflux condenser and cryotrap.
WE = working electrode, RE = reference electrode, CE =counter electrode. [59]

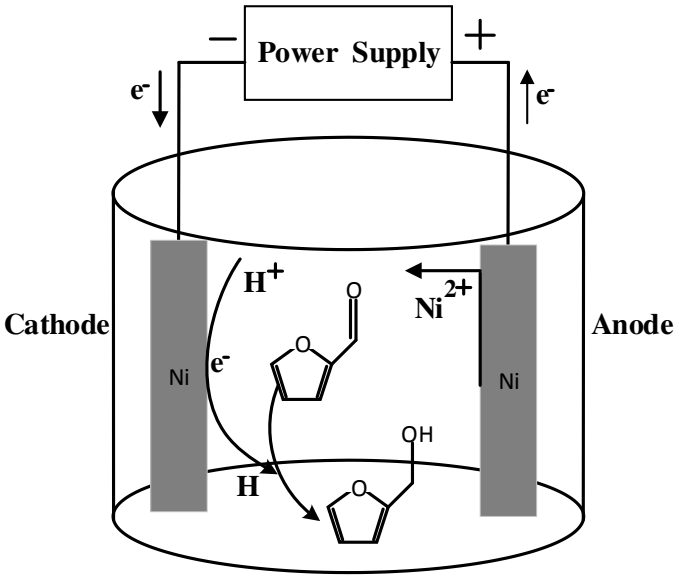

Figure 4. Electrochemical set-up with a single chamber cell for the reduction of furfural to furfuryl Alcohol [11]

1.4 Polymer Electrolyte Membrane Fuel Cell

A polymer electrolyte membrane fuel cell (PEMFC) is a type of low-temperature fuel cell that takes its name from the ion conductive polymer membrane used as the electrolyte. A typical PEMFC assembly consists of two gas diffusion media (carbon paper), two electrodes made of a carbon layer loaded with catalysts and an ion exchange membrane, which is shown in Figure 5.

Feedstocks enter the reactor at the anode and cathode and flow through serpentine flow channels. Between the flow channels is the membrane electrode assembly (MEA), consisting of a hydrogen permeable membrane between two catalyst layers (the anode and the cathode) and gas diffusion layers (carbon cloth or paper upon which the catalyst layer was deposited), which is shown in Figure 6.

The reactor provides temperature control, gas distribution, current collection, water draining and mechanical support of the PEMFC assembly [69]. Compared to one chamber and H-Cell cell

reactor, the PEMFC reactor has a smaller internal resistance, due to its highly conductive and thin membrane electrolyte assembly (MEA), resulting in significantly less electric energy loss [70]. In addition, energy consumption can be further reduced if protons are supplied from hydrogen oxidation, rather than water electrolysis. Furthermore, PEMFCs can be easily scaled up by simply stacking them, and the space-time yield of ECH using PEMFC reactors is superior to the other methods. PEMFC can be easily applied in space limited areas like stationary, transportation, and portable/micro power generation sectors [71].

Figure 6 depicts the concept of the electrocatalytic reduction of biomass-derived oxygenates using a PEM reactor. Water or H_2 is fed into the anode where protons and electrons are produced. The protons migrate through the PEM to the cathode, where they reduce the biomass-derived molecules. The reaction procedure is shown in the last chapter (Eq. 1 to Eq. 6)

Organic compounds ECH by PEMFC reactors were also reported by many researchers [35, 37, 38, 51, 58]. Green *et al*. reported that the main products from ECH of furfural were furfural alcohol (54-100% selectivity) and tetrahydrofurfuryl alcohol (0-26% selectivity). The better production rate was achieved by feeding pure hydrogen gas rather than from water electrolysis [58]. Alfonso *et al*. hydrogenated acetophenone and found that the selectivity of 1-phenylethanol was around 90% with only methylbenzene and hydrogen as by-products [51]. Pintauro *et al*. and An *et al.* both studied ECH of soybean oil in a PEMFC reactor at 60-90°C and atmospheric pressure. Pintauro *et al*. proved that a bimetallic cathode (Pd/Co or Pd/Fe) could increase the yield rate of the ECH process [35]. An *et al*. proved Pd-black cathode worked significantly better than Pt and the best current efficiency could reach 41% [37, 38].

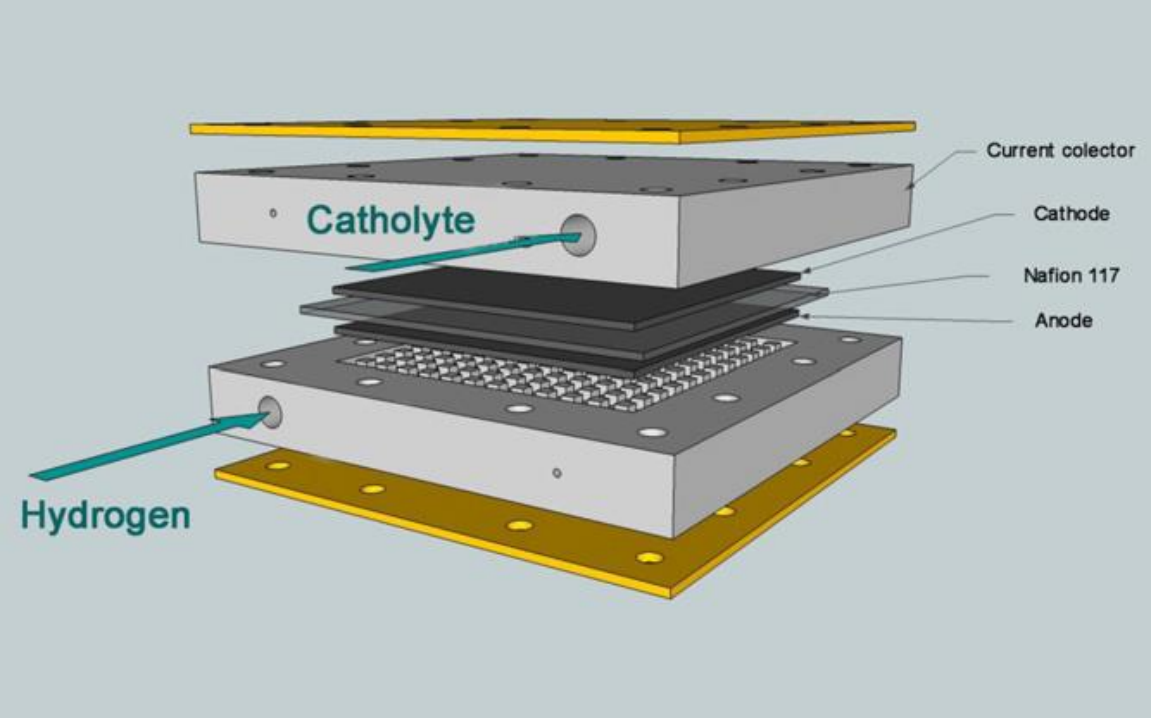

Figure 5. Scheme of Polymer Electrolyte Membrane Electrochemical Reactor [51].

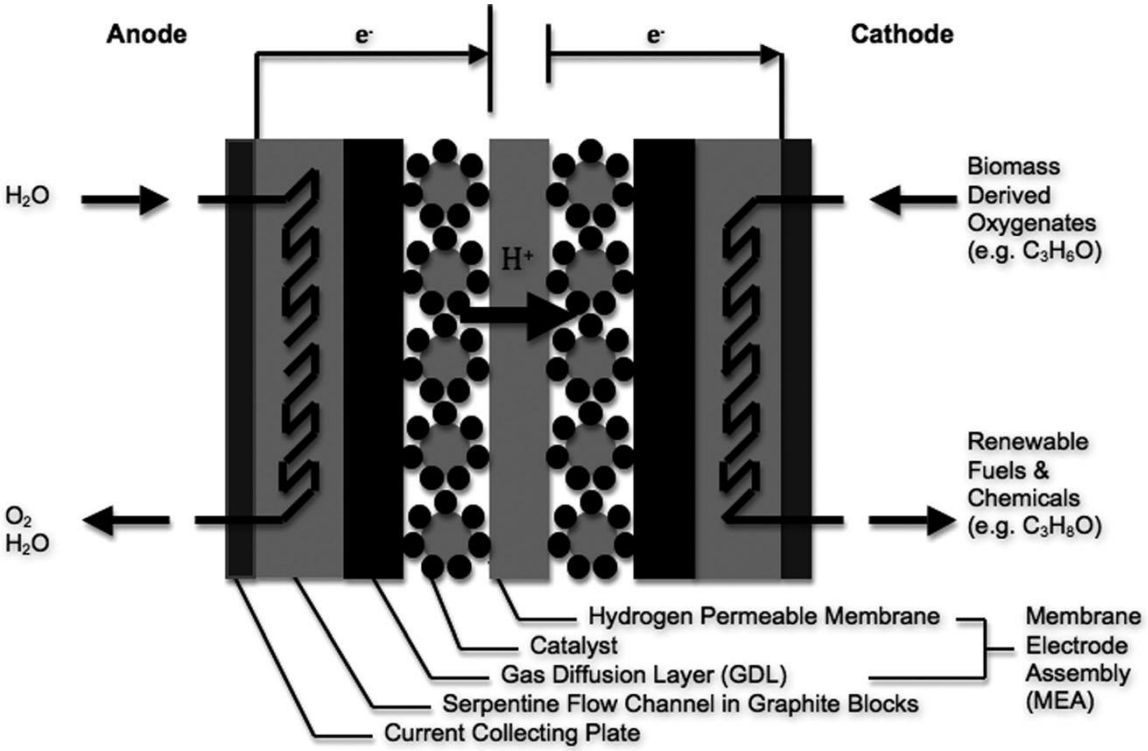

Figure 6. Schematic of the electrocatalytic PEM reactor for the reduction of acetone to isopropanol [72].

1.5 Method and Procedure

Pyrolysis is a traditional lignin biomass utilization method. The liquid products bio-oil and solid products bio-char [73-76] are the main value-added products from lignin pyrolysis [77-79]. Due to the narrow application and low quality, using the pyrolysis method to produce bio-oil and bio-char cannot bring sufficient economic benefits [26, 27, 80-84].

Three lignin value added processes are designed in this paper, as shown in Figure 7.

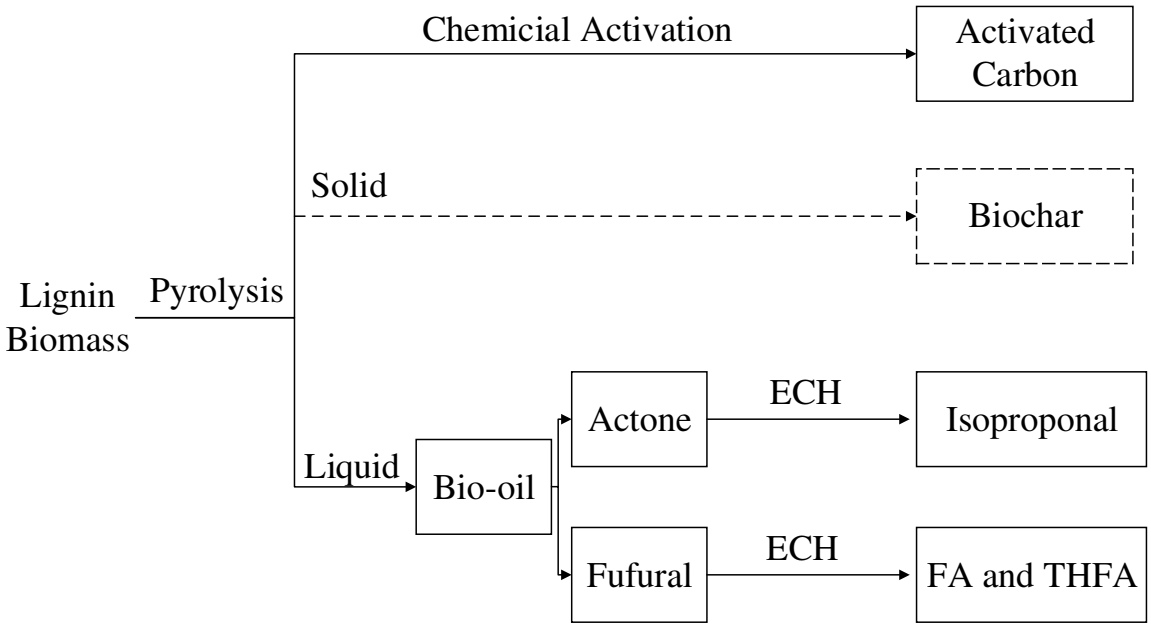

Figure 7. The designed lignin value added processed

Therefore, two methods were designed to improve the quality of lignin bio-products. Instead of direct pyrolysis, chemical activation (pyrolysis) was introduced in this dissertation. Compared to bio-char, the lignin chemical activation product lignin-activated-carbon is usually believed to be a more extensive application. Three different control parameters were selected to optimize the activation process: activation temperature, activation time, and heating rate. The activation effect of $ZnCl_2$ and H_3PO_4 were compared. Iodine No., Methylene Blue No, Surface area, Yield percentage, and Ash percentage were selected to evaluate the qualities of products.

Furfural and acetone are believed to be two main compounds of lignin-bio-oil[26, 27]. The electrochemical hydrogenation method was investigated in this dissertation to upgrade oil and obtain more valuable products, such as isopropanol, Tetrahydrofurfuryl alcohol, and 2-Methyltetrahydrofuran. A novel electrochemical hydrogenation reactor, a polymer electrolyte membrane fuel cell was applied in the experiment. Four different control parameters, including RH, operating temperature, input current density, and input voltage, were assessed to identify the optimized operating conditions for ECH of acetone. The degradation of membranes due to contamination of the polymer electrolyte membrane fuel cell, the mitigation methods and the effective working life of the polymer electrolyte membrane fuel cell were also investigated.

The objectives of this study are: (1) find effective ways to improve the value of lignin bio-products; (2) explore the best chemical activation condition of lignin biomass, and compare the activation effects by using the different activation chemicals $ZnCl_2$ and H_3PO_4; (3) pursue the optimized ECH condition of furfural and acetone; (4) evaluate the degradation of FEMFC membranes, estimate FEMFC effective working life and recommend methods to mitigate membrane pollution.

CHAPTER 2

PREPARATION OF ACTIVATED CARBON FROM UN-HYDROLYZED BIOMASS RESIDUE (LIGNIN)

In this chapter, un-hydrolyzed (UHS) biomass residue generated from enzymatic hydrolysis of corn stover was used for activated carbon production. Activated carbons were prepared by a high-temperature chemical activation method, with phosphoric acid and Zinc chloride ($ZnCl_2$) as the activation agents. A factorial design was used to optimize the activation process and five different parameters (pretreatment methods, impregnation ratio, activation time, activation temperature, and temperature increasing rate) were analyzed with respect to their influence on BET surface area and pore volume. At the optimized activation condition (i.e., co-precipitation pretreatment method, impregnation ratio 1.5, activation time 60 min, activation temperature 500°C and heating rate 60°C/min), activated carbon is obtained with surface areas and pore volumes approaching 1117 m^2/g and 0.12 cm^3/g, respectively. The capacity of methylene blue adsorption from aqueous solutions could reach 279 mg/g and adsorption isotherm fits the Langmuir model. Iodine number of the prepared activated carbon was comparable to that of commercially available material. The prepared activated carbon was characterized using SEM, XRD, FT-IR, TGA, and EDS.

2.1 Background

In this study, we used un-hydrolyzed solids (UHS) for ACs production. Bioethanol from lignocellulosic biomass is a promising alternative fuel source [85]. During the production of bioethanol, about one-third of biomass is recovered as un-hydrolyzed solids (UHS). The UHS resulting from enzymatic hydrolysis are difficult to convert into useful chemicals due to high moisture content, aromatic content, and bioactivity. However, it is a carbon-rich residue which mainly consists of lignin and unconverted sugars, depending upon the types of biomass pretreatment used in the earlier stages [86]. The production of cellulosic biofuel is estimated to increase more than five times, from the years 2015 to 2022. Therefore, the UHS residue generation will also increase. For example, a ton of lignocellulosic biomass generates approximately 60 gals of bioethanol, and 250 kg UHS residue during the production of cellulosic ethanol or butanol from biomass. According to the US Energy Independence and Security Act of 2007 (EISA), 36 billion gallons per year (BGY) of biofuels will be mandated to be produced by 2022, whereby 16 BGY will form lignocellulosic biomass [87]. Thus, the approximate generation of UHS will be 67.2 million tonnes per year, by 2022. The carbohydrate composition of UHS is introduced in Table 3.

Table 3. Carbohydrates composition of UHS[88].

Sample	Glucan,wt%	Xylan,wt%	Arabinan wt%	Lignin, wt%	Ash,wt%
UHS	13.90	5.79	1.05	52.49	12.32
RSD	<1.5	<1.2	<1.0	<2.0	<2.0

At present, several biochemical and thermochemical methods are being developed and have proved to efficiently produce lignocellulosic biofuels [88]. The bioethanol production from lignocellulosic biomass has already been demonstrated at pilot/demo-scale but cost-effectiveness

is still significantly below the EISA envisioned requirement [89]. Thus, the efficient utilization of UHS has a positive impact on making biofuels cost competitive.

Ammonia Fiber Explosion (AFEX) is a physiochemical process used for the pretreatment of corn stover under moderate temperatures (60-100 ℃) and high pressure (250-300 psi) for 5 minutes with liquid anhydrous ammonia, followed by released pressure. During this procedure the conversion of cellulose and hemicellulose to fermentable sugars is completed. AFEX treatment offers unique advantages than other biomass treatments, such as almost all the ammonia could be restored and recycled through the procedure, there is no liquid stream produced and cellulose and hemicellulose are well preserved without much degradation during the process [90-92].

The objectives of the present study are to (1) find an efficient method of making activated carbon from UHS, (2) optimize the process conditions to achieve the maximum BET surface area, (3) compare the activation effects by using different activation chemicals, $ZnCl_2$ and H_3PO_4, and (4) characterize ACs for its physio-chemical properties.

2.2 Materials and Methods

2.2.1 Material

Un-hydrolyzed biomass supplied by Biomass Conversion Research Laboratory at Michigan State University is solid residue remaining after the enzymatic hydrolysis of pretreated corn stover for bioethanol production. The Ammonia Fiber Explosion (AFEX) process was used for the pretreatment of corn stover. UHS was produced using a high-pressure stainless steel vessel. The element composition of UHS is shown in Table 2.

2.2.2 Activation Method

Activated carbon was produced by a typical one-step activation process. Prior to activation, the UHS was dried at 65°C for 48 hours and then ground to obtain a powder. H_3PO_4-UHS feedstock was prepared by soaking the UHS powder in H_3PO_4 85 wt% at 80°C for 15 minutes and then drying in an oven at approximately 80°C for 14 hours. $ZnCl_2$ and UHS feedstock was prepared by mixing the $ZnCL_2$ solution with UHS at 80°C for 7 hours. The resulting mixture's suspension that was directly dried at 110 °C for 48 h was labeled co-precipitation $ZnCl_2$ and UHS feedstock. The suspension that was dried after filtration was labeled filtration $ZnCl_2$ and UHS feedstock.

The impregnation ratio of $ZnCl_2$ and H_3PO_4 was calculated by the following equation:

$$\text{Impregnation ration} = \frac{\text{weight of mixture after impregnation} — \text{weight of UHS}}{\text{weight of UHS}} \qquad (1)$$

The impregnation ratio in this study ranged from 0.09 to 3.

The dried feedstock was activated in a quartz tube reactor (Diameter 2.7 cm; Length 56 cm). Three different control parameters were selected to optimize the activation process: activation temperature, activation time, and heating rate. The ranges of these parameters are from 400 to 600°C, 60 to 90 minutes, and 7 to 125°C/min, respectively. The activation process was taken under an N_2 flow condition. The experimental setup is shown in Figure 8.

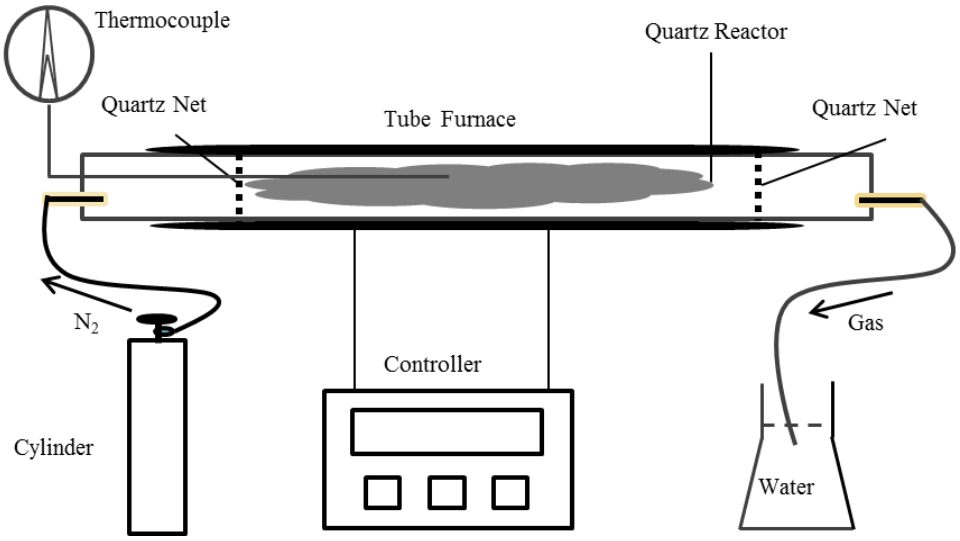

Figure 8. Schematic diagram of experimental setup.

After activation, the reactor with the primary products was cooled down to room temperature. The final product was obtained after washing once with 100 mL hot acid (20 minutes, 1:6 HCl) and four times with 1 L deionized water (25 minutes).

The entire activation step is shown in Figure 9.

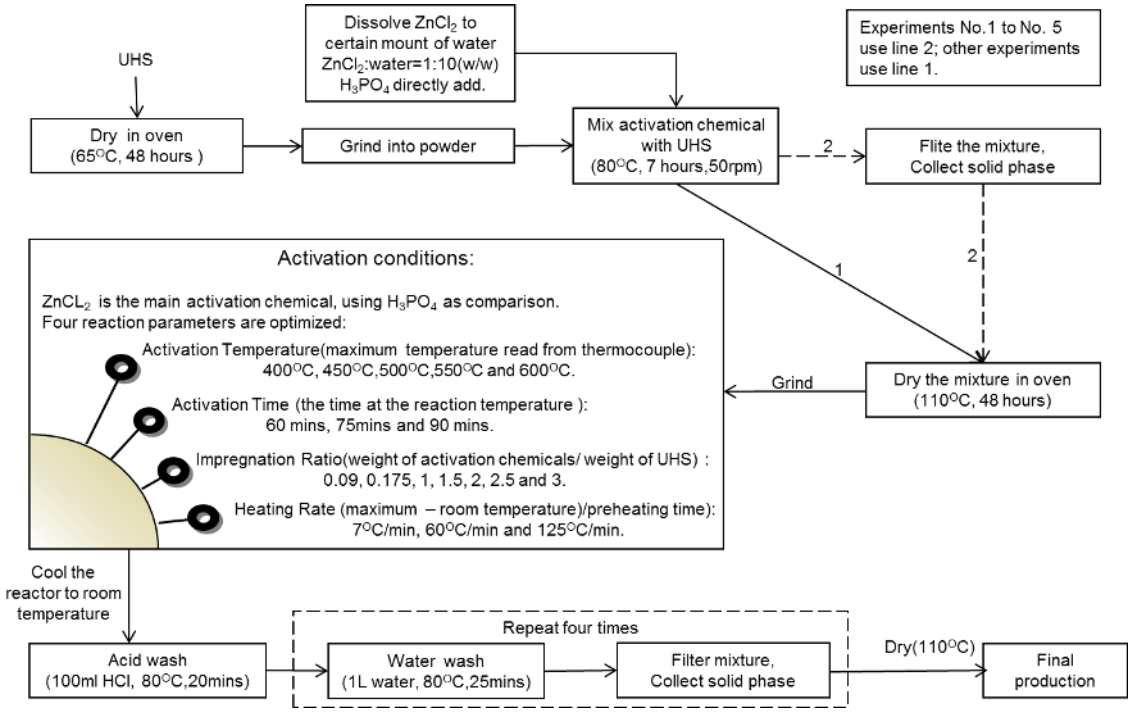

Figure 9. Schematic diagram of $ZnCl_2$ activation

2.3 Products Analysis

2.3.1 Elemental analysis

The component percentages of C, H, and N were measured by combustion analyzer and the amount of other elements were measured by energy-dispersive spectrometry (EDS).

2.3.2 Scanning electron microscopy (SEM)

Scanning electron microscopy (SEM) images were recorded on a JEOL JSM-6060LV microscope, and accelerating voltage was kept at 15.0 kV. The dry powdered samples were coated with gold to increase electrical conductivity.

2.3.3 Bulk density, moisture content, ash content, and Particle size

Bulk density was determined by the volume weight method; moisture and ash content was determined by the gravimetric method. Particle size was estimated from SEM images. Triplicated measurements were taken to measure Bulk density, moisture content, ash content, and the results show the average value.

2.3.4 Iodine number

Iodine number was determined following the standard test (ASTM Standard D4607-94). Instead of potassium iodate, potassium permanganate was selected to titrate sodium thiosulfate standard solution. The ratio of sample to adsorption solution was changed from 1g activated carbon with 1 L of 0.1 N iodine solution to 50 mg product with 40 mL of 0.03 N iodine solution. Triplicated measurements were taken and the result shows the average value.

2.3.5 Surface area and pore volume

Surface area was analyzed with a nova 2000e device. Before adsorption experiments, products were degassed under dynamic vacuum condition at 65ºC for 12 hours. The adsorption

and desorption of N_2 were performed at temperature 77.3 K. The Brunauer−Emmett−Teller (BET) model was selected to determine specific surface areas of the sample with relative pressures of P/P0 = 0.01 - 0.3. The total pore volume (Vt) was determined form the uptake at p/p0=0.99 by using the Barrett-joner-halenda method. Surface Area Analyzer with 5% accuracy, only the R^2 >0.99 the value of surface area will be adopted. A duplicated experiment was taken for BET measurement, using the average value drawing graph and raw data also was shown in the graph.

2.3.6 Thermo-gravimetric analyses (TGA)

Thermo-gravimetric analyses (TGA) were carried out by the instrument Q5000 v3.6 build 253. The samples were contained in alumina pans. The mass was recorded with temperature increasing, with 20 mL/min of N_2 flow condition. The temperature increasing rate was 10ºC/min with a range from 20ºC to 900ºC.

2.3.7 Fourier transform infrared (FTIR) spectra

Fourier transform infrared (FTIR) spectra measurement was acquired by using Nicolet 6700 at room temperature. Before analysis, the sample was dried in a vacuum oven at 80°C. Spectra were collected at a resolution of 4 cm^{-1}, and a range of 390-4000 cm^{-1}.

2.3.8 X-Ray Diffraction analyzer

XRD is used for identifying the atomic and molecular structure (usually for crystal), in which the crystalline atoms cause a beam of incident X-rays to diffract into many specific directions. A 5^{th} generation Miniflex x-ray diffractometer was used for X-ray analyses, 2θ was selected from 0^o to 45^o.

2.3.9 Acid surface group

Acid surface groups were determined by the Boehm titration method. Three allots of 100 mg samples were suspended in a 25 mL aqueous solution with 0.02 mol/L base. The bases used here were NaOH, $NaHCO_3$, and Na_2CO_3. After 24 h of agitation, solids were filtered off and elutes were titrated with 0.02 N HCl. The amount of acidic functional groups was determined according to the consumption of the base.

2.3.10 Methylene Blue (MB) dye adsorption

MB is one kind of heterocyclic dye compound, which is widely used in the textile industry. The molecular size of MB is around 1.6 nm × 0.7 nm. It is used to indicate the sorbent's ability to function as activated carbon for removing mesoporous molecules or large molecules from aqueous solutions [93].

Referring to the ASTM C837 method, Methylene Blue (MB) dye adsorption experiment was designed to determine the impact of initial MB concentration, pH, and adsorption time, with regard to adsorption equilibrium capacity.

For the experiment with varying initial MB concentrations, 20 mg of selected products were mixed with 20 mL aqueous MB solutions at varying initial concentrations (Co) to get suspensions. The suspensions were placed on a platform shaker for 24 h to ensure adsorption equilibrium. After the allotted time, solids were filtered off, and the eluate was collected for analyses. Equilibrium concentrations of MB were determined by ultraviolet-visible (UV-vis) spectrophotometry at a wavelength 665 nm. The calibration curve was obtained by standard solutions of MB. The adsorbed amount of MB at equilibrium (Qe, mg/g) was calculated by the following equation:

$$Q_e = \frac{(C_0 - C_e)V}{W} \qquad (2)$$

where C_o and C_e are the initial and equilibrium concentrations [mg/L], respectively. V is the volume of the solution [L], and W is the weight of products used [g].

Adsorption capacity with respect to time was tested to study adsorption kinetics of MB. For each experiment, 20 mg of selected products were mixed with 20 mL aqueous MB solutions, with 400 mg/L initial concentration. The amount of MB adsorption with regard to adsorption time (q_t, mg/g) was calculated by the following formula:

$$q_t = \frac{V(C_0 - C_t)}{w} \quad (3)$$

where C_t is the concentration of MB at a specific time [mg/L].

The adsorption of MB was studied under different pH conditions. For each experiment, 20 mg of selected product was mixed with 20 mL aqueous MB solution with 400 mg/L initial concentration 400 mg/L. Na_2CO_3, $NaHCO_3$, and HCL solutions were used to adjust different pH values. The suspensions were placed on a platform shaker for 24 hours to ensure reaching adsorption equilibrium. The concentration of MB (C_e) was determined by UV-vis spectrophotometry.

Every ultraviolet-visible (UV-vis) spectro-photometry measurement was duplicated, using the averaged value drawing graph and raw data also was shown in the graph.

All the experiments are shown in Table 9 (Seen in appendices).

2.4 Results and discussion

The surface and particle features of UHS and representative activated carbon were examined by SEM measurement and the results are shown in Figure 10. UHS particles show high heterogeneity in both size and the shape (Figure 10a and 10b). The visually observed particle size ranges from tens to hundreds of micrometers. If zoomed in to the surface of the particle, we

could clearly see that the UHS particle has a very smooth surface with low porosity (Figure 10c). After chemical activation with $ZnCL_2$ and H_3PO_4, the morphology characteristics have changed significantly. The result shows a relatively homogeneous particle size distribution with an average of around 70 µm (Figure 10d). Highly porous structures were successfully obtained on the activated carbon through the chemical activation reaction. The micro-scale pore size was visually estimated to be approximately 20µm through SEM imaging (Figure 10e and 10f).

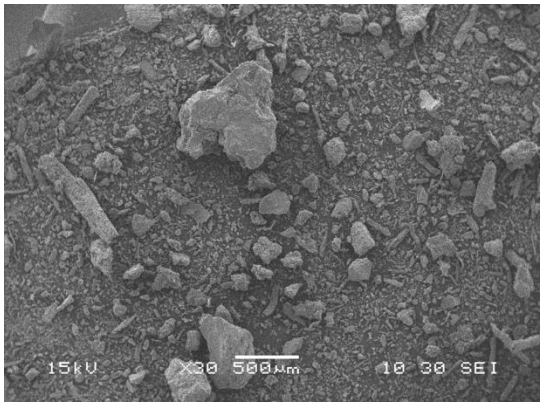

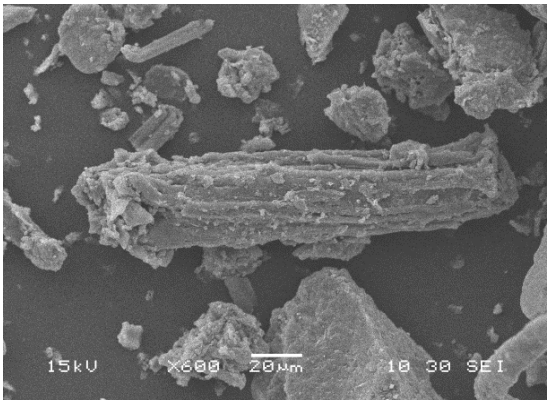

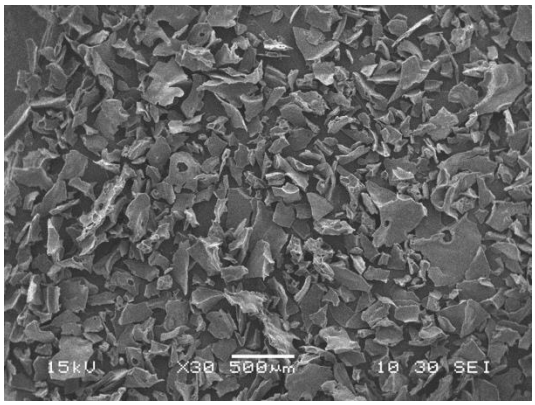

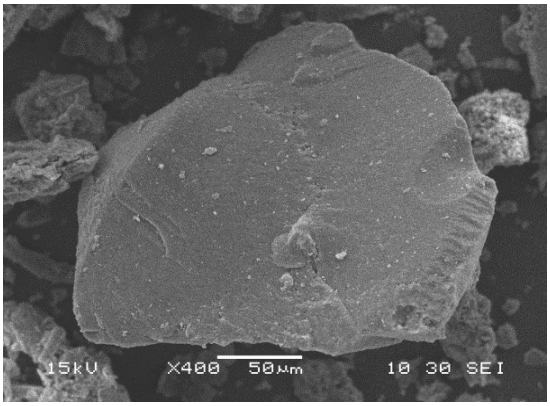

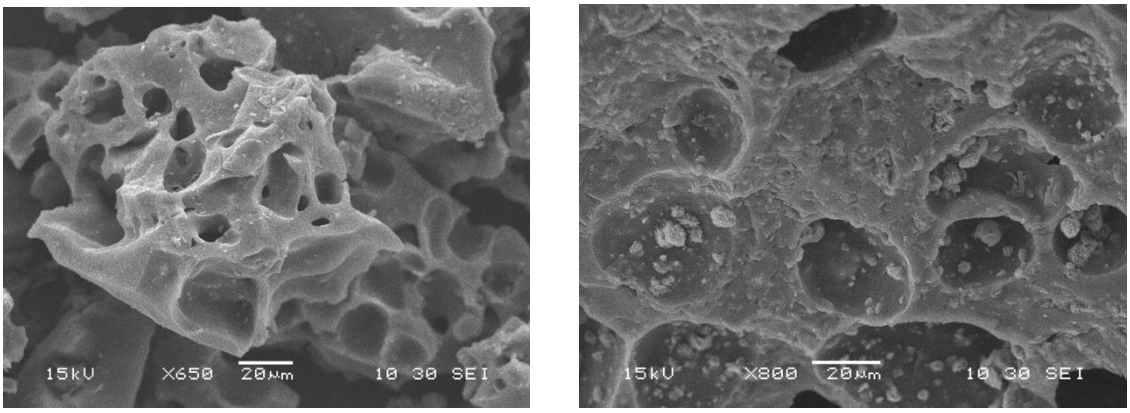

Figure 10. Scanning electron microscopy (SEM) images of UHS (a, b, c), $ZnCl_2$-AC (d, e) and H_3PO_4-AC (f) prepared from UHS.
$ZnCL_2$ activation at 500°C, 2.5 impregnation ratio, 1 h activation time 62.5 ºC/min heating rate and H_3PO_4–AC prepared from UHS, H_3PO_4 activation at 500 ºC, 1.7 impregnation ratio, 1 h activation time,52.8 ºC/min heating rate.

Table 4 presents the elemental components and ash content result of activated carbon and UHS. By comparison with the UHS components, the activated carbon produced by a chemical agent of H_3PO_4 retains similar element composition, except that P is present in the product of activated carbon during the chemical activation process. In contrast, the $ZnCl_2$ activation process obviously increases the C amount from 53.70% to 75.67%, while reducing the O component from 38.79% to 18.14%. This indicates that the $ZnCl_2$ chemical activation procedure was more distinctly reacted and Zn was totally removed by a hot acid rinse, followed by hot water wash. The effect of this reaction is also reflected in the SEM images which show that the carbon produced by $ZnCl_2$ activation has a better porous structure than that by H_3PO_4 (Figure 10e and 10f).

Table 4. Elemental and ash analysis

Sample	Moisture wt%	Ash wt%	Bulk Density (g/mL)	C wt%	H wt%	O wt%	N wt%	Cl wt%	Zn wt%	P wt%
UHS	6.9	13.0	0.64	53.70	4.04	38.79	2.44	0.39	-	-
UHS-$ZnCl_2$ AC	10.6	27.6	0.21	75.67	0.77	18.14	2.55	0.62	-	-
UHS-H_3PO_4 AC	6.3	19.4	0.53	49.41	-	35.52	1.35	-	-	9.53

$ZnCl_2$-AC prepared from UHS, $ZnCl_2$ activation at 500°C, 1.5 impregnation ratio, 1 h activation time, 62.5°C/min heating rate; H_3PO_4–AC prepared from UHS, H_3PO_4 activation at 500ºC, 1.7 impregnation ratio, 1 h activation time, 52.8°C/min heating rate.

Activation temperature is a very important parameter for the development of porous structures in activated carbon, and the response curve could indirectly indicate the activation temperature. TGA of feed stocks (Figure 11) shows the response of weight change with increasing temperature. From 20°C to 180°C, the weight loss is due to the moisture release. The results show that the water content in the three samples is less than 10% of the total weight. From 180°C to 400°C, the weight loss is due to the process of lignin releasing volatiles: ether group, carboxyl, and carbonyl group convert to CO, CO_2, and CH_4. Significant weight loss was observed in temperatures from 400°C to 600 °C, especially for the case of $ZnCl_2$ and UHS 2:1 mixture. This range has the highest decreasing rate of weight loss (more than 50%) and suggests that the best activation temperature should be in this region. According to research by Macedo et al. (2008) [94], fused $ZnCl_2$ volatile in this region. Also, Macedo et al. believe that activation chemicals like $ZnCl_2$ could promote the release of water molecules from organic compounds and formation of less volatilized aromatic compounds. Compared to the $ZnCl_2$-UHS mixture, the H_3PO_4-UHS mixture does not show any drastic weight lost region. According to Rubner et al. (2014)[95], lignocellulose constituent degradation could be deformed and be “dragged-out” over a wide temperature range when using H_3PO_4 as activation chemical agent.

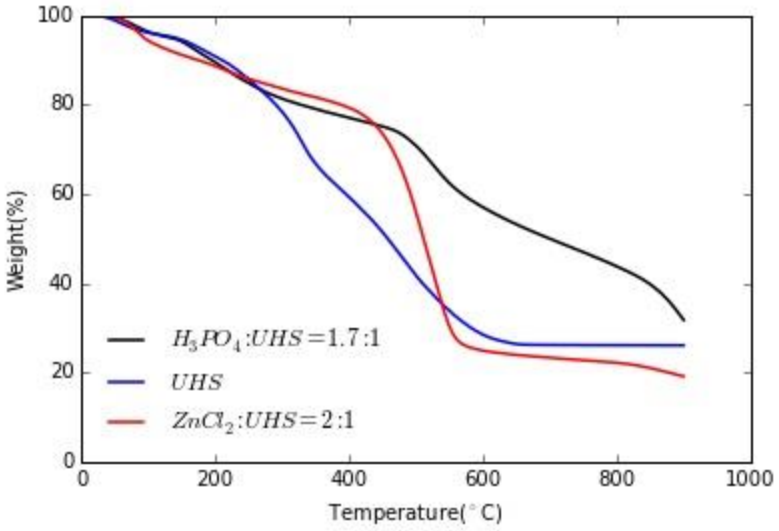

Figure 11. TGA curves of varied feed stocks

Total weight loss for chemical and UHS mixture samples was approximately 75% at temperatures above 650ºC. This implies that the yield percentage should reach a very high number.

The yield percentage measurement could indicate the output efficiency of activated carbon. It could be calculated by the following equation:

$$\text{Yield percentage}(\%)=\frac{\text{Yield weight of AC}}{\text{Input weight of UHS}}\times 100\% \quad (4)$$

The yield percentage is affected by reaction time, heating rate, reaction temperature, and impregnation ratio (shown in Figure 12). Specifically, with temperature increases from 400ºC to 600ºC, the yield percentage first decreases and the lowest amount happens at temperature 500ºC and then increases back, but the highest yield percentage is at 400ºC (Figure 12a).

The yield percentage is shown to be not proportional to the change of the impregnation ratio, and the results show that when the impregnation ratio is bigger than 1, the yield percentage has no big changes (Figure12b).

The yield percentage is inversely proportional to the change with heating rate (Figure 12c) and not very sensitive to the change of reaction time. The yield percentage could be stabilized at a certain impregnation ratio, temperature, and heating rate with 1 h (Figure 12d).

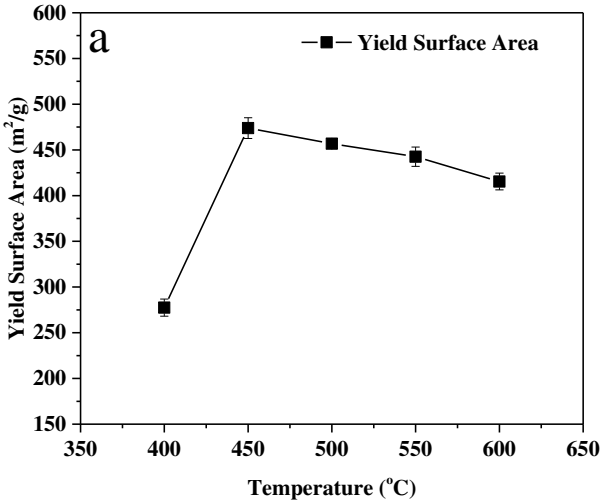

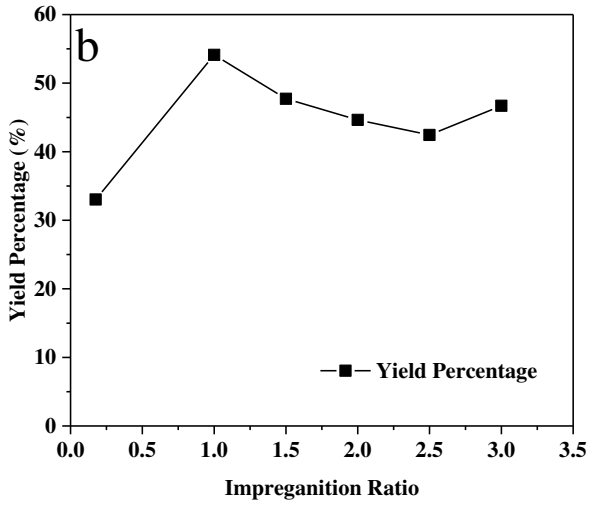

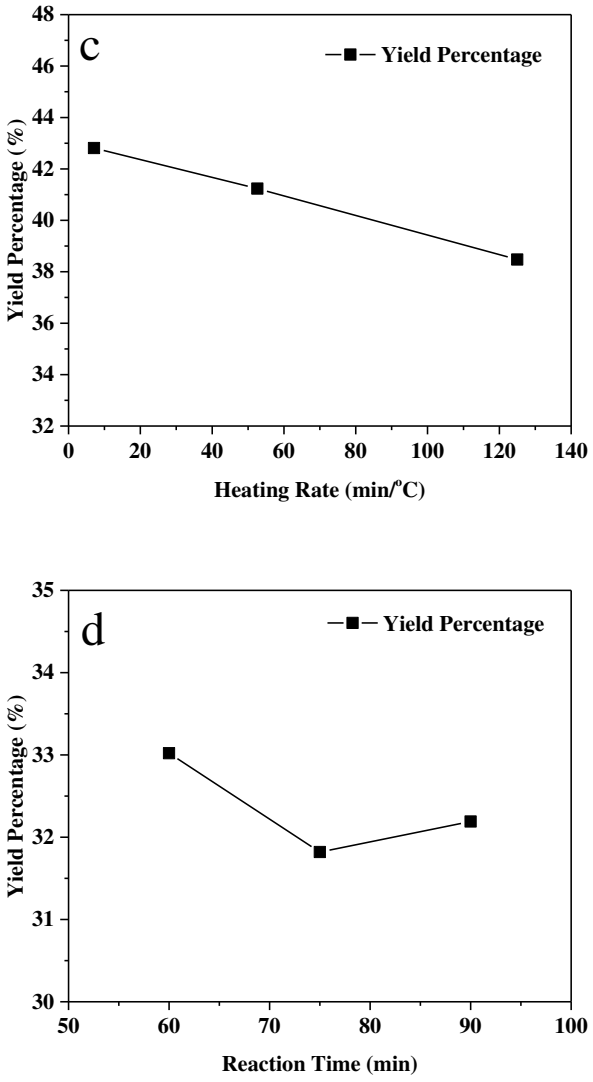

Figure 12. The yield percentage relationship with reaction time, heating rate, reaction temperature, and impregnation ratio
(a) Yield percentage as a function of activation temperature: activation time is 60 mins, the heating rate is around 60 mins/°C, the impregnation ratio is around 2, and activation chemical agent is $ZnCl_2$; (b) Yield percentage as a function of impregnation ratio: heating rate is around 10 min/°C, temperature is around 500°C, activation time is 60mins, and activation chemical agent is $ZnCl_2$; (c) Yield percentage as a function of heating rate: activation time is 90mins, temperature is around 500°C, impregnation ratio is around 2, and activation chemical agent is $ZnCl_2$; (d) Yield percentage as a function of reaction time: heating rate is around 10 min/°C, temperature is around 500°C, impregnation ratio is around 0.175, and activation chemical agent is $ZnCl_2$

Porous volume and surface area of activated carbons determine their adsorption quality. The results from the yield percentage investigation experiment show that the optimum reaction conditions when using $ZnCl_2$ as the activation chemical agent are activation temperature of

500°C, impregnation ratio of 1.5- 2, a heating rate of 60°C/min, and reaction time between 60 to 75 minutes. Activation temperature and impregnation ratio have a more significant impact on the surface area than temperature increasing rate and reaction time.

The surface area of the representative UHS-$ZnCl_2$ activated carbon sample was up to 1117 m^2/g under the reaction conditions of 60 minutes activation time, approximately 60 mins/°C heating rate, and an impregnation ratio of 1.5. The pore volume of a representative UHS-$ZnCl_2$ activated carbon sample was as high as 0.52 cc/g under the conditions of 60 minutes activation time, approximately 60 mins/°C heating rate, and around 3 impregnation ratio.

Comparing with $ZnCl_2$, the activation chemical agent with H_3PO_4 shows relatively little effect on the surface area and pore volume activated carbon off. For instance, the surface area and pore volume just reach 365.1m^2/g and 0.0479 ccs/g respectively, under activation time of 60 minutes, approximately 50 mins/°C heating rate, and an impregnation ratio of 1.7.

According to the experimental results, $ZnCl_2$ is a better activation chemical than H_3PO_4 for UHS activation.

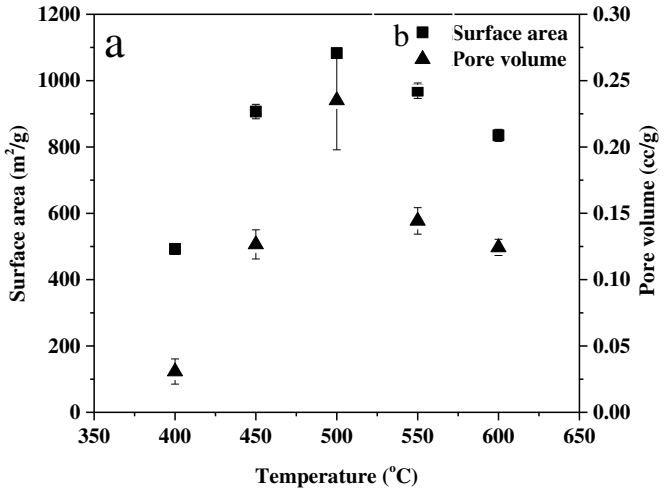
a
b
Surface area
Pore volume
Surface area (m²/g)
Pore volume (cc/g)
Temperature (°C)
1200
1000
800
600
400
200
0
0.30
0.25
0.20
0.15
0.10
0.05
0.00
350
400
450
500
550
600
650

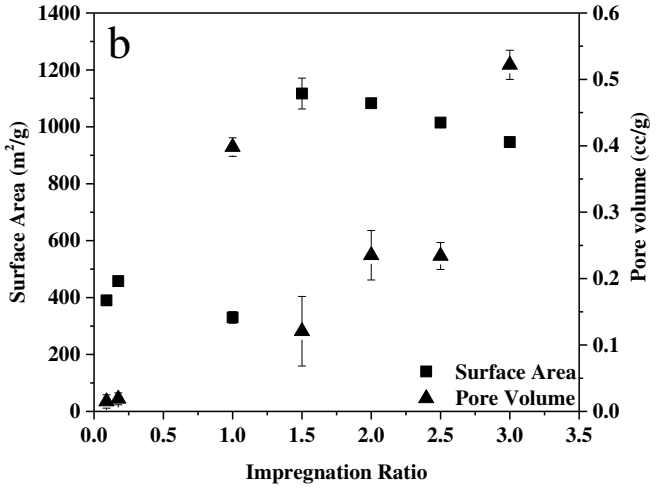
b
Surface Area
Pore Volume
Surface Area (m²/g)
Pore volume (cc/g)
Impregnation Ratio
1400
1200
1000
800
600
400
200
0
0.6
0.5
0.4
0.3
0.2
0.1
0.0
0.0
0.5
1.0
1.5
2.0
2.5
3.0
3.5

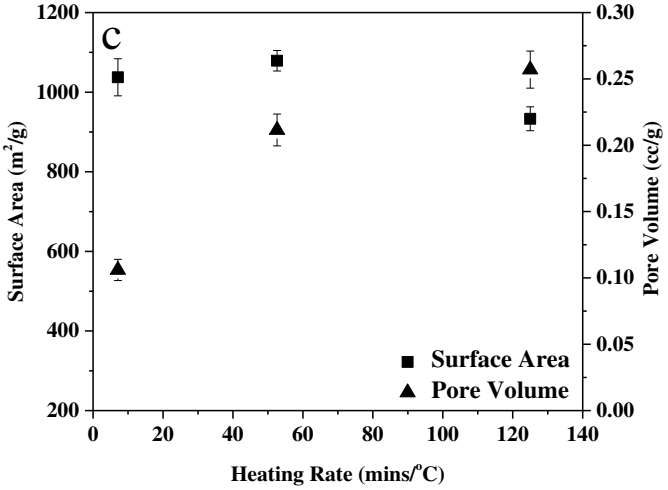
c
Surface Area
Pore Volume
Surface Area (m²/g)
Pore Volume (cc/g)
Heating Rate (mins/°C)
1200
1000
800
600
400
200
0.30
0.25
0.20
0.15
0.10
0.05
0.00
0
20
40
60
80
100
120
140

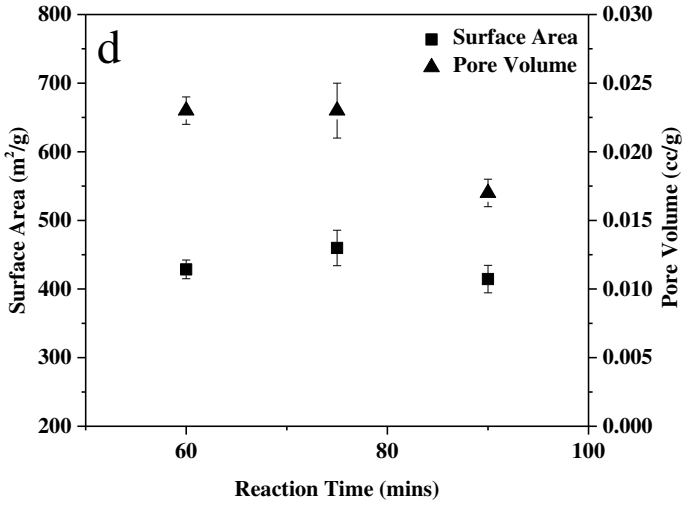

Figure 13. The surface area and pore volume relationship with Temperature, Impregnation, Heating rate and reaction time.
(a)Surface area and pore volume as a function of activation temperature: activation time is 60 mins, the heating rate is around 60 mins/℃ and impregnation ratio is 2; (b) Surface area and pore volume as a function of impregnation ratio: activation time is 60 mins, the heating rate is around 60 mins/℃ and activation temperature is 500℃; (c) Surface area and pore volume as a function of heating rate. Activation time is 90 mins, the temperature is around 500℃ and impregnation ratio is around 2; (d) Surface area and pore volume as a function of reaction time: heating rate is around 10min/ ℃, the temperature is around 500℃ and impregnation ratio is around 0.175.

Yield surface area could show the combined effect between yield and surface area; it could be calculated by the following equation:

$$\text{Yield Surface Area} = \text{yield percentage} \times \text{surface area} \quad (5)$$

Yield Surface area VS activation temperature is shown in Figure 14.

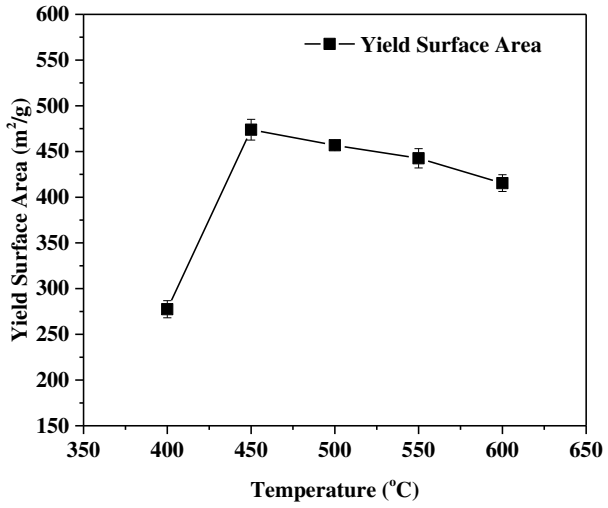

Figure 14. Yield surface area as a function of activation temperature.
Activation time is 60 mins, the heating rate is around 60 mins/℃ and impregnation ratio is 2.

When the temperature reaches 450℃, the yield surface area has the maximum value of 459m^2/g, the decrease is slow. The uptake of MB was studied on the activated carbon with a surface area of 1077 m^2/g. The observed methylene blue adsorption results show that there is a good affinity for MB on to UHS-$ZnCl_2$ activated carbons. Q_e could reach 186 mg/g at the initial pH of 4.8, while Q_e is 279 mg/g at the pH value of 10. The isotherm was measured by subjecting the samples to aqueous solutions of MB, with different initial concentrations, at room temperature and an equilibration time of 7 hours.

Figure 15 shows the experimental isotherm of MB on UHS-$ZnCl_2$ activated carbon. To some extent, the result moderately fits with the Freundlich model. The expression of the Freundlich model is Q_e =101.9C_e^0.1143 with R^2=0.988 to get K and N numbers.

The kinetics of MB adsorption are presented in Figure 16. From the change of C_t with uptake time, the equilibrium time of MB adsorption between 3 to 4.5 hours.

Figure 17 shows the significance of the effect of pH on the adsorption capacity of UHS-$ZnCl_2$ activated carbon. When pH value was below 7, Q_e was stable around 175 mg/g. The Q_e is proportional to the change of pH value once the pH exceeds 7.

Deng et al. have explained this phenomenon by the zero charge pH theory. There is a very special pH point for activated carbon called the point zero charge (PZC). At this special pH point, there is no charge on the surface of activated carbon. When $pH < pH_{PZC}$, both H^+ and MB are adsorbed, which means the capacity to MB adsorption was reduced. Once $pH > pH_{PZC}$, the surface of the activated carbon is negatively charged, which increases the adsorption capacity of positively charged MB molecules [96].

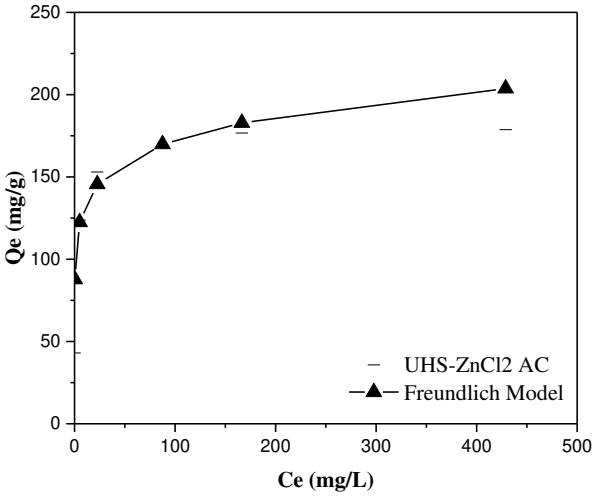

Figure 15. Q_e changes with C_e.
Adsorption time=7h, pH=4.8, activated carbon was prepared at 500°C, 62.5ºC/mins heating rate, 2 impregnation ratio, and 60 min reaction time.

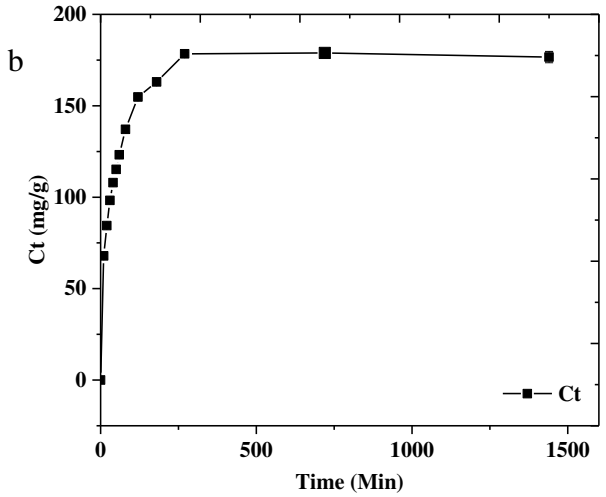

Figure 16. C_t changes with uptaking time.
pH=4.8, initial MB concentration=400mg/L, activated carbon was prepared at 500°C, 62.5 °C/mins heating rate, 2 impregnation ratio, and 60 min reaction time.

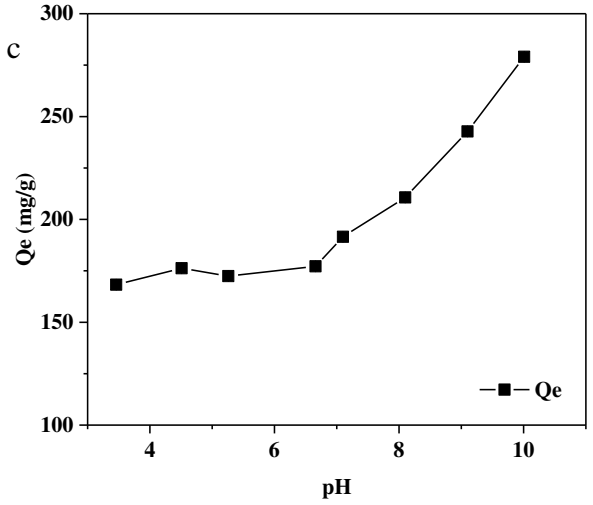

Figure 17. Q_e change with pH of UHS-$ZnCl_2$.
Adsorption time=7h, initial MB concentration =400mg/L, activated carbon was prepared at 500ºC, 62.5 °C/mins heating rate, 2 impregnation ratio, and 60 min reaction time.

Table 5 shows that the UHS-$ZnCl_2$ activated carbon contained 0.7 cmol/L acid groups, most of which were relatively strong acids (e.g., phosphoric, lactonic, and carboxylic). Compared with

physical activation for commercial activated carbon (Norit, GAC 1240), chemical activation with $ZnCl_2$ introduced fewer acid groups on the interfaces of the activated carbons.

Table 5. Surface functional group comparison from UHS-$ZnCl_2$ and commercial AC
(UHS-$ZnCl_2$ AC prepared from UHS at 500ºC with impregnation ratio 1.5 at heating rate 60ºC/min and activation time 1h)

Type	Phenolic (cmol/L)	Lactonic (cmol/L)	Carboxylic (cmol/L)	Total (cmol/L)
UHS-$ZnCl_2$ AC	0.1	0.2	0.4	0.7
Coal AC (Norit, GAC 1240)	0.3	0.5	0.2	1.0

FT-IR analysis was used to determine the functional groups of activated carbon and to estimate the compositions. Commercial activated carbon used as a control in FT-IR responses is Aqua Nuchar. The activation condition for UHS-$ZnCl_2$ AC used in FT-IR analyses is impregnation ratio of 2, 500°C activation temperature, 52.6 °C/min heating rate, and a 90 minute reaction time. Activation conditions for UHS-H_3PO_4 AC are impregnation ratio of 8, activation temperature of 600°C, 52.1 °C/min heating rate, and a 90 minute reaction time.

As shown in Figure 18, UHS, UHS-$ZnCl_2$ AC, UHS-H_3PO_4 AC, and commercial AC have very similar FT-IR curves. Peaks at 1600cm^{-1} and between 1000 and 1300 cm^{-1} are from the aromatic ring C-C band and C-H band and all the four curves have these two peaks. Peaks at 3300 cm^{-1} and 1315 cm^{-1} probably are from the phenolic hydroxyl (Ar)O-H, which is observed from UHS. The peak at 1690 cm^{-1}, which is present in UHS-$ZnCl_2$ AC and commercial AC samples, implies that carboxyl (C=O) may exist. The peak at 680-900 cm^{-1} is from the substituted aromatic ring which is shown in all four curves. The wide peak between 1000-1300cm^{-1} in UHS-H_3PO_4 AC curve may due to C=P and C-P band stretching vibrations. Alcoholic hydroxyl (O-H) peak at 1410 cm^{-1} is only observed in the UHS curve. In summary, this indicates that chemical activation does not destroy the aromatic structure, while it only removes phenolic hydroxyl (Ar) O-H. The results also indicate that alcoholic hydroxyl (O-H)

may be converted to carboxyl(C=O). The percentage of both H and O was reduced due to these conversions.

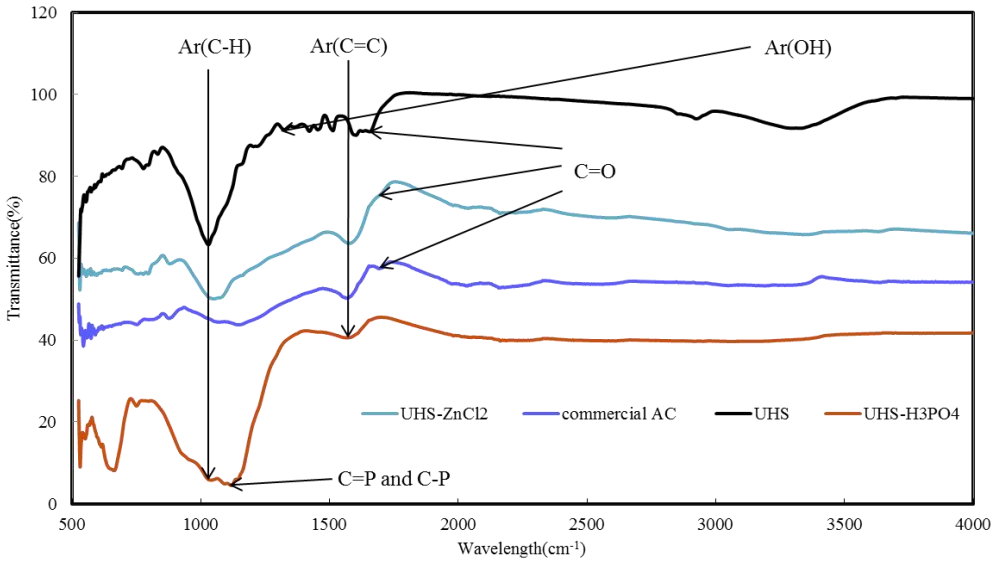

Figure 18. FT-IR spectra of activated samples, commercial activated carbon, and UHS

X-Ray diffraction (XRD) analyses were used to determine molecular structure (usually for crystal), in which the crystalline atoms cause a beam of incident X-rays to diffract into many specific directions. XRD was used in this study to estimate the composition of UHS and activated carbon samples.

Activation conditions for UHS-$ZnCl_2$ AC used in XRD analyses are impregnation ratio of 2, the activation temperature of 500°C, a heating rate of 52.6 °C/min, and a reaction time of 90 minutes. Activation conditions for UHS-H_3PO_4 AC are impregnation ratio of 8, the activation temperature of 600°C, a heating rate of 52.1 °C/min and a reaction time of 90 minutes.

The results show a broad diffraction peak corresponding to the graphitic ordering in molecular planes near 26º in $ZnCl_2$ activated carbon, which is more compared to H_3PO_4 sample[97]. And there is a SiO_2 peak observed on all the three samples due to residual materials

after carbonization and activation processes at the used temperatures. There is 4.67 wt% Si in UHS; SiO_2 is generated by the activation process. SiP_2O_7 and H_3PO_4 peaks were observed in UHS-H_3PO_4 AC curve, which indicates that P was introduced to the activated carbon produced by the addition of activation chemical agent, H_3PO_4.

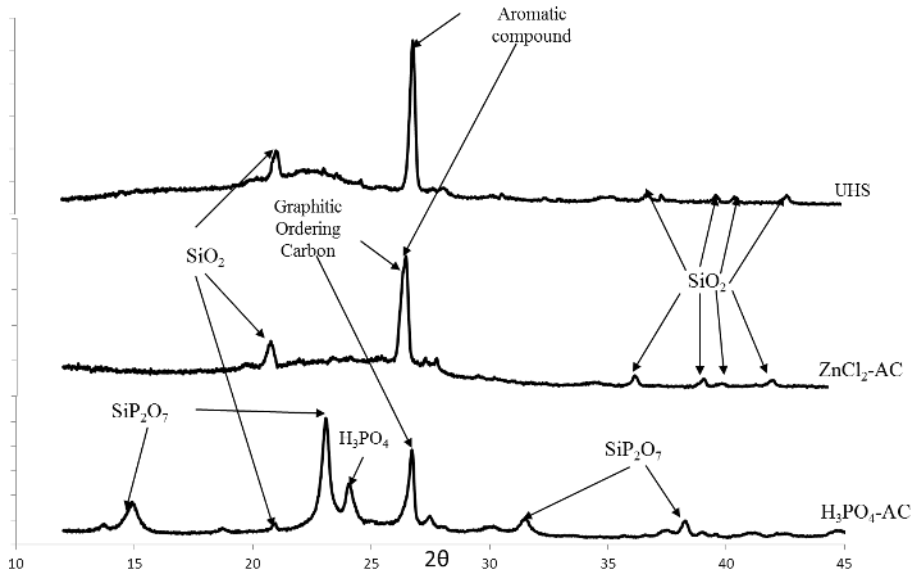

Figure 19. XRD spectra of activated samples and UHS

Compared to commercial AC (Table 6), UHS- $ZnCl_2$ AC has similar Iodine number, Methylene Blue number, and surface area, but a better yield percentage. This indicates that high-temperature $ZnCl_2$ activated carbon method is a possible way of utilizing UHS residue. Relatively high ash content, higher bulb density, oxygen percentage, and relatively lower carbon element, pore volume are the main shortage of UHS-$ZnCl_2$ AC.

Table 6. Commercial AC and UHS-$ZnCl_2$ AC Comparison

	Iodine No. (mg/g)	Methylene Blue No. (mg/g)	Surface area (m^2/g)	Yield percentage (%)	Ash content (%)	Bulb density (g/mL)	Oxygen Percentage (wt%)	Carbon Percentage (wt%)	Pore Volume (cm^3/g)
$ZnCL_2$-AC	939.5	187.5	1117	42~57	27.6	0.21	12~18	73~81	0.12~0.52
Commercial AC	900~ 1050	135~ 210	800~ 2000	20~40	2~4	0.48~ 0.54	3~7	90~94	0.2~0.7
H_3PO_4-AC			365	82	19.4	0.53	35.5	49.4	0.05

2.5 Conclusions

Un-hydrolyzed solid from biomass was applied to prepare good quality activated carbons through a single stage chemical activation process. $ZnCl_2$ and H_3PO_4 were used as impregnating agents and $ZnCl_2$ was tested to most effectively produce ACs. The optimal experimental condition is that when the activation time is 60 minutes, the impregnation ration is between 1.5 to 2, the heating rate is 60 ℃/mins, and an activation temperature around 500℃. With the best activation conditions, the carbons produced have a surface area of around 1117 m^2/g, and the yield percentage could reach around 50%. Comparing to Commercial AC, UHS-$ZnCl_2$ AC has similar Iodine No., Methylene Blue No, Surface area, better Yield percentage, which makes high-temperature $ZnCl_2$ activated carbon method is a possible way of utilizing un-hydrolyze biomass residue. In addition, the Zinc residues could be totally removed through the acid wash and water wash which increased the purity of the activated carbon produced. In comparison, the activated carbon produced by the H_3PO_4 agent has a relatively low surface area and a high amount of phosphorus residue.

CHAPTER 3

ELECTROCHEMICAL HYDROGENATION OF ACETONE TO PRODUCE ISOPROPONAL

Electrochemical hydrogenation (ECH) of acetone is a relatively new method to produce isopropanol. It provides an alternative way of upgrading bio-fuels with less energy consumption and chemical waste as compared to conventional methods. In this chapter, a Polymer Electrolyte Membrane Fuel Cell (PEMFC) hardware was used as an electrochemical reactor to hydrogenate acetone to produce isopropanol and diisopropyl ether as a byproduct. High current efficiency (59.7%) and selectivity (>90%) were achieved, while ECH was carried out in mild conditions (65ºC and atmospheric pressure). Various operating parameters were evaluated to determine their effects on the yield of acetone and the overall efficiency of ECH. The results show that an increase in humidity increased the yield of propanol and the efficiency of ECH. The operating temperature and power supply, however, have less effect. The degradation of membranes due to contamination of PEMFC and the mitigation methods were also investigated.

3.1 Background

Propanol is an important organic raw material in chemical production, two isomers 1-propanol and isopropanol are widely used in the paint, medicine and pesticide industries [98]. Compared to 1-propanol, isopropanol has more extensive and important applications. Along with ethanol, n-butanol, and methanol, isopropanol belongs to the group of alcohol solvents, about 6.4 million tons of which were utilized worldwide in 2011 [99]. Isopropanol is primarily produced by combining water and propene in a hydration reaction, through either an indirect or direct process. In an indirect process, propene reacts with sulfuric acid and forms a mixture of sulfate esters. Subsequent hydrolysis of those esters by steam produces isopropanol. In a direct hydration process propene reacts with water or steam at high pressure (200 to 300 atm) and high temperatures (230 to 270 °C), in the presence of solid or supported acidic catalysts [100, 101]. Isopropanol is produced by a direct combination of propene and water. Both processes require intensive energy input and use of corrosive chemicals.

Thermal hydrogenation of acetone is a relatively new and more advanced method to produce isopropanol, where acetone is hydrogenated either in the liquid or gas phase over a Raney nickel or copper and chromium oxide mixture[102]. Compared to the aforementioned conventional methods, thermal hydrogenation can be carried out at a lower temperature (75 °C) with up to 35% yield rate. However, an elevated temperature (350 to 400°C) is still required to enable fully activated catalysts. In addition, handling corrosive chemicals remains a problem [103].

Electrochemical hydrogenation (ECH) provides a more energy efficient and environment-friendly method of upgrading organics, by integrating both the electrochemical and catalytic methods [42]. In this chapter, ECH of acetone to produce isopropanol was demonstrated using a PEMFC reactor at ambient pressure. Various factors that impact the yield of propanol were

investigated, including current density, temperature, relative humidity (RH), and membrane degradation. The main objective of this work was to evaluate the appropriate pathways of ECH of bio-oil components using a PEMFC reactor.

3.2 Materials and Method

3.2.1 Material and experimental setup

The experiments were performed using a standard PEMFC hardware (Scribner Associates Inc., USA) with an active area of 25 cm^2. Such standard PEMFC hardware has been widely used for PEMFC evaluation tests [51, 104]. Commercially available MEAs were purchased from Ion Power Inc., USA. The MEAs consist of Nafion® 117 membranes sandwiched with porous carbon-based electrodes, each of which has a Pt loading of 0.3 mg/cm^2. Micro-porous carbon papers (SIGRACET® 10BC) were trimmed and used as gas diffusion layers (GDLs) for both electrodes. Teflon gaskets were used to seal the assembly. A pair of graphite bipolar plates with flow patterns was used to distribute flows and enclose the assembly. All the temperatures were acquired via K-type thermocouples (OMEGA, USA). A fuel cell test station (850e, Scribner Associates Inc., USA) was used to control temperatures, flow rates, and humidity. It was also used for data acquisition.

Ultra-high purity (99.999%) N_2 (Airgas, USA), and filtered shop air were connected to the fuel cell test station and supplied to the PEMFC through the purge line. They were used for purging the system and making current and voltage curve, respectively, and were cut off while the ECH experiment was running. The ultra-high purity (99.999%) H_2 (Airgas, USA) and Deionized (DI) water tanks were purged through the anode side of the reactor, using the fuel cell test station. H_2 was the electrons donator and deionized (DI) water tank was used for adding humidity to H_2. Acetone (Fisher Scientific, Certified ACS Reagent Grade) was injected into the

cathode side of the reactor by a syringe pump (MTI Corporation, EQ-300sp-LD). A direct current (DC) power supply (Tektronix, PWS 4205) was used to supply DC power for ECH. The positive probe was connected to the anode, while the negative probe was connected to the cathode. While ECH was running, electrons were deprived of H_2 and transferred to the cathode through the DC power supply. Acetone was the electron acceptor and reacted with the produced protons. The products from the cathode outlet were collected by airbags (Tedlar®), which were held by the water bath. The room temperature water bath was used for condensing the unreacted acetone and products. The cell temperature was controlled by the fuel cell test station. The exhaust gases and byproducts from the anode were condensed in a knock-out bottle prior to venting out. The schematic diagram of the whole experimental setup is shown in Figure 20.

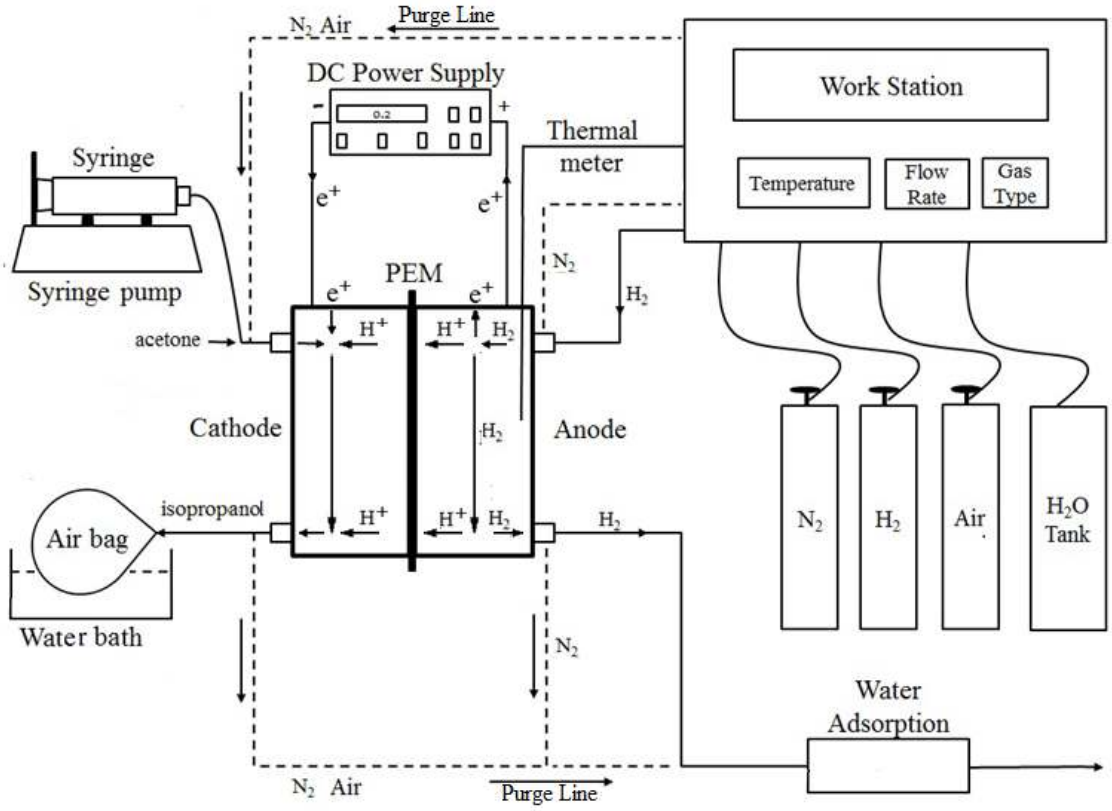

Figure 20. Schematic diagram of the experimental setup

3.2.2. Electrochemical hydrogenation and characterization

All the PEMFCs were assembled in accordance with the standard assembly procedure of fuel cell hardware[105]. Prior to each ECH experiment, a new membrane was conditioned based on the standard protocol [105] for at least 24 hours, until it reached a fully functional state. Current-voltage (I-V) sweeps were performed to establish the baseline data for the following ECH experiments.

In each ECH experiment the acetone and H_2 flow rates were controlled at 6 ml/hr and 0.25 slpm, respectively. The voltage was consistent for each reaction; the current was recorded every five minutes. Four different factors, including cell temperature, RH, supplied voltage, and membrane degradation, were investigated to identify the optimized operating conditions. The operating conditions were in the range of 55 °C to 80 °C, 0.01 V to 0.02V, and 35 % to 90 %, respectively. I-V scans were conducted before and after ECH to characterize the membrane degradation.

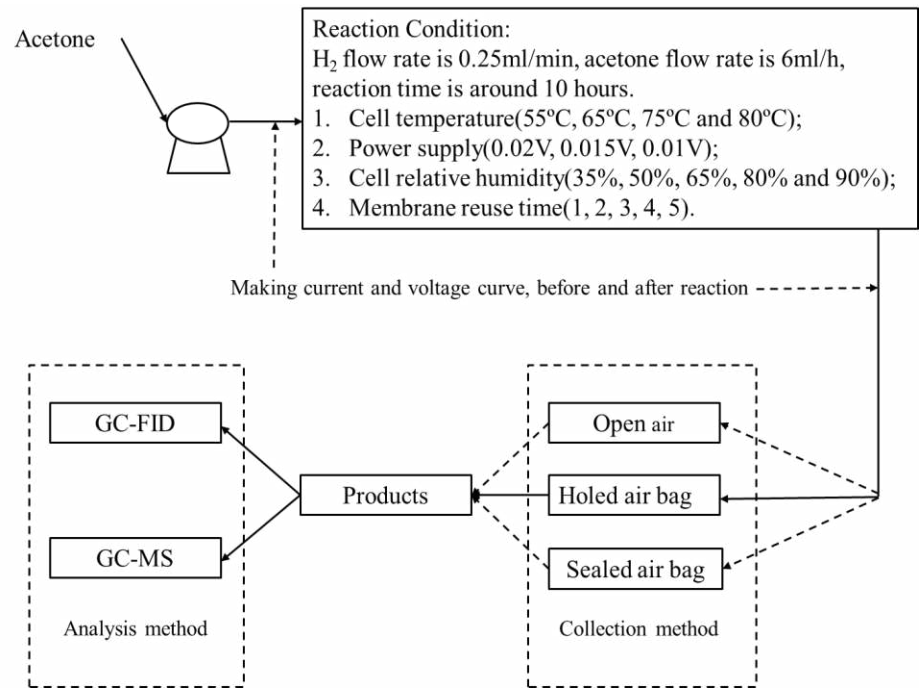

Figure 21. Flowchart of the experiment

The flow chart of the ECH experimental operation is shown in Figure 21. Initially, three collection methods, including the dead end, were partially confined and an open end was evaluated to identify the best means for accurate collection of products. In the partially confined method, products were collected by airbags with pressure relief valves, which prevents pressure buildup while trapping the products. In the other two collection methods, although the products were condensed by room temperature water bath, dead-end still resulted in too much back pressure accumulation, whereas open end failed to collect enough products for analysis. Therefore, partially confined airbags were used for all the experiments. The pressure differential of two electrodes can be controlled by airbags confined extent. Green *et al*. proved that a suitable pressure differential between the anode and cathode could decrease cross-over and increase conversion [72]. Dadda *et al*. believed that water transport in the membrane of a PEMFC is influenced by a convective force, resulting from a pressure gradient [106]. Many researchers also point out the importance of flow pressure [107].

The collected samples were analyzed by a gas chromatography-mass spectroscopy (Shimadzu, GC-MS-QP2010 SE), using a Shimadzu (SH-Rxi-5Sii) MS column (length: 30 m, inner diameter: 0.25 mm). Volume quantitative analysis was conducted by another gas chromatograph (SRI Instrument, 8610C), using a Restek (MXT-WAX) column (length: 30 m, inner diameter: 0.53 mm). Helium was used as a carrier gas for both gas chromatographs.

3.3 Results and Discussion

3.3.1 Product characterization

Both the liquid and gaseous products were analyzed by GC-MS. Unreacted acetone (C_3H_6O), isopropanol (C_3H_8O), and diisopropyl ether ($C_6H_{14}O$) were detected in the liquid products. Unreacted acetone, diisopropyl ether, and isopropanol were found in the gaseous and liquid products.

The reactions on both electrodes are catalyzed by Pt. While applying a DC voltage, protons formed at the anode are electrochemically pumped to the cathode. The protons then react with acetone to produce isopropanol and diisopropyl ether. The most feasible reaction pathways at the cathode are shown below:

$$2H^+ + 2e^- \xrightarrow{Pt} 2H_{ads} \quad (a)$$

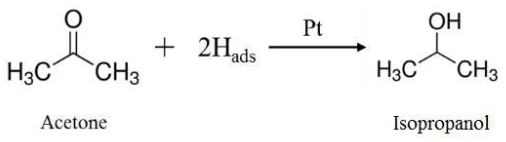

(b)

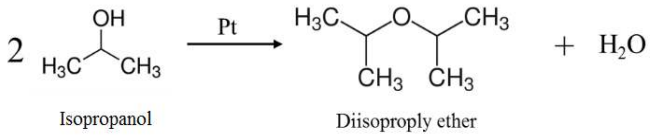

Isopropanol Diisoproply ether (c)

Electrosorbed hydrogen is formed on Pt surface by reduction of H+ (eq.(a), where H_{ads} is the electrosorbed hydrogen). Hydrogenation of the C=O bond then proceeds as in catalytic hydrogenation through the reaction of the acetone with the electyrosorbed hydrogen (eq(b)). As a result, isopropanol, which is the main product generated. Two isopropanol molecules may also combine together and free one water, generating diisoproply ether as a byproduct is formed (eq. (c)). Note that hydrogen gas can also be regenerated, which is an unfavorable electrochemical reaction during ECH. Hydrogen regeneration reduces the efficiency by electrochemically pumping useless hydrogen through the MEA, resulting in a reduction of the yield rate of products.

Each MEA had undergone at least three ECH experiments before replacement. In order to minimize the impacts of MEA degradation on ECH experiments, the results of the I-V scans, which were carried out prior to the experiments, were compared to the baseline performance of each MEA. If the I-V curve demonstrated an obvious deflection from the baseline performance, then the MEA needs to be replaced. The components detected in the products were isopropanol, diisopropyl ether, acetone, and water, with their volumetric percentages ranging from 12% to 16%, 1% to 2%, 69% to 75%, and 11% to 14%, respectively. Note that abundant acetone was supplied to the cathode to prevent fuel starvation. As a result, the maximum conversion rate of acetone to isopropanol was 23%. The selectivity of isopropanol was calculated more than 90%. Acetone was also detected in the anode due to crossover and will be discussed later. The produced isopropanol can be easily separated from the mixture using extraction and distillation,

which are two widely adopted methods in the industry [108] and therefore not discussed in detail here.

Three different control parameters, including RH, operating temperature, and input voltage, were assessed to identify the optimized operating conditions for ECH of acetone. All the operating parameters used in the experiments are shown in Table 10 (seen in the appendices).

RH is a very important parameter that affects the performance of PEMFCs [107, 109-113]. Figure 22a shows a typical impact of RH on the product yield during ECH of acetone. It was obviously evidenced that higher humidity promoted a higher yield of isopropanol. The composition of isopropanol in the products increased from 4.9% to 16.1%, while RH climbed from 35% to 90%. humidity had such a significant impact because the MEA usually uses a perfluorosulfonic acid membrane (e.g. Nafion®) as the electrolyte. A high or nearly saturated humidity (RH >80%) is usually required to obtain practical performance because the conductivity of perfluorosulfonic acid membrane membranes depends on the water content. Higher humidity means higher conductivity, resulting in better performance [114-117]. Water management is critical for PEMFC operation. Sufficient water must be absorbed into the membrane to ionize the acid groups, whereas excess water can cause flooding issues and thus diminish the performance [72]. The inlet RH of the electrodes must be controlled to prevent both membrane dry out and electrode flooding. Although better performance is usually obtained by increasing RH, excess moisture may result in water flooding that hinders gas transport [118]. In the present experiments, RH was maintained between 35% and 90% to prevent either water starvation or over saturation. In fact, many researchers have investigated the mechanism of humidity influence. It is generally believed that RH can impact electro-osmotic drag, water diffusion, membrane ionic conductivity, and water back diffusion flux in the MEAs, which

consequently influence the performance [119, 120]. Elevated RH can greatly improve the PEMFC performance, through increasing the membrane conductivity [121, 122], the catalyst activities [121, 123], the electrode kinetics [124, 125], and the mass transfer rates [126, 127].

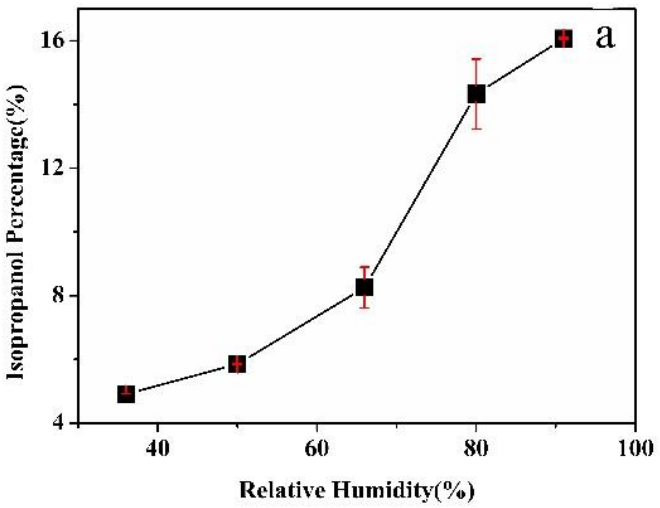

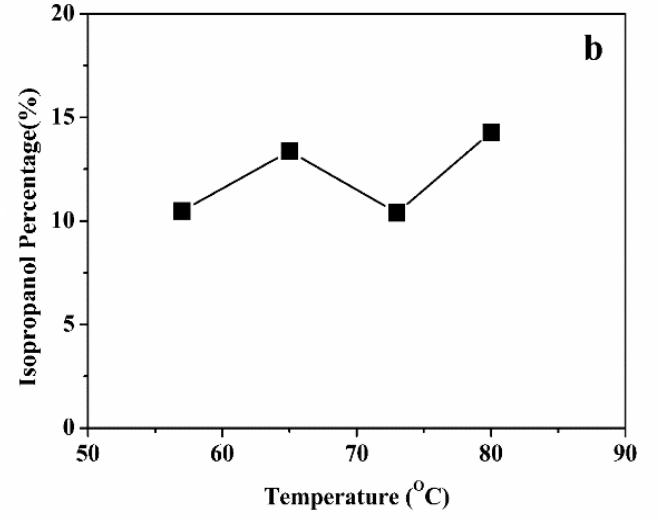

Figure 22. Isopropanol yield (percentage) change as a result of (a) RH and (b) temperatures.
H_2 and acetone flow rates were 0.25 L/min and 6 ml/hr, respectively.
(a) The ECH experiments were conducted for 5 times at 65 °C. Each ECH experiment was repeated twice; (b) The ECH experiments were conducted for 4 times at 80% RH.

Operating temperature is the second factor that was assessed in this study. Generally, the temperature was found to have a slightly positive impact on the product yield. As shown in Figure 22b, the isopropanol yield percentage of products varied between 9.3% and 14.3%, when the temperature increased from 55ºC to 80 ºC. However, the temperature seemed to have minimal effect on the total efficiency.

The results agreed with the findings from the literature. Singh *et al.* [47] investigated ECH of phenol by Pt accordance with increasing temperature. It was believed that dehydrogenated phenol adsorbents easily block the active sites of Pt at higher temperatures. The ECH efficiency was claimed to be directly correlated with the adsorption properties of acetone, hydrogen, and propanol onto the Pt/C catalyst. Murillo and Chen [128] used temperature programmed desorption (TPD) to monitor the desorption and decomposition property of propanol in a wide temperature range on the Pt surface. According to their research, propanol decomposition peaked at 65 ºC and 117 ºC. In the present research, the operating temperature ranged from 55ºC to 80 ºC, between which propanol decomposition could happen at a higher temperature (above 80 ºC). Decomposition of propanol was believed to cause the decrease of its yield. Therefore, increasing the operating temperature in the range does not necessarily result in an increase in the product yield.

Finally, the influence of applied voltage on the product yield was also investigated. Generally, the input voltage has no obvious impact on the product yield. In the experiments, the voltage ranged from 10 mV to 20 mV, with 5 mV increments. At 10 mV and 15 mV, the yield of isopropanol was 15.9% and 17.0%, respectively. Diisopropyl ether was not detected in both cases. However, when the input voltage was increased to 0.02V, the volumetric percentage of isopropanol produced was up to 16% and about 1% diisopropyl ether was detected.

3.3.2 System analysis

Selectivity, H_2 utilization, and current efficiency are selected to evaluate the hydrogenation efficiency. Selectivity represents the yield of desirable products. As the major product, higher isopropanol selectivity was pursued. The selectivity is calculated based on the following equation [54, 60], where acetone unreacted is excluded:

$$Selectivity = \frac{Moles\ of\ Desired\ Product}{Total\ Moles\ of\ Product} \times 100\% \qquad (1)$$

In the present research, H_2 was supplied to the anode to produce protons for ECH reactions on the cathode. Due to gas diffusion resistance, gas crossover, and hydrogen regeneration on the cathode, some H_2 was wasted. The H_2 utilization is directly related to the overall ECH efficiency. Higher H_2 utilization percentage is desired since more hydrogen will be actually involved in the ECH process. The actual amount of H_2 used to produce isopropanol can be derived from the amount of product. The H_2 utilization is calculated by the following equation:

$$H_2\ Utilization = \frac{Atomic\ Hydrogen\ Used\ for\ Faraday\ Current}{Total\ Atomic\ Hydrogen\ Supplied} \times 100\% \qquad (2)$$

During the ECH process, acetone reacts with $M(H)_{ads}$ to produce isopropanol and byproducts on the cathode. Concurrently, H_2 regeneration happens and is an unfavorable process simply because it wastes energy. The H_2 regeneration reaction is affected by supplied voltage, temperature, humidity, and catalyst. Hereby, current efficiency (shown below) is used as an important parameter to determine how efficient H_2 is used for the ECH process [54, 60].

$$Current\ Efficiency = \frac{Current\ used\ for\ the\ ECH\ process}{Total\ Faraday\ current} \times 100\% \qquad (3)$$

The total efficiency is defined by the H_2 utilization multiplying the current efficiency, as shown in the following equation:

$$Total\ Efficiency = H_2\ Utilization \times Current\ Efficiency \quad (4)$$

Figure 23a shows the impact of temperature on H+ utilization, current efficiency, and total efficiency in a typical set of experiments. As the operating temperature increased from 50 ºC to 80 ºC, H+ utilization increased from 1.5% to 6.0%, whereas current efficiency decreased from 28% to 18.5%. Temperature affects H+ utilization and current efficiency differently. Higher ionic mobility and catalytic activities are achieved with higher operating temperatures, resulting in higher H_2 utilization. Consequently, the electrochemical conversion and reaction rates increase with elevated temperatures [72]. However, Figure 4a indicates that although elevated operating temperature enabled more hydrogen being involved in reactions, yet the yield of products did not increase or even decreased. That resulted in a loss of current efficiency, which means most extra protons produced were somehow wasted. The conclusion can also be evidenced by the curve of the total efficiency, which remained almost flat. Note that the total efficiency was low because abundant H_2 was supplied to the system to minimize the impact of fuel starvation and gas diffusion resistance. Practically, stoichiometric flow can be fed to the system based upon the actual current. In their experiments of ECH of acetone, Sara *et al*. observed that the current efficiency increased while the cell temperature increased from 25 ºC to 50 ºC, which seems to contradict our results [72]. However, in the present research, PEMFCs were operated in a recommended range between 50 ºC and 80 ºC to achieve the best performance. The reduction of current efficiency is believed mainly due to propanol decomposition, as mentioned in 3.1. Another minor reason was acetone vaporization, since the boiling point of acetone is 56 ºC.

Acetone gasification might have a negative impact on the hydrogenation reactions on the cathode, due to increased pressure and thus higher diffusion resistance.

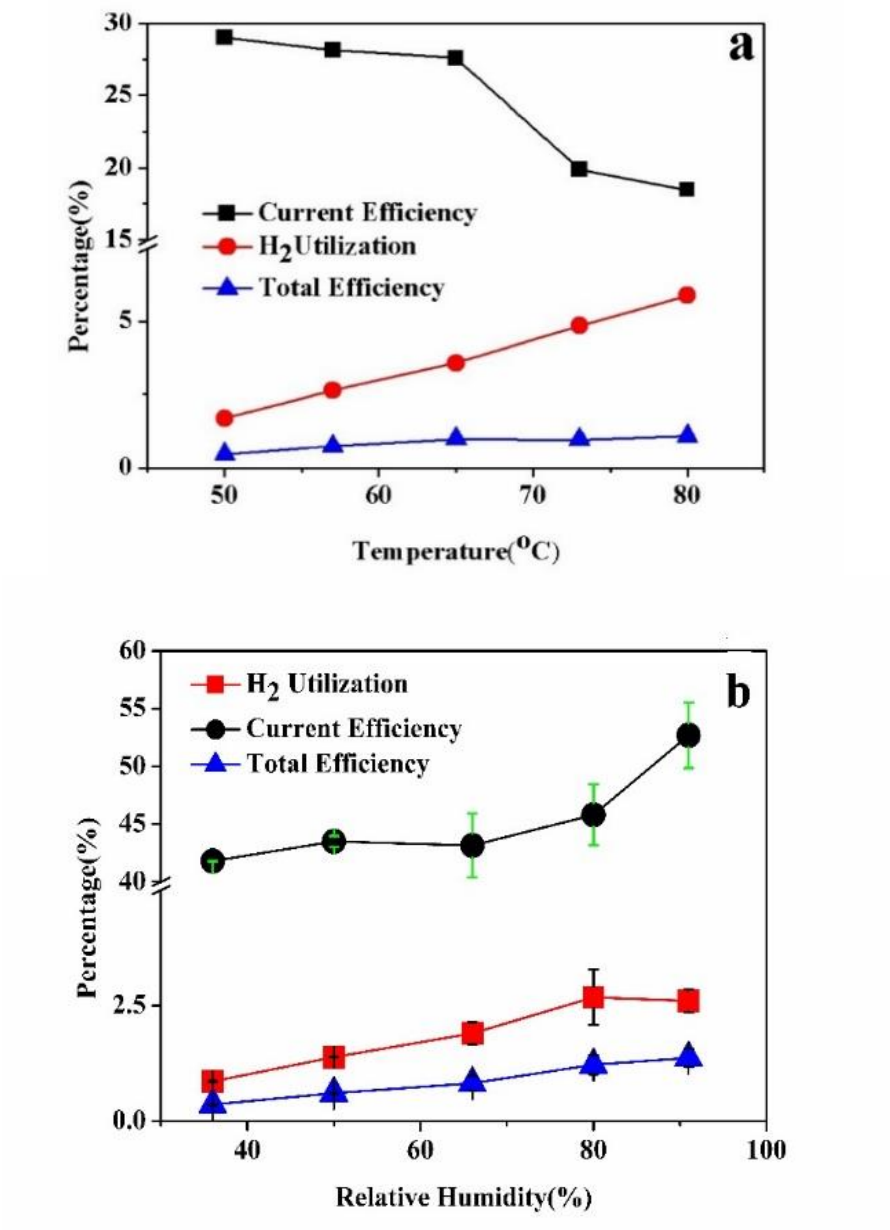

Figure 23. H_2 Utilization, Current Efficiency, and Total efficiency calculated at different (a) temperatures and (b) RH.
H_2 and acetone flow rates were 0.25 L/min and 6 ml/hr, respectively.
(a) The ECH experiments were conducted for 5 times at 80% RH; (b) The ECH experiments were conducted for 5 times at 65 °C. Each ECH experiment was repeated twice.

Figure 23b shows the impact of RH on H_2 utilization, current efficiency, and total efficiency. The operating temperature was set at 65 ºC, and the RH was controlled by setting the humidifier's temperature. It is seen that higher RH resulted in better efficiencies. As the RH ranged from 35% to 90%, the H_2 utilization increased from 0.9% to 2.8%, and the total efficiency increased from 0.4% to 1.5%. A sudden hike of the current efficiency was observed when ramping the RH from 80% up to 91%. It can be concluded that higher RH is favorable for ECH of acetone and will result in a higher yield of products. It has been proved that higher ionic conductivity can be achieved when MEAs become more hydrated [121-123, 129-132]. Practically, high RH is required to maintain the best fuel cell performance. The higher water content in the Nafion membrane will ease proton transport, i.e. less ionic resistance. As a result, more protons can be created and transported to the cathode for ECH. Typically >80% RH is recommended [114-117, 133], which explains that a hike in the current efficiency was observed when the RH surpassed 80%.

The present research shows that the performance of ECH of acetone is correlated with RH, input voltage, and temperature, in which RH has the most obvious effect. It is suggested that the optimized operating conditions are RH of 80% or more, the input voltage of 0.02 V or less, and temperature of between 50 ºC and 55 ºC. The obtained maximum H_2 utilization and maximum current efficiency achieved in the present experiments were 5.9% and 59.7%, respectively. To further increase those efficiencies, stoichiometric flow control is strongly recommended.

3.3.3 MEA degradation

Long-term durability is one important factor that affects the practical applications of ECH using PEMFC reactors. Nowadays, commercial MEAs are fairly durable for their common roles as power sources. The ECH process, however, involves organics that may contaminate MEAs

and thus shorten their lifetime. To our best knowledge, very limited research has been conducted to evaluate the impacts of contaminants on the durability of ECH. In the past decade, extensive research has been carried out on mitigating contamination of PEMFCs from impurities, including CO, CO_2, H_2S, NO_x, SO_x, and hydrocarbons [134, 135]. Impurities may contaminate one or more components of the MEA, resulting in performance degradation. Three major contamination effects were identified as the poisoning of the electrode catalysts, a decrease of the ionic conductivity, and an increase of the mass transfer resistance.

Additionally, the crossover is another factor that negatively impacts the PEMFC performance. Crossover of organic compounds during hydrogenation using PEMFCs has been reported [136, 137]. One immediate drawback is the loss of fuel and/or products, which decreases the efficiency. Furthermore, contaminants not only poison just one electrode but also may crossover and further poison the catalyst on the other electrode [33].

To investigate the impacts of MEA degradation on the present hydrogenation tests, polarization scans (V-I sweeps) were performed after each test [56]. The black curves in Figure 5 were the baseline data recorded for the fresh MEAs prior to ECH tests. After each test, pure N_2 was purged for at least 10 hours to remove all the temporary contaminants. The effects of RH and temperature on the MEA degradation were also evaluated.

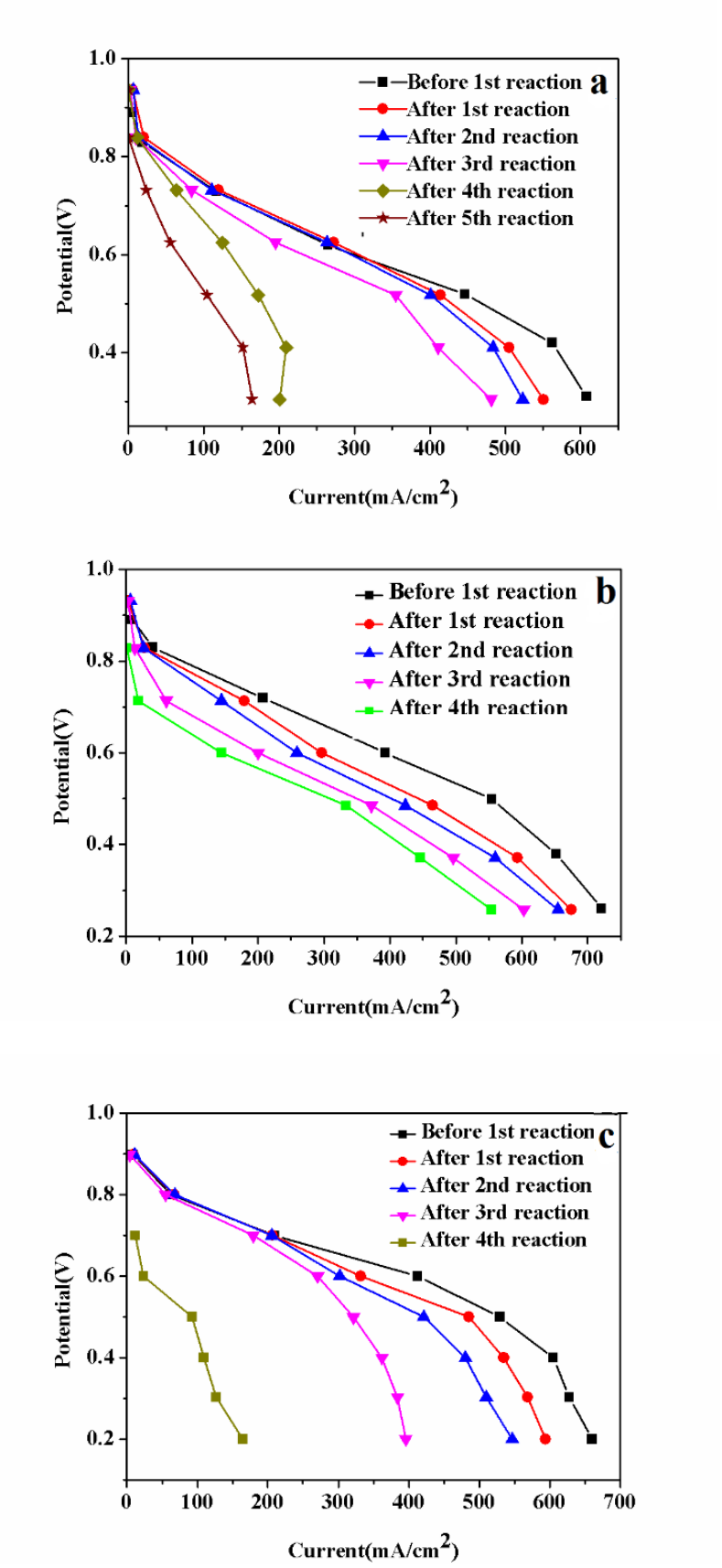
a
Before 1st reaction
After 1st reaction
After 2nd reaction
After 3rd reaction
After 4th reaction
After 5th reaction
Potential(V)
Current(mA/cm2)
b
Before 1st reaction
After 1st reaction
After 2nd reaction
After 3rd reaction
After 4th reaction
Potential(V)
Current(mA/cm2)
c
Before 1st reaction
After 1st reaction
After 2nd reaction
After 3rd reaction
After 4th reaction
Potential(V)
Current(mA/cm2)

Figure 24. V-I scans performed during three sets of ECH experiments.
(a) The ECH experiments were conducted for 5 times at 65 °C and 80% RH; (b) The ECH experiments were conducted for 4 times at 65 °C but different RH. The RH of the four reactions are 65%, 65%, 50%, and 50%, respectively; (c) The ECH experiments were conducted 5 times at 80% RH but different temperatures. The temperature of four reactions are 80 ºC, 73 ºC, 57 ºC, and 50 ºC, respectively; The black curves were the baseline data recorded for the fresh MEAs prior to ECH tests. After each test, pure N_2 was purged for at least 10 hours to remove all the temporary contaminants.

Figure 24a shows the results of five sets of V-I measurements performed on a PEMFC, which underwent five 10-hour long ECH experiments. Both the ECH experiments and V-I measurements shown in Figure 26a were conducted at 65 ºC with 80% RH. It clearly shows that the MEA performance degraded as more ECH tests were conducted, especially after the third ECH experiment. The open circuit voltage (OCV) dropped a lot starting from the 4th V-I scan, which indicates that crossover became significant. It implied that pinholes might form due to degradation.

Figure 24b shows the effect of RH on MEA degradation during ECH. For the ECH experiments conducted in Figure 24b, RH was reduced to 65% for the 1st and 2nd tests and was further reduced to 50% for the 3rd and 4th tests. Note that in order to compare with the same baseline data (the black curve in Figure 24b), all the V-I scans were performed using the same operating conditions that have been used for the baseline scan. The results illustrate that reducing RH was able to mitigate the degradation to some extent. It is believed that less RH resulted in less mass transport via the MEA, which eventually extended the lifetime of the catalysts. However, permanent damage to the MEA still existed, as seen from the general trend of the V-I scan. Similar to what was observed in Figure 24a, purging with pure N_2 could not remove permanent contaminants.

Last but not least, the effect of operating temperature on the MEA degradation was investigated, as shown in Figure 24c. For the ECH experiments conducted in Figure 5c, the operating temperatures were 80 ºC, 73 ºC, 57 ºC, and 50 ºC, while maintaining the same RH.

Again, all the V-I scans were performed using the same operating conditions as those used for the baseline scan (black curve in Figure 24c). The results show that temperature variation has no observable impact on MEA degradation. In other words, changing the operating temperature did not mitigate degradation.

Figure 25 showsthe trends of current efficiency, H_2 utilization, and total efficiency using the same MEA for several ECH experiments. Figure 25 shows that as the MEA degraded, current efficiency, H_2 utilization, and total efficiency all decreased. Until a method of contamination mitigation is found, it is acceptable to use one MEA three times.

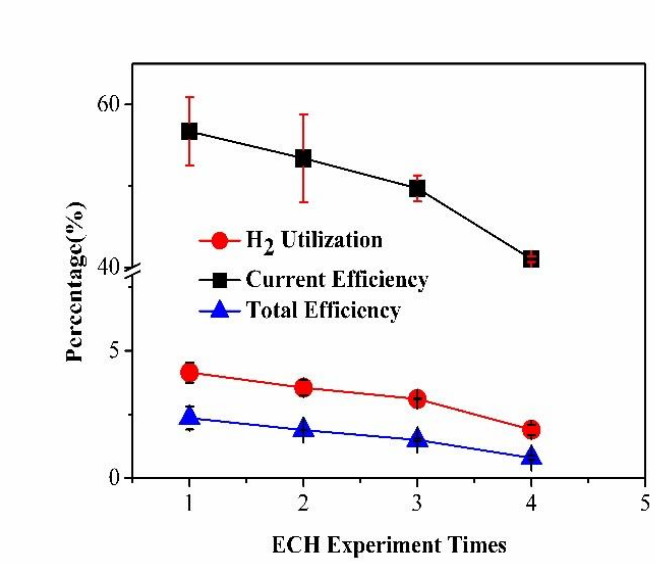

Figure 25. H_2 Utilization, Current Efficiency and Total efficiency as a function of ECH experiment times.
The ECH experiments were conducted for 4 times at 65 °C and 80% RH. H_2 and acetone flow rates were 0.25 L/min and 6 ml/hr, respectively. After each test, pure N_2 was purged for at least 10 hours to remove all the temporary contaminants. Each ECH experiment was repeated twice.

Usually, the lifespan of a PEMFC under steady-state operation can be very long, up to thousands of hours [138-143]. However, catalyst contamination is the major factor that diminishes the PEMFC performance and very likely results in significant degradation [144-146]. In fact, many organic compounds are able to contaminate the MEA. Those compounds include acetaldehyde, toluene, propane, vinyl acetate, methyl methacrylate, acetonitrile,

dichloromethane, acetylene, chlorobenzene, formic acid, methanol, ethanol, phenol, butane, acetone, and naphthalene [147-149], and the list is expanding. The main reason that so many contaminants were found is that the catalysts used in common MEAs are Pt-based. Pt is a premium catalyst, but also sensitive to so many contaminants. The MEAs used in the present research contain pure Pt as the catalyst. Although developing a non-Pt catalyst is beyond the scope of the present research, in order to further conduct durable ECH experiments, MEAs with contamination tolerant catalysts need to be used.

Reactant and product crossing over is another possible reason that caused the MEA degradation. Liquids that contained mainly acetone were detected at the anode side during the ECH experiments. Those liquids not only decrease the fuel utilization but also further contaminate the anode catalyst. Feasible solutions to this issue include adopting thicker MEAs, feeding gaseous feedstock instead of liquid, and using non-Pt catalyst [150].

In summary, to minimize the MEA contamination using the current setup, keeping low RH is suggested. To solve the problem essentially, novel non-Pt catalysts need to be developed, such as Pd and Ni-based catalysts [151, 152]. Despite the fact that a wide range of metals can be used as electrocatalysts at the cathode, those with the strong capability of hydrogen absorption are desired.

3.4 Conclusions

Electrochemical hydrogenation of acetone using a PEMFC reactor was successfully demonstrated in the present research. The results proved that ECH can be a feasible way of hydrogenating acetone to produce isopropanol in mild conditions. In the experiments, the main product obtained was isopropanol with a selectivity of approximately 90%. A small amount (about 1%) of diisopropyl ether was also obtained as a byproduct. The mild operation conditions,

including low temperature and ambient pressure, are the greatest advantages of the proposed ECH method. The present research suggests that the optimized conditions for ECH of acetone using a PEMFC reactor include an operating temperature around 65 ℃ and relative high RH.

Contamination impact using the PEMFC reactor during ECH was also investigated. It was concluded that organic compounds are able to contaminate the MEAs, resulting in serious degradation. However, the methods to mitigate contamination are limited. The present research only demonstrated that lower RH could help reduce contamination. Eventually, novel non-Pt catalysts need to be developed for durable ECH process.

CHAPTER 4

HYDROGENATION OF FURFURAL USING A POLYMER ELECTROLYTE MEMBRANE REACTOR

The electrochemical hydrogenation of biomass-derived compounds in a polymer electrolyte membrane reactor presents a promising method that minimizes energy consumption and chemical waste as compared to conventional methods. In this paper, a Polymer Electrolyte Membrane Fuel Cell (PEMFC) hardware was used as an electrochemical reactor to hydrogenate aqueous solutions of furfural into furfuryl alcohol (FA, 6-15% selectivity), tetrahydrofurfuryl alcohol (THFA, 0-2% selectivity), 2-Methyltetrahydrofuran (MTHF, 12-31% selectivity), 1-Pentanol(10-33%, selectivity), 2-Pentanone(MPK, 1-15% selectivity) and (S)-(+)-2-Pentanol (2-Pentanol, 15-44% selectivity). High current efficiency (85.27%) was achieved. Various operating parameters were evaluated to determine their effects on the yield of products and the overall efficiency of ECH. The results show that an increase in humidity of anode increased the yield of products and H_2 utilization. High current density significantly increased the H_2 utilization while having less effect on the product's yield. Cell temperature between 50 °C and 80 °C had a negative effect on furfural conversion. The degradation of membranes due to contamination of PEMFC and the mitigation methods were also investigated.

4.1 Background

Furfural is a versatile compound in the fragrance industry and is produced from the acid-catalyzed dehydration of xylan contained in lignocellulose. Many different lignocellulosic residues could be used for furfural production, like corncob, sugarcane bagasse, rice husk, olive stones and wheat bran [153, 154].

Furfural is already produced with an amount of more than 200 000 tons per annum from lignocellulosic biomass and is the most common industrial chemical derived from renewable resources[155, 156].

Furfural cannot be used directly as a fuel due to its tendency to polymerize at room temperatures [157]. However, Furfural is believed as one of the platform chemicals which can be used as a starting reagent to produce other high value-added products, like the vapor phase hydrogenation of furfural is commonly used to produce 2-Methyltetrahydrofuran and furfuryl alcohol [158, 159]. Through the hydrogenation and acid– base catalyzed reactions, furfural could be upgraded to biofuels. The complete value chain of furanic biofuels is shown in Figure 26 [160].

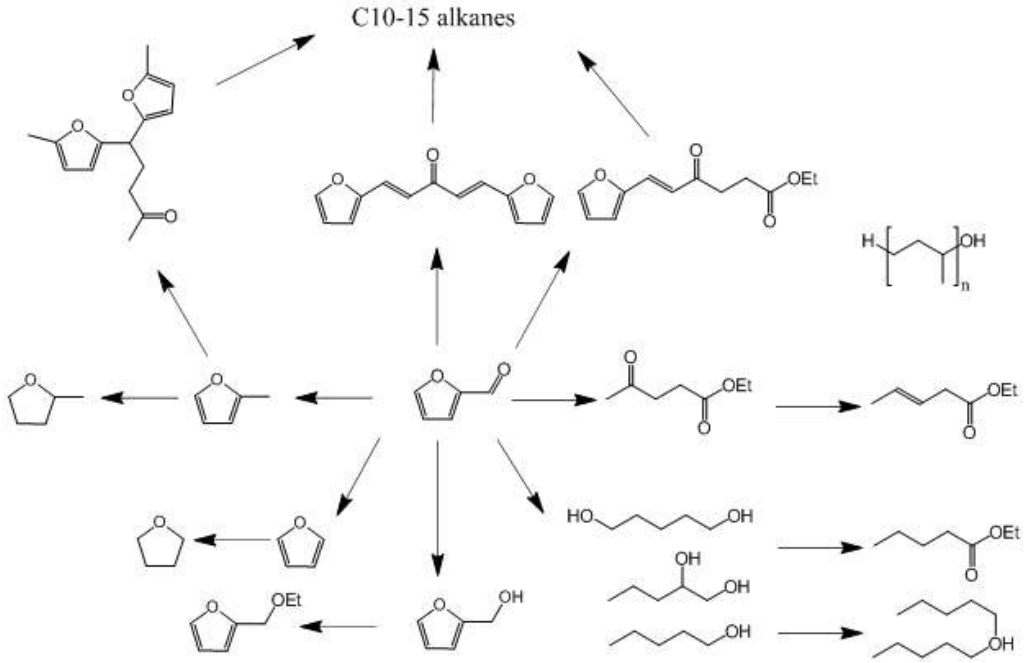

Figure 26. Furfural platform for biofuels

Furfural derivatives are prepared traditionally by the catalytic hydrogenation method. For instance, there are two ways to produce furfuryl alcohol (FA) by hydrogenation of furfural: vapor-phase hydrogenation and liquid-phase hydrogenation. In vapor-phase hydrogenation, the experiment could be carried out atmospheric, while high temperature (170°C -300°C) is required. Depending on the type of catalyst used, hydrogenation of furfural can give, besides furfuryl alcohol, a variety of products such as 2-methylfuran, 2-pentanol, 2-methylretrahyfrofuran(MTHF), 2-pentanone(MPK), 1,5- pentanediol, and tetrahydrofurfuryl alcohol (THFA) [161, 162]. Hydrogenation of furfural in liquid phase requires high pressures (0.1-2MPa) and temperatures (170°C -350°C). Ring-opening products like 1-pentanone, 2-pentanone, 1-pentanol, 1-pentanol, 1,2-pentanediol and 1,5-pentanediol are formed [163, 164]. Catalyst residues are the main drawback of this method [165]. Overall, both processes require intensive energy input and use corrosive chemicals.

Furfuryl alcohol is an important fine chemical for the polymer industry. It is mainly used for the production of dark thermostatic resins resistant to acids, bases and various solvents; liquid resins for galvanic bath-tube, and resins used for strengthening ceramics. It is also widely used as a solvent, e.g. phenolic resins or pigments of low solubility [158, 162, 166-169].

2-methylretrahyfrofuran is an important intermediate in fine chemical industrial practices, which is mainly used for the synthesis of crysanthemate pesticides, perfume intermediates and chloroquine lateral chains in medical intermediates [162, 170, 171]. The potential of 2-methyl furan as biofuels has been corroborated by Langue *et al.* [160]. 2-methyl furan is also used as a gasoline blend[172]. Pentanol can be used as a solvent for coating CDs and DVDs. Pentanol has all the properties necessary to replace gasoline as an internal combustion fuel, and used as fuel blend [173-176].

Electrochemical hydrogenation (ECH) is believed to be a more energy saving and environmentally-friendly method to upgrade organics, by integrating both the catalytic and the electrochemical methods. In this paper, ECH of furfural to produce furfuryl alcohol (FA), tetrahydrofurfuryl alcohol (THFA,), 2-Methyltetrahydrofuran (MTHF), 1-Pentanol, 2-Pentanone (MPK) and (S)-(+)-2-Pentanol (2-Pentanol) was demonstrated using a PEMFC reactor at ambient pressure. 2(3H)-Furanon,5-methyl-(FM) and Gamma-Valerolactone(GV) were also identified in the products, which were probably from the hydrogenation of furfural impurity, 2-Acetylfuran, and 2-Methyl-2-furaldehyde(MF). Various factors that impact the yield of propanol were investigated, including current density, temperature, relative humidity (RH), reaction time and membrane degradation. The main objective of this work was to evaluate the appropriate alternative pathway of furfural hydrogenation to conventional hydrogenation techniques using a PEMFC reactor.

4.2 Material and Method

4.2.1 Material and experimental setup

The experiments were performed using a standard PEMFC hardware (Scribner Associates Inc., USA) with an active area of 25 cm^2. Such standard PEMFC hardware has been widely used for PEMFC evaluation tests [51, 104]. Commercially available MEAs were purchased from Ion Power Inc., USA. The MEAs consist of Nafion® 117 membranes sandwiched with porous carbon-based electrodes, each of which had a Pt loading of 0.3 mg/cm^2. Micro-porous carbon papers (SIGRACET® 10BC) were trimmed and used as gas diffusion layers (GDLs) for both electrodes. Teflon gaskets were used to seal around the assembly. A pair of graphite bipolar plates with flow patterns was used to distribute flows and enclose the assembly. All the temperatures were acquired via K-type thermocouples (OMEGA, USA). A fuel cell test station (850e, Scribner Associates Inc., USA) was used to control temperatures, flow rates, and humidity. It was also used for data acquisition.

Ultra-high purity (99.999%) N_2 (Airgas, USA), and filtered shop air were connected to the fuel cell test station and supplied to the PEMFC through the purge line. They were used for purging the system and making current and voltage curve, respectively, and were cut off while the ECH experiment was running. The ultra-high purity (99.999%) H_2 (Airgas, USA) and Deionized (DI) water tanks were purged through the anode side of the reactor, using the fuel cell test station. H_2 was the electrons donator and deionized (DI) water tank was used for adding humidity to H_2. Furfural (98+%, Fisher Scientific, Acros Organics, USA) was injected into the cathode side of the reactor by a syringe pump (MTI Corporation, EQ-300sp-LD). A direct current (DC) power supply (Tektronix, PWS 4205) was used to supply DC power for ECH. The positive probe was connected to the anode, while the negative probe was connected to the

cathode. While ECH was running, electrons were deprived of H_2 and transferred to the cathode through the DC power supply. Furfural was the electron acceptor and reacted with the produced protons. The products from the cathode outlet were collected by airbags (Tedlar®), which were held by the water bath. Room temperature water bath was used for condensing the unreacted furfural and products. The cell temperature was controlled by the fuel cell test station. The exhaust gases and byproducts from the anode were condensed in a knock-out bottle prior to venting out. The schematic diagram of the whole experimental setup is shown in Figure 27.

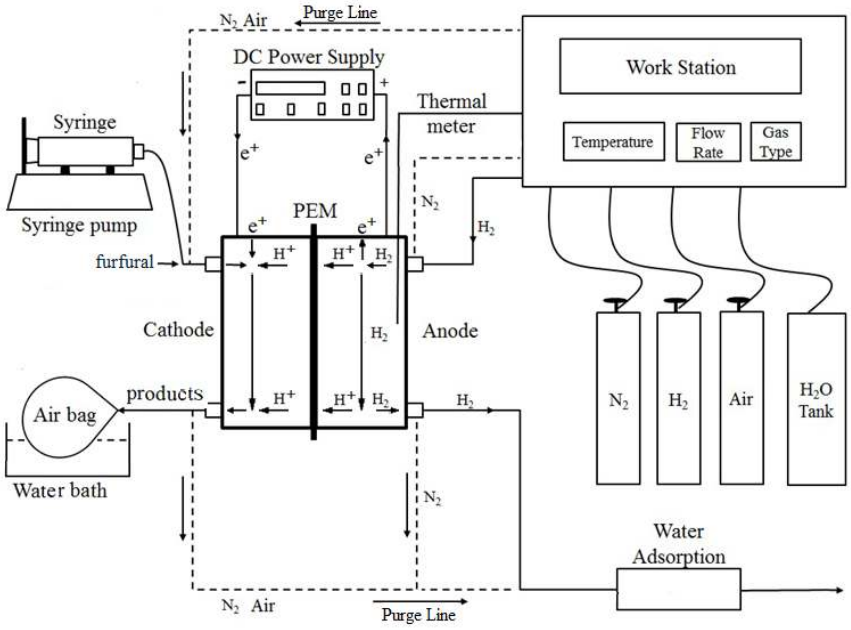

Figure 27. Schematic diagram of the experimental setup.

4.2.2 Experimental characterization

All the PEMFCs were assembled in accordance with the standard assembly procedure of fuel cell hardware [56]. Prior to each ECH experiment, a new membrane was conditioned based on the standard protocol [56] for at least 24 hours, until it reached a fully functional state.

Current-voltage (I-V) sweeps were performed to establish the baseline data for the following ECH experiments.

In each ECH experiment, the 5% furfural solution and H_2 flow rates were controlled at 12 ml/hr and 0.15 slpm or 0.25 slpm, respectively. The voltage was consistent for each reaction; the current was recorded every one minute. Four different factors, including cell temperature, RH, current density, reaction time and membrane degradation, were investigated to identify the optimized operating conditions. The operating conditions were in the range of 55 °C to 80 °C, 40 % to 100 %, 20mA/cm^2 to 200mA/cm^2 and 60 minutes to 220 minutes, respectively. I-V scans were conducted before and after ECH to characterize the membrane degradation.

After each experiment, the system was washed by water and air for 24 hours, respectively. A 5% HCl solution also was tested to wash the system. Products were collected by airbags with pressure relief valves. The airbag was immersed into room temperature water bath. The pressure differential of two electrodes can be controlled by airbags confined extent. Green *et al*. proved that a suitable pressure differential between the anode and cathode could decrease cross-over and increase conversion [72]. Dadda *et al*. believed that water transport in the membrane of a PEMFC is influenced by a convective force, resulting from a pressure gradient [106]. Many researchers also point out the importance of the flow pressure [107].

The product volume and weight were recorded after the reaction. The collected samples were extracted by 3 to 5 ml methylene dichloride (DCM). The extracted samples were quantitatively and qualitatively analyzed by a gas chromatography-mass spectroscopy (Shimadzu, GC-MS-QP2010 SE), using a (Restek, Rxi-1ms) MS column (length: 30 m, inner diameter: 0.25 mm). Helium was used as a carrier gas for gas chromatography. The standard curves of products were made by GC-MS using MTHF (99+%, Fisher Scientific, Fisher

Scientific, Acros Organics, USA), 2-Acetyluran (99%, Fisher Scientific, Acros Organics, USA), MPK(99+%, Fisher Scientific, Acros Organics, USA), FA(98%, Sigma Aldrich, Alfa Aesar, USA), 1-pentanol(99+%, Fisher Scientific, Acros Organics, USA), GV(98+%, Sigma Aldrich, Alfa Aesar, USA), (s)-(+)-2-pentanol(97+%, Fisher Scientific, Acros Organics, USA), THFA(99+%, Fisher Scientific, Acros Organics, USA), MF(98+%, Fisher Scientific, Acros Organics, USA) and FM(98%, Sigma Aldrich, Alfa Aesar, USA).

The flow chart of the ECH experimental operation is shown in Figure 28.

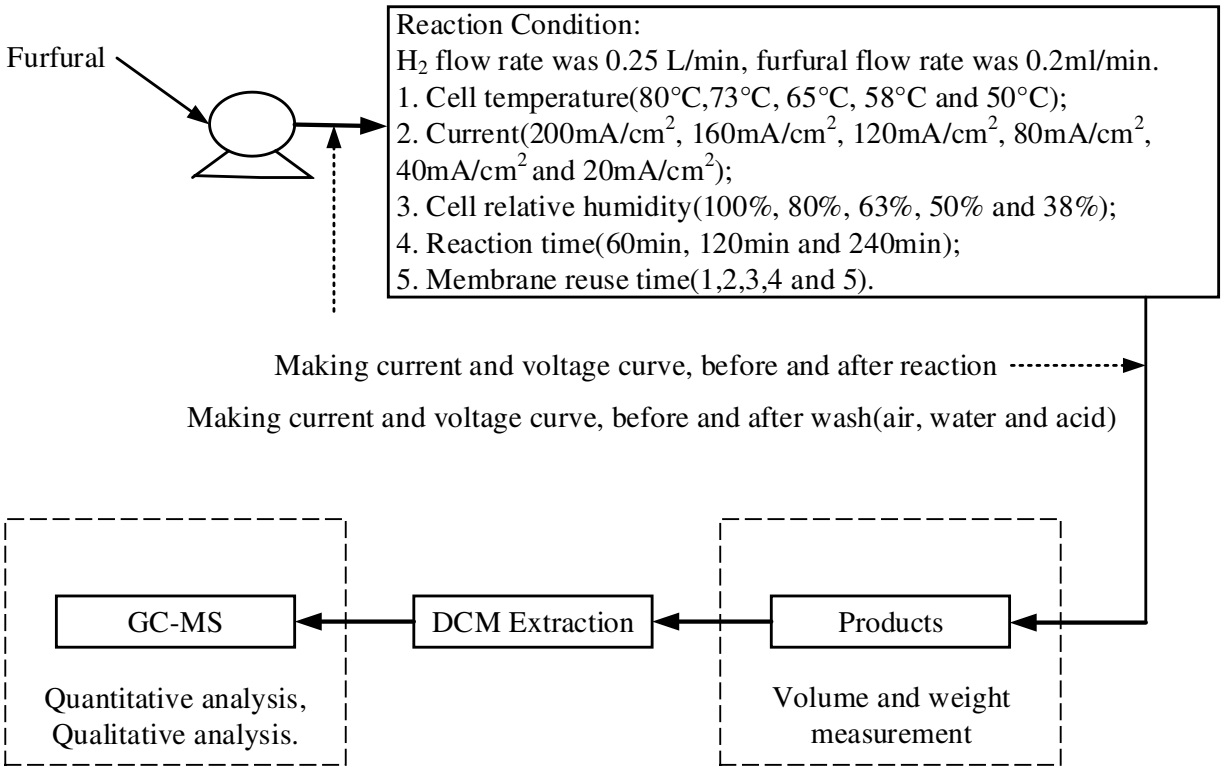

Figure 28. Flowchart of the experiment.

4.3 Results and Discussion

4.3.1 Product characterization

Both furfural and the liquid products were analyzed by GC-MS. Two impurities of 5-Methyl-2-furaldehyde (MF, $C_6H_6O_2$) and 2-Acetylfuran ($C_6H_6O_2$) were detected in the initial

furfural sample. Except furfural and the impurities, eight products of furfuryl alcohol (FA, $C_5H_6O_2$, 6%-15% selectivity), tetrahydrofurfuryl alcohol (THFA, $C_5H_{10}O_2$, 0%-2% selectivity), 2-Methyltetrahydrofuran (MTHF, $C_5H_{10}O_2$, 12%-31% selectivity), 1-Pentanol($C_5H_{12}O$, 10%-33%, selectivity), 2-Pentanone(MPK, $C_5H_{10}O$, 1%-15% selectivity), (S)-(+)-2-Pentanol (2-Pentanol, $C_5H_{12}O$, 15%-44% selectivity), 2(3H)-Furanon,5-methyl-(FM, $C_5H_6O_2$, 0%-2% selectivity) and Gamma-Valerolactone (GV, $C_5H_8O_2$, 0%-3% selectivity) were found in the liquid.

The reactions on both electrodes were catalyzed by Pt. while applying a DC voltage protons formed at the anode were electrochemically pumped to the cathode. The protons then reacted with furfural to produce products. The most feasible reaction pathways at the cathode are shown in Figure 29.

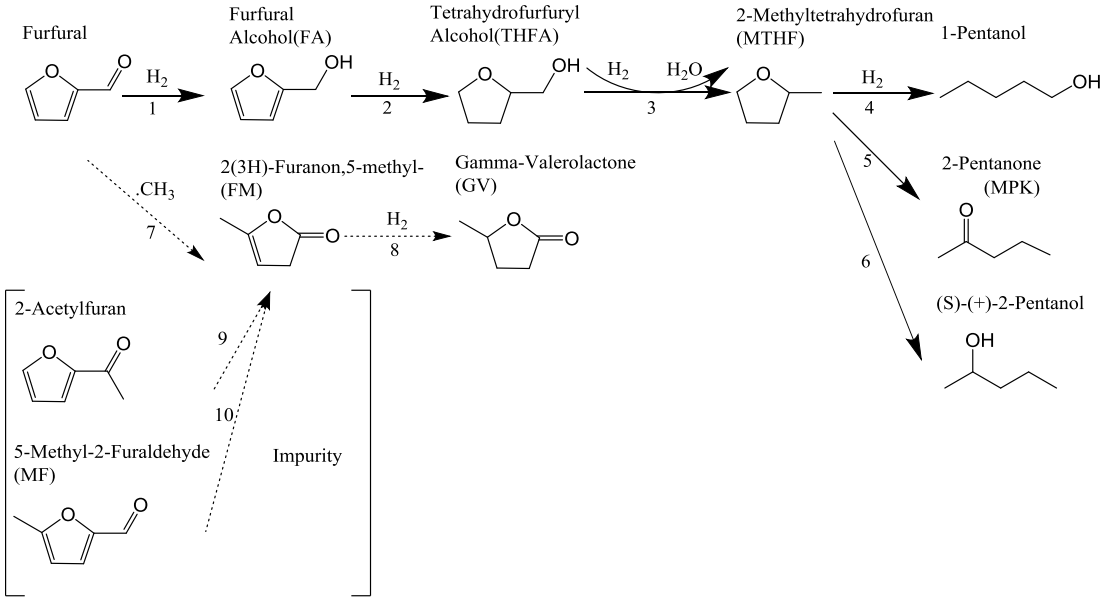

Figure 29. Furfural hydrogenation pathway

Electrosorbed hydrogen (H_{ads}) was formed on Pt surface by reduction of H^+, and then H_{ads} reacts with furfural and intermediate products. The first reaction was the hydrogenation of the

furfural C=O bond with the product of FA (Rea.1), then the FA C=C bond was hydrogenated with the corresponding saturated chemicals THFA generation (Rea.2). THFA converted to MTHF through dehydration reaction (Rea.3). The carbon ring-opening of MTHF was the ultimate hydrogenation process, and the final products are 1-pentanol, 2-pentanol, and 2-pentanone (Rea 4, 5, 6). Although FM and GV are detected in products, they cannot be confirmed as furfural hydrogenation products (Rea 7, 8). The most possible source of them was furfural impurity hydrogenation (Rea 9, 10). The reason will be explained in the following chapters.

According to the various product concentrations (Figure 30), 2-pentanol, 1-pentanol, and MTHF were the main products, others are by-products. The yield of products is determined by the catalyst type. Green *et al*. reported that the Pt/C catalyst has a higher electrochemically active surface area and lower overpotential than Pd/C. Furfural hydrogenation over Pd/C could produce four products of FA, THFA, MF, and MTHF, compared to the only product of FA by Pt/C [58]. Platinum has long been known as a furfural hydrogenation catalyst [158, 177, 178] and favors the side and consecutive reactions such as hydrogenolysis of the C-O bond and ring-opening [179]. In this paper, Pt was used as the catalyst for all the experiments.

The electrocatalytic hydrogenation of aqueous solutions of 5 wt% furfural in a continuous PEMFC reactor was investigated, as shown in Figure 30. Three different control parameters, including RH, temperature and current density were assessed to identify the optimized operating conditions for ECH furfural. All the operating parameters used in the experiments are shown in Table 11 (seen in the appendices).

RH is a very important parameter that affects the performance of PEMFCs [107, 109-113]. Figure 30a shows a typical impact of RH on the product yield during ECH of furfural. It was

obviously evidenced that higher humidity slightly promoted the yield of 2-pentanol (100 ppm to 150 ppm), 1-pentanol (55 ppm to 110 ppm), FM (4 ppm to 23 ppm) and MTHF (83 ppm to 115 ppm), while FA, GV, MPK, and THFA concentration were constant or slightly descended. Compared to C=O and C=C hydrogenation, the higher temperature contributed more to the ring-opening reaction, since the selectively of ring-opening product 1-pentanol increased from 16% to 24% with the RH increasing from 40% to 100%. The reason why humidity had such an impact is that the MEA usually uses a perfluorosulfonic acid membrane (e.g. Nafion®) as the electrolyte. A high or nearly saturated humidity (RH >80%) is usually required to obtain practical performance because the conductivity of perfluorosulfonic acid membrane membranes depends on the water content. Higher humidity means higher conductivity, resulting in better performance [114-117]. Water management is critical for PEMFC operation. Sufficient water must be absorbed into the membrane to ionize the acid groups, whereas excess water can cause flooding issues and thus diminish the performance [72]. The inlet RH of the electrodes must be controlled to prevent both membrane drying out and electrode flooding. Although better performance is usually obtained by increasing RH, excess moisture may result in water flooding that hinders gas transport [118]. In the present experiments, cathode side water was from furfural solution, while anode water was supplied by RH and cathode water crossing over. RH selection should be determined by target products and reaction time. According to Figure 5a, if the preferred product was FA, less than 50% RH should be selected. Correspondingly, more than 80% RH could favor the yield of preferred product 2-pentanol and 1-pentanol. The amount of crossing over water was easily accumulated, with the extension of reaction time. To prevent either water starvation or over saturation, RH could be adjusted with time.

Nowadays, the mechanism of humidity influence has been investigated by many researchers. It is generally believed that RH can impact electro-osmotic drag, water diffusion, membrane ionic conductivity, and water back diffusion flux in the MEAs, which consequently influence the performance [119, 120]. Elevated RH can greatly improve the PEMFC performance, through increasing the membrane conductivity [121, 122], the catalyst activities [121, 123], the electrode kinetics [124, 125], and the mass transfer rates [126, 127].

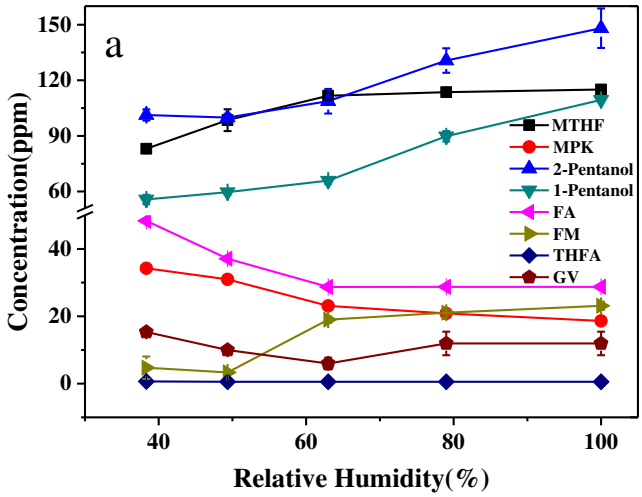

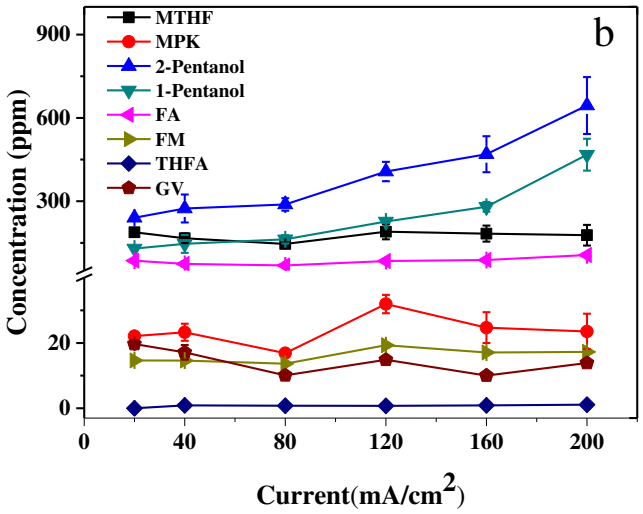

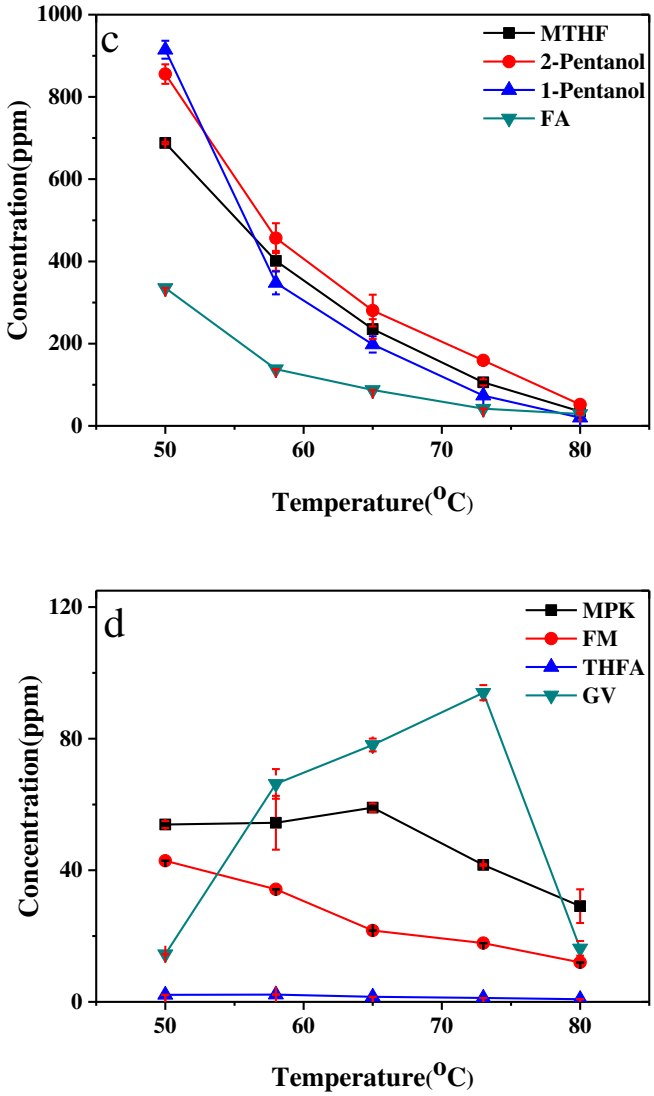

Figure 30. Products change as a result of (a) current, (b) RH and (c) (d) temperatures.
H_2 and furfural solution flow rates were 0.25 L/min and 12 ml/hr, respectively. Products concentration were identified three times. (a) The current ECH experiments were conducted for 6 times at 65 °C; (b) The ECH experiments were conducted for 5 times at 65 °C and 80% RH; (c) (d) The ECH experiments were conducted for 5 times at 80% RH.

Operating current density was the second factor assessed in this study. Figure 30b shows the influence of current density on the product yield during ECH of furfural. The concentrations for all the main products of 2-pentanol, 1-pentanol, FA and MTHF were more than 200ppm. Correspondingly, the by-product's concentration was less than 30ppm. Therefore, the yield of the main products was maximized. It is also proved that an increase of current density had an

obviously positive influence on the yield of 2-pentanol (240ppm to 644ppm) and 1-pentanol (130ppm to 468ppm), while other products' concentrations were almost constant. At the maximum current density of 200mA/cm^2, 2-pentanol and 1-pentanol achieved their maximum selectivity, 44%, and 32%, respectively. In temperature and RH experiments, the cell current density changed with time by fixing voltage at 0.02V. Different from them, the current density was constant in this set, while the input voltage changed with time (Figure 31). In these experiments, the operating temperature, RH, H_2 flow rates and furfural solution flow rates were set at 80%, 65 ℃, 0.25 L/min and 12 ml/hr. Figure 31 shows the input voltage was determined by the required current density. 0.05V to 0.27V voltage was required to maintain 200mA/cm^2 (black line), while the voltage number decreased to 0.01 with 20mA/cm^2 current density (green line). In addition, due to the decrease of PEMFC membrane performance, the input voltage was elevated with the extension of reaction time. Green *et al*. found that higher applied voltage was favorable for current density elevation and also demonstrated that the input voltage significantly impacted on the type of products, due to the difference of standard cell potentials required by each reaction, such as THFA was only present at a power input of 0.3 W [58]. This experiment proved that when the input voltage was below 0.27V, the yield of products is impacted by current density, rather than determined by the input voltage.

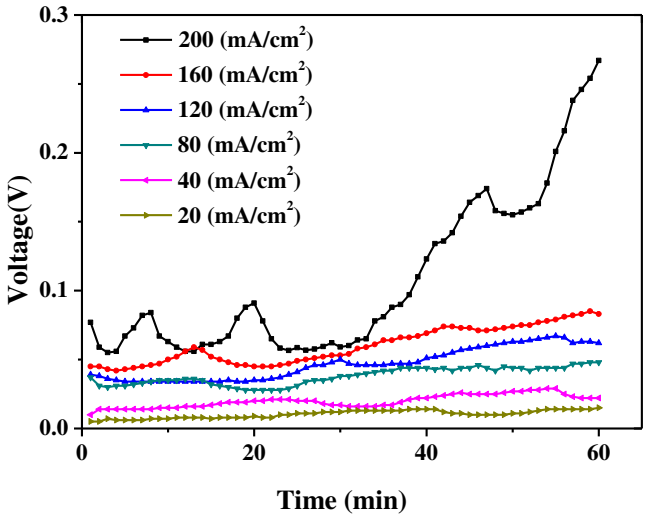

Figure 31. The change of voltage with time at different currents.

Operating temperature was another factor assessed in this study andis shown in Figure 30c and 30d. Generally, the temperature was found to have a significantly negative impact on the yield of MTHF, FA, 2-pentanol, and 1-pentanol, while a slightly negative influence on MPK, THFA, and MF was also evidenced. The only exception was GV, for which the maximum concentration appeared at 73 ℃. The maximum decrease was from 1-pentanol, whose concentration declined from 920 ppm to 20 ppm when the temperature increased from 55℃ to 80 ℃. At 80 ℃, meanwhile, 1-pentanol reached the minimized selectivity of 26%. Therefore, the optimized temperature seemed to be room temperature. The results agreed with some findings from the literature. Singh *et al*. [47] investigated the ECH of phenol by Pt accordance with increasing temperature. It was believed that dehydrogenated phenol adsorbents easily block the active sites of Pt at higher temperatures. Li *et al.* investigated ECH of bio-oil and the results show that the electrochemical efficiency for guaiacol reduction decreased from 17% at 50 °C to 10% at 80 °C [66]. Green et al. investigated the ECH of furfural by Pt/C catalyst with increasing temperature. The results indicate that the increase in temperature promotes water electrolysis of

hydrogen gas but not furfural hydrogenation [58]. Room temperature ECH was also recommended by many researchers [34, 50, 51, 57, 58].

In sum, room temperature, high current density, and high RH are recommended to optimize the yield of products, especially for ring-opening products.

4.3.2 System analysis

Selectivity, H_2 utilization, and current efficiency are selected to evaluate the hydrogenation efficiency. Selectivity represents the yield of products. The selectivity is calculated based on the following equation [54, 60], where furfural unreacted is excluded:

$$Selectivity = \frac{Moles\ of\ Desired\ Product}{Total\ Moles\ of\ Product} \times 100\% \qquad (1)$$

In the present research, H_2 was supplied to the anode to produce protons for ECH reactions on the cathode. Due to gas diffusion resistance, gas crossover, and hydrogen regeneration on the cathode, some H_2 was wasted. The H_2 utilization is directly related to the overall ECH efficiency. Higher H_2 utilization percentage is desired since more hydrogen will be actually involved in the ECH process. The actual amount of H_2 used to produce products can be derived from the amount of product. The H_2 utilization is calculated by the following equation:

$$H_2\ Utilization = \frac{Atomic\ Hydrogen\ Used\ for\ Faraday\ Current}{Total\ Atomic\ Hydrogen\ Supplied} \times 100\% \qquad (2)$$

During the ECH process, furfural reacts with $M(H)_{ads}$ on the cathode. Concurrently, H_2 regeneration happens and is an unfavorable process simply because it wastes energy. The H_2 regeneration reaction is affected by current density, temperature, humidity, and catalyst. Hereby, current efficiency (shown below) is used as an important parameter to determine how efficient H_2 is used for the ECH process [54, 60].

$$Current\ Efficiency = \frac{Current\ used\ for\ the\ ECH\ process}{Total\ Faraday\ current} \times 100\% \qquad (3)$$

The total efficiency is defined by the H_2 utilization multiplying the current efficiency, as shown in the following equation:

$$Total\ Efficiency = H_2\ Utilization \times Current\ Efficiency \qquad (4)$$

Figure 32a shows the impact of temperature on H_2 utilization, current efficiency, and total efficiency in a typical set of experiments. As the operating temperature decreased from 50 ºC to 80 ºC, H_2 utilization decreased from 3.3% to 1.1%, current efficiency decreased from 11.7% to 2.5%. Temperature negatively affected H_2 utilization and current efficiency. Figure 32a indicates that with elevated operating temperature, less hydrogen being involved in reactions and more current electrons wasted. Note that the total efficiency was low because abundant H_2 was supplied to the system to minimize the impact of fuel starvation and gas diffusion resistance. Practically stoichiometric flow can be fed to the system based upon the actual current. It used to believe that higher ionic mobility and catalytic activities are achieved with elevated operating temperatures, resulting in higher H_2 utilization, better current efficiency, more electrochemical conversion, and faster reaction rates [42, 43, 180]. Actually, the temperature influence on ECH reaction is controversial. It is claimed to be correlated with properties of reactants. Singh *et al*. believed that dehydrogenated phenol adsorbents easily block the active sites of Pt at higher temperatures, according to his ECH of phenol result[47]. Green *et al.* electrocatalytically hydrogenated acetone and furfural in the same proton-exchange-membrane (PEM) reactor at the same catalysts. The results demonstrated the different influence of temperature on ECH efficiency. The acetone conversion, reaction rate, and current efficiency increased with

increasing temperature. However, the ECH furfural results indicated that the increase in temperature cannot improve furfural hydrogenation [58, 72].

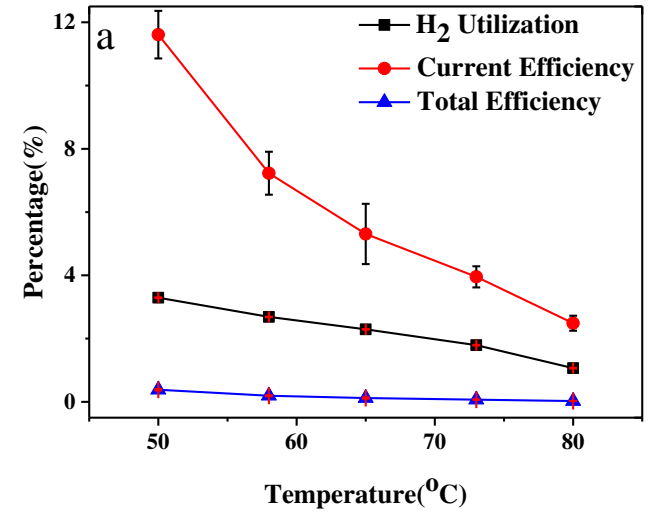

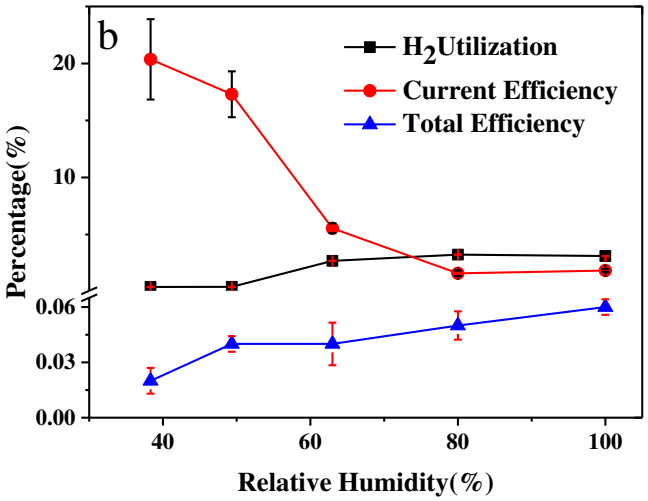

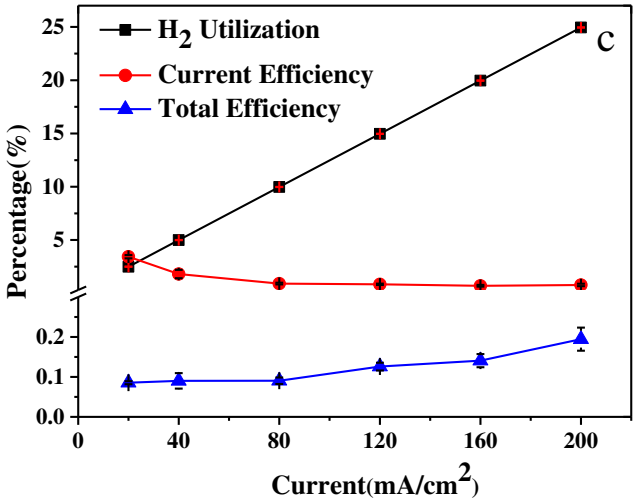

Figure 32. H_2 Utilization, Current Efficiency, and Total efficiency calculated at different (a) temperatures, (b) RH and (c) Current.
H_2 and furfural flow rates were 0.25 L/min and 12 ml/hr, respectively. Products concentrations were identified three times. (a) The ECH experiments were conducted for 5 times at 80% RH; (b) The ECH experiments were conducted for 5 times at 65 °C; (c) The current ECH experiments were conducted for 6 times at 65 °C and 80% RH.

Figure 32b shows the influence of RH on H_2 utilization, current efficiency, and total efficiency. The operating temperature was set at 65 ℃, and the RH was controlled by setting the humidifier's temperature. It was seen that higher RH resulted in worse current efficiencies and better H_2 utilization. As the RH ranged from 40% to 100%, the H_2 utilization increased from 0.4% to 3.1%, and the current efficiency decreased from 20% to 1.9%. A sudden descent of current efficiency from 17.3% to 5.6% was observed when ramping the RH from 50% up to 63%; meanwhile, the H_2 utilization hiked slightly. In this experiment, anode water was supplied by RH and cathode water crossing over. It has been proved that higher ionic conductivity can be achieved when MEAs become more hydrated [121-123, 129-132]. With the ionic conductivity increasing, it is favorable for anode H_2 to protonate and generate current electrons, which is expressed as the increase of H_2 utilization. After sufficient hydration of MEAs, elevating RH cannot improve H_2 utilization, which was shown in the range of RH 63% to 100%. Different

from the anode side, sufficient water was supplied to cathode side by furfural solution. Therefore, the change of RH cannot bring directly impact on cathode reaction. It was also demonstrated that higher RH resulted in a slightly higher yield of products, which was shown in Figure 30a. This phenomenon of H_2 utilization and products increasing with current efficiency decreasing in the same time was due to higher RH generating more current electrons, but the increased current elections were only partially utilized by cathode side organics. With the HR increasing, total efficiency was improved significantly, which increased from 0.02% to 0.06%. Practically, high RH is required to maintain the best fuel cell performance. The higher water content in the Nafion membrane will ease proton transport, i.e. less ionic resistance. As a result, more protons can be created and transported to the cathode for ECH. Typically >80% RH is recommended by many researchers [114-117, 133]. Accordingly, although the current efficiency is not optimized, >80% RH is still suggested.

Figure 32c shows the influence of current density on H_2 utilization, current efficiency, and total efficiency. The operating temperature and RH were set at 65 ℃ and 80%, the current density was constant and controlled by current (DC) power supply. The changing trend of input voltage with reaction time was shown in Figure 31. It has been seen that the higher current density required a higher input voltage to maintain. In Figure 32c, H_2 utilization was proportional to the fixed current and achieved the top 25% at 200 mA/cm^2, which was the maximum affordable current of the PEMFC system. The current efficiency was significantly descended at the current density between 20 mA/cm^2 and 40 mA/cm^2 and then maintained at 0.9%. Higher current density means more electrons were deprived from H_2, which corresponded to H_2 utilization elevation. However, not all the increasing electrons could be utilized by organics, which resulted in the stagnant or even decreasing current efficiency. Because total efficiency

significantly increased from 0.08% to 0.19% over the range of 20 mA/cm^2 to 200 mA/cm^2, high current density is commended with ignoring the operation lifetime of the reactor. Some researchers reported the influence of current density on furfural electrochemical hydrogenation. Niles *et al.* investigated the electrochemical conversion of furfural to 2-methylfuran and of 5-hydroxymethylfurfural to 2,5-dimethylfuran. It indicated that the furfural conversion rate corresponded to the current density and suggested increasing the electrode surface area to improve current efficiency [59]. Green *et al*. used a continuous-flow electrocatalytic membrane reactor for the reduction of aqueous solutions of furfural into furfuryl alcohol, tetrahydrofurfuryl alcohol, 2-methylfuran, and 2-methyl tetrahydrofuran and found that higher applied voltage was favorable for current density elevation [58]. Li *et al*. studied electrocatalytic hydrogenation of furfural to furfuryl alcohol and 2-methylfuran. It indicated that the current density also strongly affected the product yield and electrochemical efficiency [54].

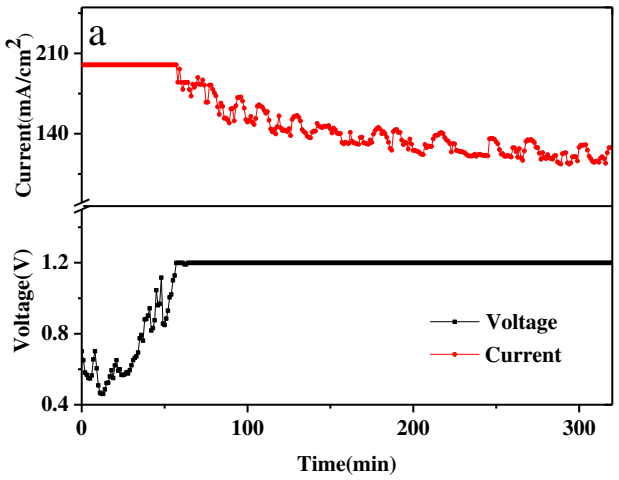
a
Current(mA/cm2)
210
140
Voltage(V)
1.2
0.8
0.4
Voltage
Current
0
100
200
300
Time(min)

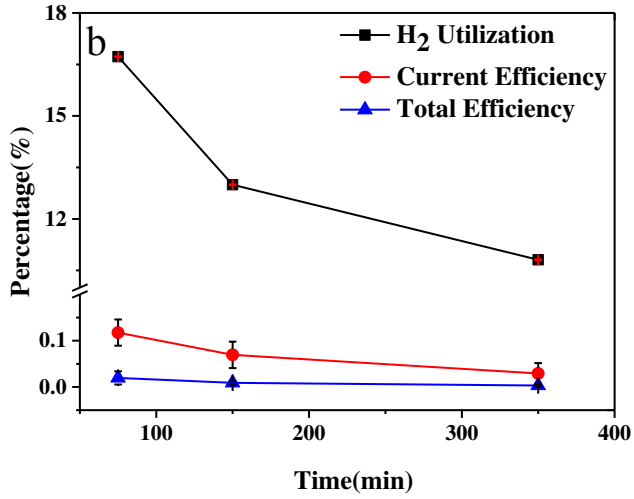
b
H2 Utilization
Current Efficiency
Total Efficiency
Percentage(%)
18
15
12
0.1
0.0
100
200
300
400
Time(min)

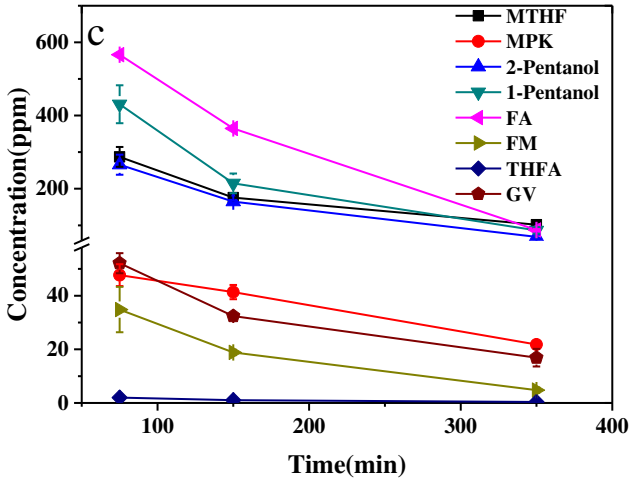
c
MTHF
MPK
2-Pentanol
1-Pentanol
FA
FM
THFA
GV
Concentration(ppm)
600
400
200
40
20
0
100
200
300
400
Time(min)

Figure 33. The change of voltage and current with time(a), the comparison of products(c), H_2 utilization (b), current efficiency (b), and total efficiency (b) between different voltage and current.
A constant current was 180 mA/cm^2, at first 60min. A constant current was 1.2V, at between 60min to 350min. Product was collected time times, at 60min, 150min, and 350min, and then were identified three times. The ECH experiments were conducted at 65 °C, 80% RH, 12 ml/hr furfural flow rates and 0.15 L/min H_2 flow rate.

The comparison between the current fixed ECH method and input voltage fixed method was investigated, and the result was shown in Figure 33. The experiment was conducted at 65 °C, 80% RH, 12 ml/hr furfural flow rates and 0.15 L/min H_2 flow rate. Products were collected at 60 minutes, 120 minutes, and 350 minutes. At the first hour, to keep current density constant at 200 mA/cm^2, which was the maximum affordable current density of the system, the voltage was elevated from 0.5V to 1.2.V. between 60 minutes and 350 minutes, the current density cannot be maintained at 180 mA/cm^2, though voltage was still 1.2V. This trend was shown in Figure 8a. It indicated that due to the degradation of MEAs with time, which will be discussed in the next chapter, high current density maintenance required more input voltage, in another words, more energy. It is corresponding to Figure 6. similar phenomenon was observed by other researchers [60]. As shown in Figure 33b and 33c, all the parameters including product concentration, H_2 utilization, current efficiency, and total efficiency behaved much better in the first hour than at any other time periods. The results from Figure 30b were reconfirmed by the data in Figure 33c, which demonstrated that high current results in better product yield. No new products were detected even when the input voltage was increased up to 1.2 V. Accordingly, the current fixed ECH method is recommended.

In summary, the present research shows that the performance of ECH of furfural is correlated with RH, input current density, and temperature. Specifically, temperature and input current density have a more obvious effect than the rest of the parameters. The obtained maximum H_2 utilization and maximum current efficiency achieved in the present experiments was 25% and 21%, respectively. It is suggested that the optimized operating conditions are RH

of 80% or more, the input current of 200 mA/cm^2 or more, and room temperature. To further increase those efficiencies, stoichiometric flow control is strongly suggested.

4.3.3. MEA degradation

Long-term durability is one important factor that affects the practical applications of ECH using PEMFC reactors. Nowadays, commercial MEAs are fairly durable for their common roles as power sources. The ECH process, however, involves organics that may contaminate MEAs and thus shorten their lifetime. To our best knowledge, very limited research has been conducted to evaluate the impacts of contaminants on the durability of ECH. In the past decade, extensive research has been carried out on mitigating contamination of PEMFCs from impurities, including CO, CO_2, H_2S, NO_x, SO_x, and hydrocarbons [134, 135]. Impurities may contaminate one or more components of the MEA, resulting in performance degradation. Three major contamination effects were identified as the poisoning of the electrode catalysts, a decrease of the ionic conductivity, and an increase of the mass transfer resistance.

Additionally, the crossover is another factor that negatively impacts the PEMFC performance. Crossover of organic compounds during hydrogenation using PEMFCs has been reported [136, 137]. One immediate drawback is the loss of fuel and/or products, which decreases efficiency. Furthermore, contaminants not only poison just one electrode but also may crossover and further poison the catalyst on the other electrode [33].

To investigate the impacts of MEA degradation on the present hydrogenation tests, polarization scans (V-I sweeps) were performed after each test [56], which is shown in Figure 34. The black curves in Figure 34a, 34b-1 and 34c-1 were the baseline data recorded for the fresh MEAs prior to ECH tests. Figure 34b-2 and 34c-2 were the current VS time curve of the tests, corresponding to the reaction mentioned in Figure 34b and 34c. After each test, pure N_2 and

water were purged for at least 24 hours to remove all the temporary contaminants. An HCl solution was also tested in the experiment. The effects of RH, temperature and time on the MEA degradation were also evaluated.

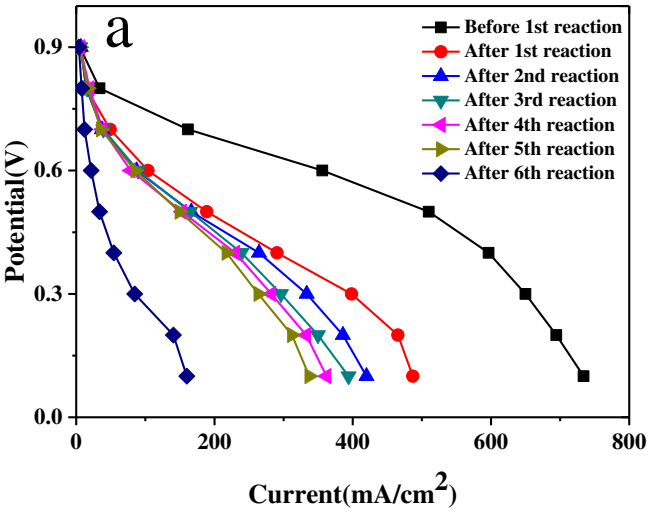

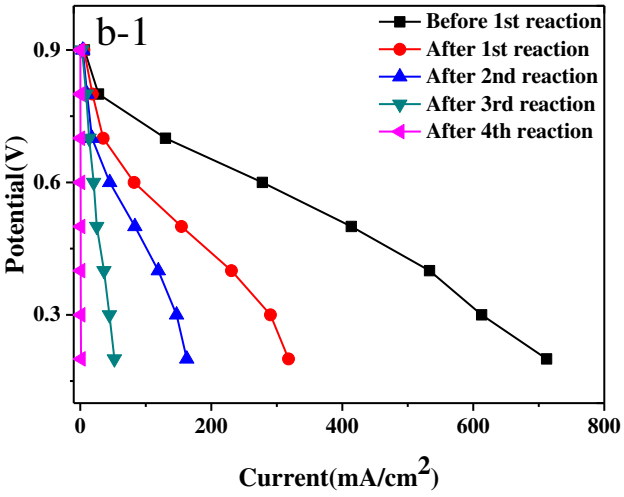

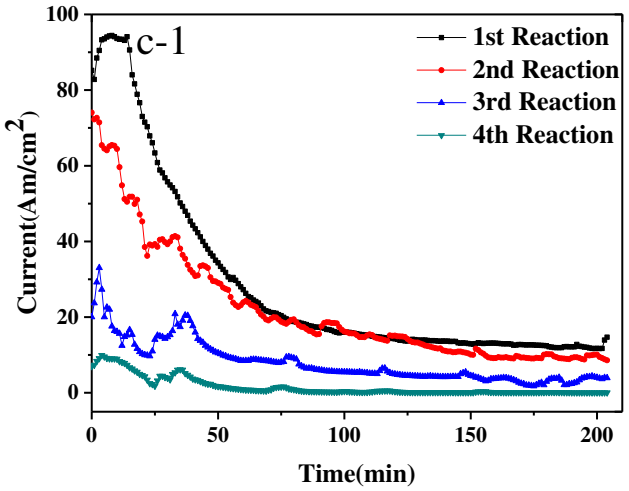
c-1
1st Reaction
2nd Reaction
3rd Reaction
4th Reaction
Current(Am/cm2)
Time(min)
0
20
40
60
80
100
0
50
100
150
200

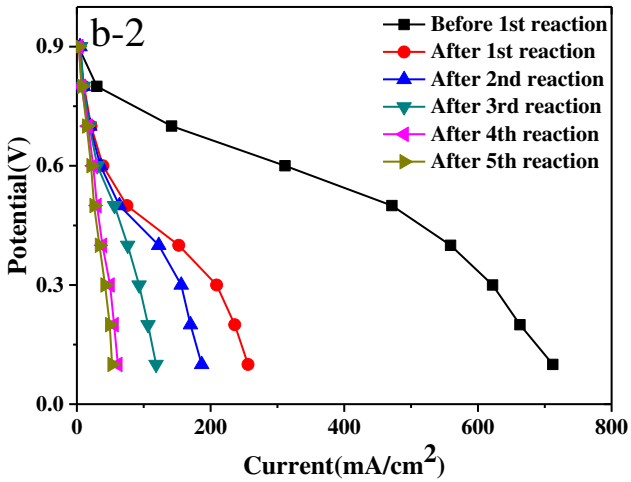
b-2
Before 1st reaction
After 1st reaction
After 2nd reaction
After 3rd reaction
After 4th reaction
After 5th reaction
Potential(V)
Current(mA/cm2)
0.0
0.3
0.6
0.9
0
200
400
600
800

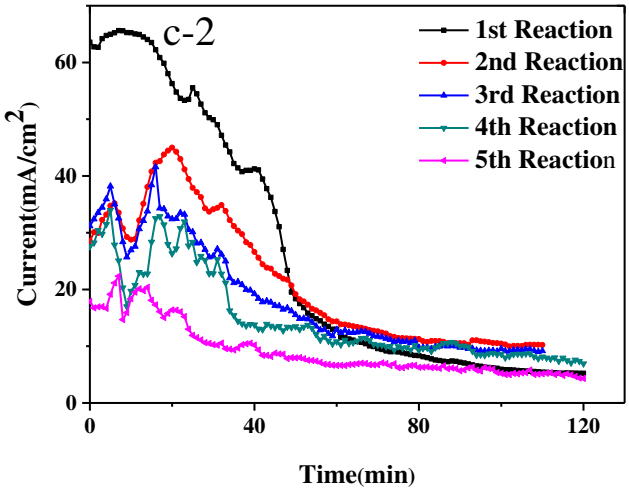
c-2
1st Reaction
2nd Reaction
3rd Reaction
4th Reaction
5th Reaction
Current(mA/cm2)
Time(min)
0
20
40
60
0
40
80
120

Figure 34. V-I scans (a) (b-1) (c-1) and current (b-2) (c-2) performed during three sets of ECH experiments.
(a) The ECH experiments were conducted for 6 times at 65 °C and 80% RH, The current of five relations are 200mA/cm^2, 160 mA/cm^2, 120 mA/cm^2, 80 mA/cm^2, 40 mA/cm^2 and 20 mA/cm^2; (b) The ECH experiments were conducted for 4 times at 65 °C but different RH. The RH of the four reactions are 100%, 63%, 50%, and 38%, respectively; (c) The ECH experiments were conducted 5 times at 80% RH but different temperatures. The temperature of five reactions is 50 ºC, 58 ºC, 65 ºC, 73 ºC, and 80 ºC, respectively. Products concentrations were identified three times. H_2 and furfural flow rates were 0.25 L/min and 12 ml/hr, respectively. The black curves were the baseline data recorded for the fresh MEAs prior to ECH tests. After each test, pure N_2 and water were purged for at least 24 hours, respectively, to remove all the temporary contaminants.

Figure 34a shows the results of five sets of V-I measurements performed on a PEMFC, which underwent five 1-hour long ECH experiments. Both the ECH experiments and V-I measurements shown in Figure 34a were conducted at 65 ºC with 80% RH. Note that in order to compare with the same baseline data (the black curve in Figure 34a), all the V-I scans were conducted using the same operating conditions that have been used for the baseline scan. It clearly shows that the MEA performance degraded as more ECH tests were conducted, especially after the fifth ECH experiment. The open circuit voltage (OCV) dropped a lot starting at the 1st V-I scan, and then the dropping trend is not obvious until the 6th ECH V-I scan which indicates that crossover became significant. It implied that pinholes might form due to degradation.

The effect of RH on MEA degradation was investigated, as shown in Figure 34b. For the ECH experiments conducted in Figure 33, the operating RH were 100%, 63%, 50%, and 38%, while maintaining the same temperature at 65 ºC for 4 hours. Again, all the V-I scans were performed using the same operating conditions as those used for the baseline scan (black curve in Figure 33b-1). Figure 34b-1 shows that the drop of V-I scans negatively correlated to the reaction RH. The current number of V-I scans at 0.5V decreased by 259 mA/cm^2, 112 mA/cm^2, 58mA/cm^2 and 24 mA/cm^2, at 100%, 63%, 50% and 38% RH, respectively. It indicated that the variation of RH from 100% to 38% has a positive impact on MEA degradation. Figure 34b-2 gave the demonstration that less RH resulted in less reaction current, leading to less mass

transport via the MEA, which eventually prolonged the lifetime of the catalysts. However, permanent damage to the MEA still existed, as seen from the general trend of the V-I scan. Similar to what was observed in Figure 34a, purging with pure N_2 and water could not remove permanent contaminants.

Figure 34c shows the effect of temperature on MEA degradation during ECH. For the ECH, five 2 hours long experiments conducted in Figure 33c, Temperature was reduced from 80 ℃ to 50 ℃, at 80% HR. The temperature of five reactions was 50 ℃, 58 ℃, 65 ℃, 73 ℃, and 80 ℃, respectively. The strongest drop of the open circuit voltage (OCV) happened at the 1st V-I scan, which was performed after the minimum 50 ℃, and then the decrease became slight. The 4th V-I scan and the 5th V-I scan were most coincided, which means the population of MEA was maximized. Again, all the V-I scans were performed using the same operating conditions as those used for the baseline scan (black curve in Figure 33c-1). The results illustrate that the most significant inefficiency of MEAs appeared at a minimum temperature of 50C. Figure 34c-2 demonstrated the current of each test, which was extremely correlated to the drop of OCV. For instance, the 1st reaction current curve was obviously higher than other, which corresponded to the strongest drop of the OCV happened at the 1st V-I scan. Accordingly, increasing temperature was recommended to mitigate the degradation to some extent. permanent damage to the MEA still existed, which was similar to temperature and current tests.

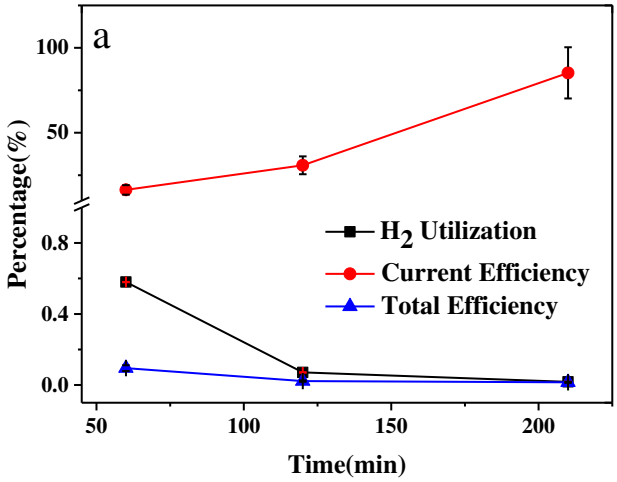
a
Percentage(%)
Time(min)
H2 Utilization
Current Efficiency
Total Efficiency

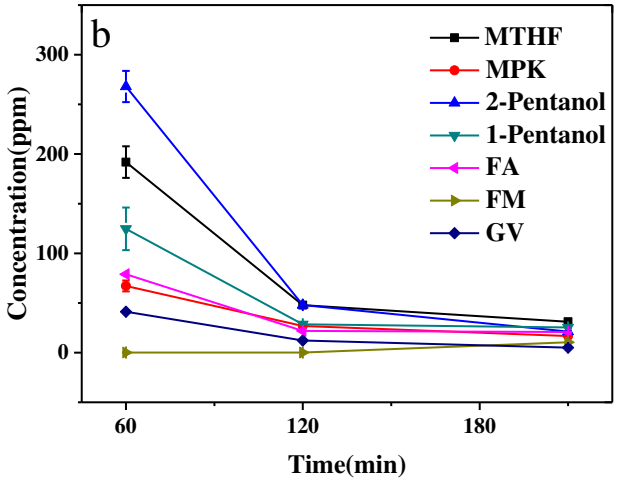
b
Concentration(ppm)
Time(min)
MTHF
MPK
2-Pentanol
1-Pentanol
FA
FM
GV

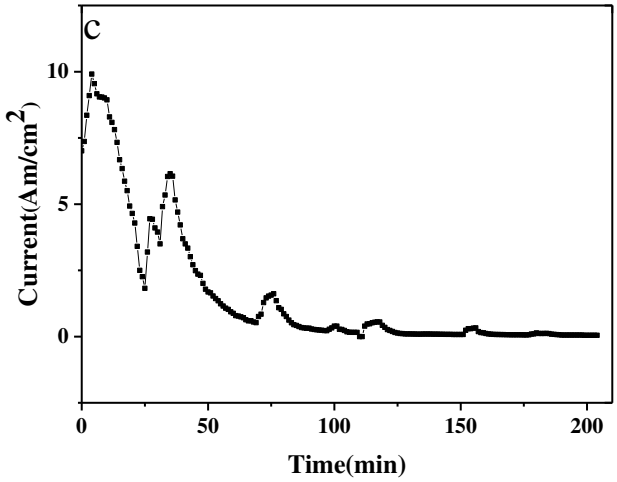
c
Current(Am/cm2)
Time(min)

Figure 35. Product (a), current efficiency (b), H_2 utilization (b) and total efficiency (b) as a function of ECH experiment time.
The ECH experiments were conducted for 220 min. The corresponding current vs time curve was shown in Figure (c).The ECH experiments were conducted at 65 °C, 80% RH, 0.02V input voltage, 12 ml/hr furfural flow rates and 0.25 L/min H_2 flow rate. Products were collected at 60 min, 120min, and 220 min and were identified three times.

Figure 35 shows that the trends of product, current efficiency, H_2 utilization and total efficiency using one MEA for 220 minutes. Products were collected at 60 min, 120min, and 220 minutes. Figure 10b shows a typical impact of reaction time on the product yield during ECH of furfural. Most of the main products of 2-pentanol, 1-pentanol and MTHF were produced at the first 60min, and then extremely descended at the time between 60 minutes and 120 minutes, eventually tended to be constant in the range of 120 minutes to 220 minutes. For instance, the yield of 2-pentanol at first 60 minutes was 268ppm and then dropped to 47ppm and 21ppm, at 120 minutes and 220 minutes, respectively. Different from the main products, by-products of GV and MPK slightly descended at the time between 60 minutes and 120 minutes. Very few mounts of MF were detected in this experiment. Figure 35a shows that the trend of current efficiency and H_2 utilization with time were totally opposite, H_2 utilization was negatively impacted by reaction time, while current efficiency was positively affected. Ultimately, 85% H_2 utilization was achieved at 220 minutes. Figure 35c exhibited that the current changed with time and proved that most of the current electrons were produced at the first hour. The Pt catalyst was commonly applied in fuel cells and proved to be an effective catalyst of depriving electrons from hydrogen [181, 182]. Although Pt has long been known as a furfural hydrogenation catalyst [158, 177, 178], the initial activity of Pt for furfural ECH by PEM reactor is not as good as Pd, Ni and Ru [41] Pt catalyst deactivation with time brings more serious influence on proton formation than the organic reduction. The deactivation of the Pt catalyst prevented anode H_2 protonation and current electrons generation, which was expressed as the decrease of H_2

utilization. Because the impact of deactivation of Pt on cathode organic reduction was not as serious as the current generation, the current efficiency was elevated with the decrease of current density.

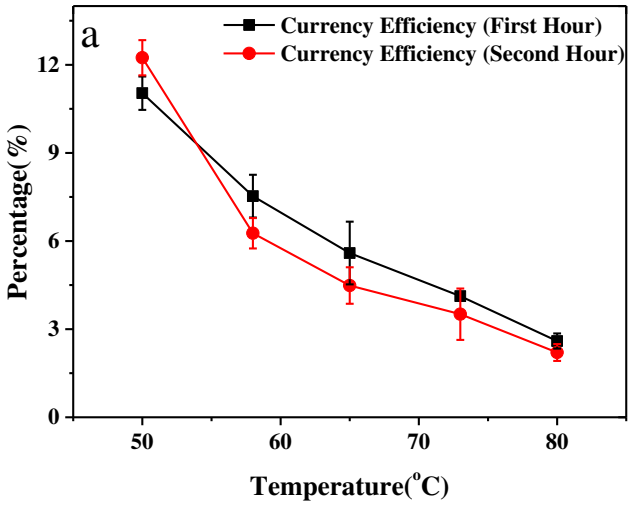

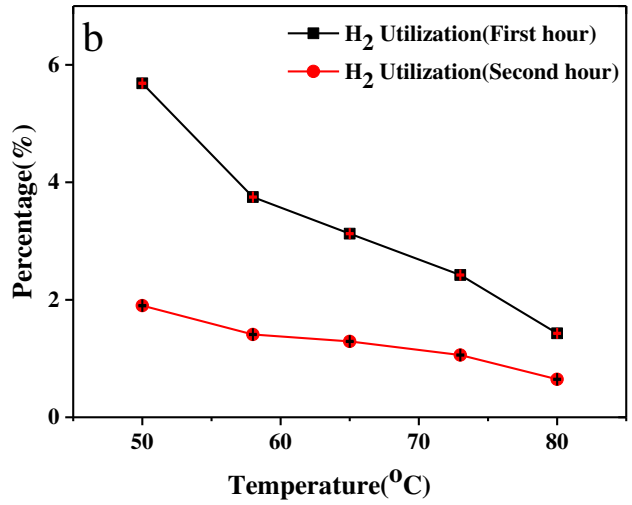

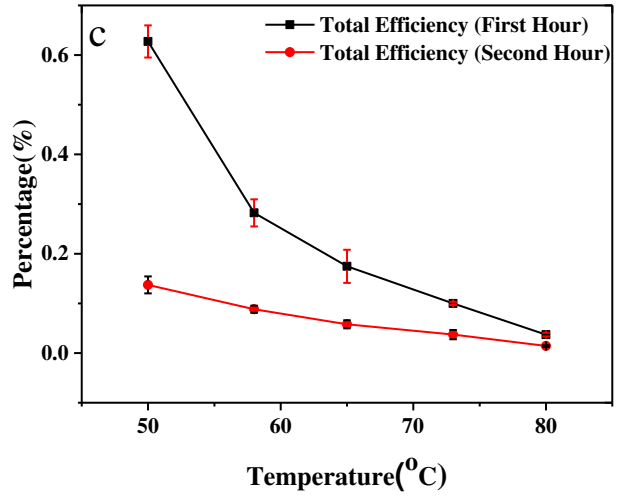
c
Total Efficiency (First Hour)
Total Efficiency (Second Hour)
Percentage(%)
0.0
0.2
0.4
0.6
50
60
70
80
Temperature(°C)

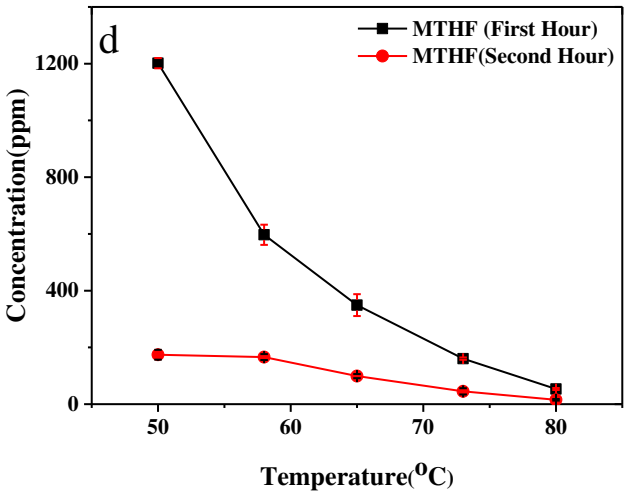
d
MTHF (First Hour)
MTHF(Second Hour)
Concentration(ppm)
0
400
800
1200
50
60
70
80
Temperature(°C)

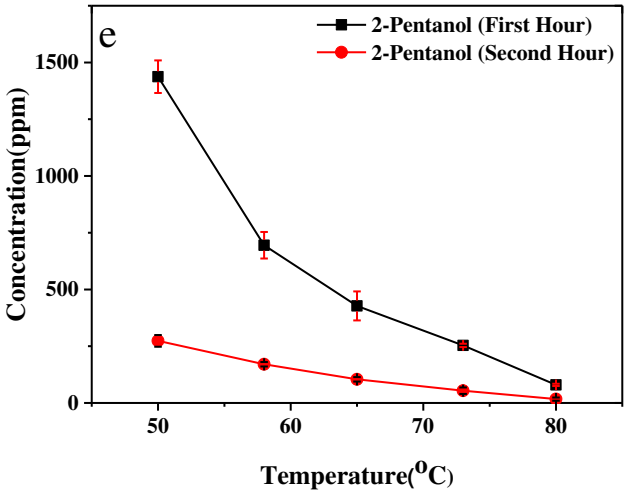
e
2-Pentanol (First Hour)
2-Pentanol (Second Hour)
Concentration(ppm)
0
500
1000
1500
50
60
70
80
Temperature(°C)

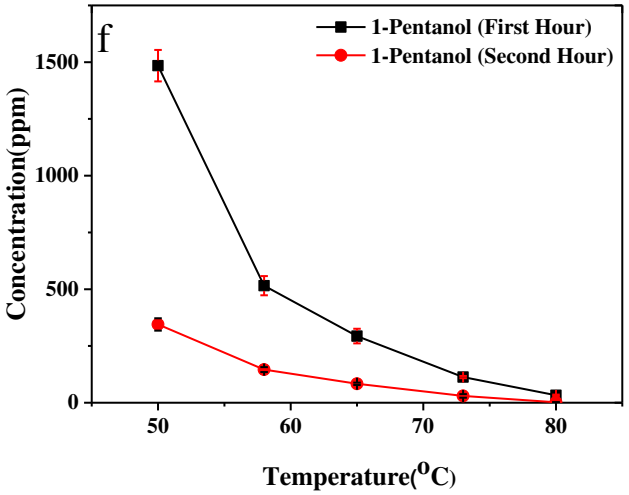
f
1-Pentanol (First Hour)
1-Pentanol (Second Hour)
Concentration(ppm)
1500
1000
500
0
50
60
70
80
Temperature(°C)

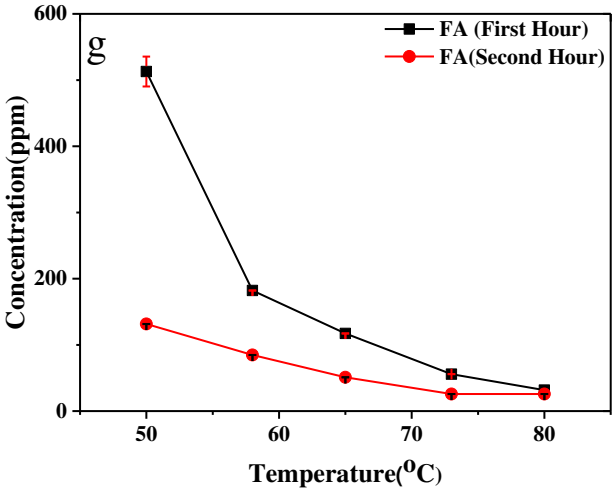
g
FA (First Hour)
FA(Second Hour)
Concentration(ppm)
600
400
200
0
50
60
70
80
Temperature(°C)

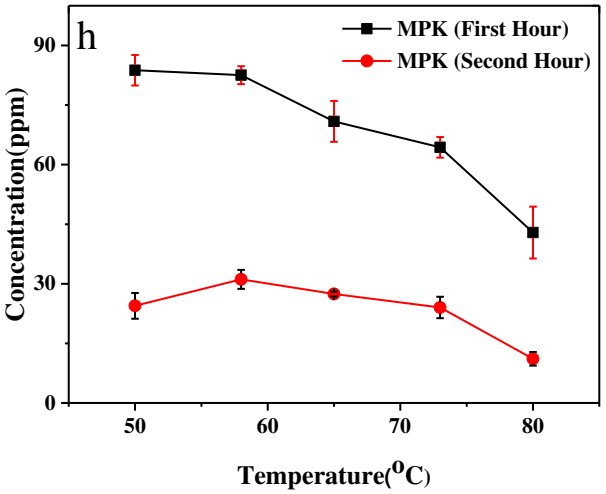
h
MPK (First Hour)
MPK (Second Hour)
Concentration(ppm)
90
60
30
0
50
60
70
80
Temperature(°C)

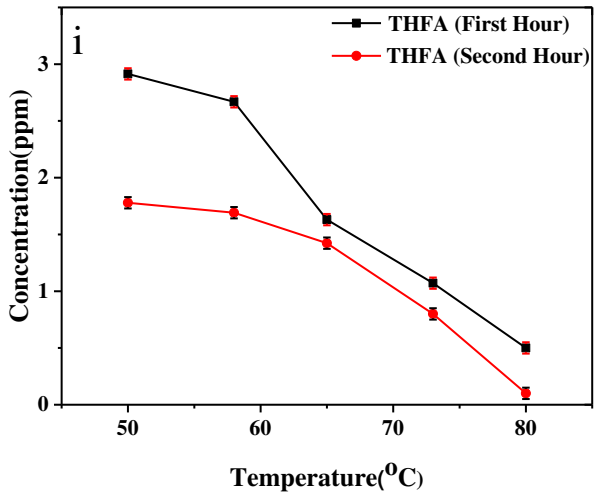
i
THFA (First Hour)
THFA (Second Hour)
Concentration(ppm)
0
1
2
3
50
60
70
80
Temperature(°C)

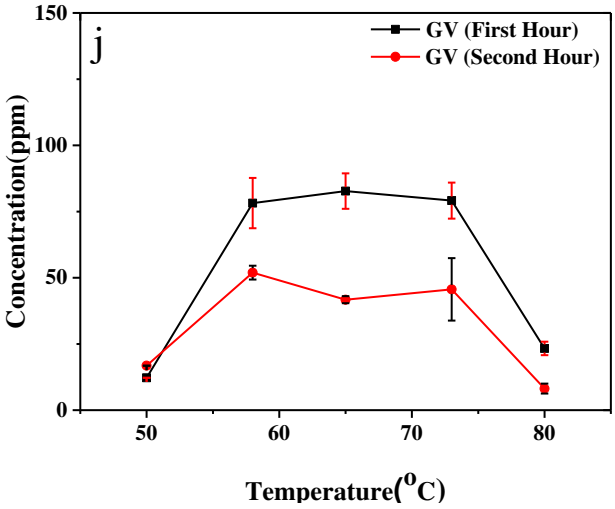
j
GV (First Hour)
GV (Second Hour)
Concentration(ppm)
0
50
100
150
50
60
70
80
Temperature(°C)

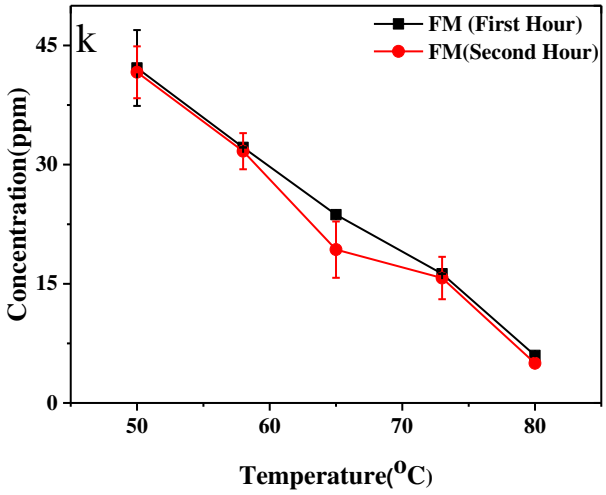
k
FM (First Hour)
FM(Second Hour)
Concentration(ppm)
0
15
30
45
50
60
70
80
Temperature(°C)

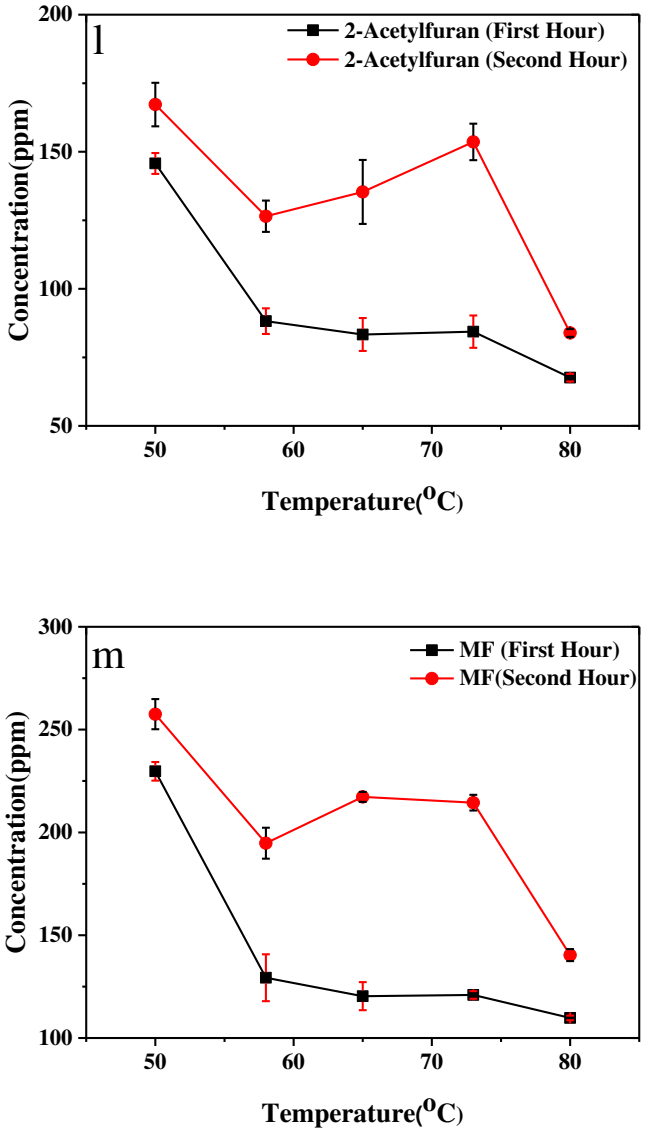

Figure 36. Current efficiency (a), H_2 utilization (b), total efficiency (c), products (d) (e) (f) (g) (h) (i) (j) (k) and impurity(l) (m) as a function of ECH experiment time.
The ECH experiments were conducted for 120 min, and the products were collected twice at 60 min and 120 min. The ECH experiments were conducted at 80% RH, 0.02V input voltage, 12 ml/hr furfural flow rates and 0.25 L/min H_2 flow rate. Products were identified three times.

Figure 36 shows the impact of temperature and reaction time on H_2 utilization, current efficiency, total efficiency and products in a typical set of experiments. Each experiment was conducted for 120 minutes, and with the products collected twice at 60 minutes and 120 minutes. Black curves in each figure expressed 1-hour collection, with red one standing for 2-hour collection. As we have already discussed the negative effects of temperature, on H_2 utilization,

current efficiency total efficiency and products previously, the discussion here will focus on the comparison of the different reaction time curve. Figure 36a, 36b, and 36c demonstrates that comparing with the current efficiency, H_2 utilization and total efficiency had a more significant drop between the 1st-hour curve and the 2nd-hour curve, which means H_2 utilization and total efficiency declined faster than current efficiency at the same operating time. It could be explained by the fact that the deactivation of Pt with time bringing more a negative effect on anode H_2 protonation than cathode organic reduction. This has been discussed in the last chapter. Compared with the first hour curve of Figure 36d, 36e, 36f and 36g, the second hour curve in these figures also took a huge descent, and it was more obvious at a lower temperature. For instance, the decrease of 1-pentanol between the first and the second-hour curve at 50°C was from 1484ppm to 345ppm, and the corresponding number was from 32ppm to 2ppm at 80°C. Obviously, with the same reaction time, at a lower temperature, furfural conversion rate was much higher, which resulted in the faster degradation of MEAs. This was why the low temperature gap between the two lines is bigger than the high temperature one. It concluded that these products of 2-pentanol, MTHF, 1-pentanol, and FA were centrally produced in the first hours and 1 hour operating time is recommended to ECH of furfural.

Compared to the main products, the by-product concentration of THFA and MPK in the ultimate product is fairly low, which is shown in Figure 36h and 36i. Especially for THFA, the maximum detected concentration was less than 3 ppm, which means the concentration change cannot be as significant as others. However, the gap between the two lines was still observable. It demonstrated that the yield of by-products decreased with reaction time extension, not as obvious as the main products.

A completely different changing trend of 1 hours curve and 2 hours curve were demonstrated in Figure 36j and 36k. The two lines of FM almost overlapped. The gaps of GV 2 lines just appeared at a temperature between 57°C and 73°C. Different from the structure of furfural, one extra $–CH_3$ is bonded to the O-C ring of FM and GV. Although traditional methods could produce FM and GV form furfural [157, 183], there was no evidence to prove that $–CH_3$ could be added to furfural and generate FM and GV by the ECH method [54-59, 184]. MF and 2-cetylfuran were detected in the initial furfural sample and determined to be an impurity. FM was very likely to form the C=C double bond hydrogenation of MF, which has a similar structure, and then FM C=C bond was hydrogenated with the corresponding saturated chemicals GV generation. Since the possibility that FM and GV transformed from furfural cannot be ruled out, the yield of FM and GV was still reported in the present research.

The concentration of MF and 2-cetylfuran with temperature and reacted hours is also shown in Figure 36l and 36m. Both the 1-hour curve and 2-hour curve are not constant, which means MF and 2-cetylfuran joined in the hydrogenation. Different from other figures, the 2-hour curve of MF and 2-cetylfuran is higher than the 1-hour curve, which means more MF and 2-cetylfuran were consumed in the first hour.

Usually, the lifespan of a PEMFC under steady-state operation can be very long, up to thousands of hours [138-143]. However, catalyst contamination is the major factor that diminishes the PEMFC performance and very likely results in significant degradation [144-146]. In fact, many organic compounds are able to contaminate the MEA. Those compounds include acetaldehyde, toluene, propane, vinyl acetate, methyl methacrylate, acetonitrile, dichloromethane, acetylene, chlorobenzene, formic acid, methanol, ethanol, phenol, butane, acetone, and naphthalene [147-149], and the list is expanding. The main reason for the discovery

of so many contaminants is that the catalysts used in common MEAs are Pt-based. Pt is a premium catalyst, but also sensitive to so many contaminants. The MEAs used in the present research contain pure Pt as the catalyst. Although developing non-Pt catalyst is beyond the scope of the present research, in order to further conduct durable ECH experiments, MEAs with contamination tolerant catalysts need to be used.

Reactant and product crossing over is another possible reason that caused the MEA degradation. Liquids that contained mainly furfural and some products were detected at the anode side during the ECH experiments. Those liquids not only decrease the fuel utilization but also further contaminate the anode catalyst. Feasible solutions to this issue include adopting thicker MEAs, feeding gaseous feedstock instead of liquid, and using a non-Pt catalyst [150].

In sum, 1 reaction hour is strongly recommended for furfural ECH to maintain the conversion rate, and then MEAs degradation should be mitigated. Some simple methods proved to be effective, such as water wash, air wash and acid wash, which is shown in Figure 37. At 0.5 V, after air wash, water wash and acid wash, the current density increased by 40mA/cm^2, 23 mA/cm^2 and 27 mA/cm^2, respectively.

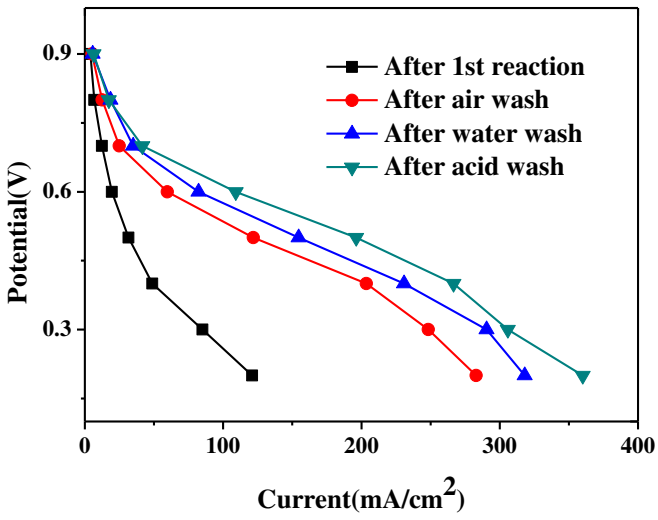

Figure 37. V-I scans after air wash, water wash, and acid wash.

Current density control was certified as a better method than input voltage control, by which MEA could be reused five times. Low operating temperature and high reaction humidity accelerated MEA's degradation. Nevertheless, it cannot be avoided, since high furfural conversation rate was also required. To solve the problem essentially, novel non-Pt catalysts need to be developed, such as Pd and Ni-based catalysts [60, 151, 152]. Despite the fact that a wide range of metals can be used as electrocatalysts at the cathode, those with the strong capability of hydrogen absorption are desired.

4.4 Conclusions

Electrochemical hydrogenation of furfural using a PEMFC reactor was successfully demonstrated in the present research. The results proved that ECH can be a feasible way of hydrogenating furfural in mild conditions (room temperature and atmosphere). The main products include 2-pentanol, 1-pentanol, FA and MTHF, while THFA and MPK are by-products. Temperature negatively impacts the product's yield, while humidity brings positive influence. Maintaining high current density by the applied voltage is a good method to increase the product's yield and accelerate furfural conversion. The mild operation conditions, including low temperature and ambient pressure, are the greatest advantages of the proposed ECH method. The present research suggests that the optimized conditions for ECH of furfural using a PEMFC reactor include room temperature, relative high RH around 80% and high current density.

Contamination impact using the PEMFC reactor during ECH was also investigated. It was concluded that organic compounds are able to contaminate the MEAs, resulting in serious degradation. However, the methods to mitigate contamination are limited. The present research demonstrated that lower RH could help reduce contamination; a high-efficiency work hour of

MEAs is 1 hour, and then simple wash is necessary to remove the temporary contamination. Eventually, novel non-Pt catalysts need to be developed for a durable ECH process.

CHAPTER 5

CONCLUSIONS AND RECOMMENDATIONS

5.1 Conclusions

The following five conclusions can be deduced from this dissertation.

(1) Chemical activation is a feasible method to produce AC from lignin biomass, ECH of lignin bio-oil compounds e.g., furfural and acetone to produce a value added product, such as FA and isopropanol by using PEMFC reactor is an effective way to improve economic benefits from lignin utilization.

(2) In comparison, the activated carbon produced by the H_3PO_4 agent has a relatively low surface area and a high amount of phosphorus residue. $ZnCl_2$ proved to be a better impregnating agent. The optimal experimental condition is that when the activation time is 60 minutes, the impregnation ration is between 1.5 to 2, the heating rate is 60ºC/mins, and an activation temperature around 500ºC. With the best activation conditions, the carbons produced have a surface area of around 1117 m^2/g, and the yield percentage could reach around 50%. Compared to Commercial AC, UHS-$ZnCl_2$ AC has similar Iodine No., Methylene Blue No, Surface area, better Yield percentage, which makes the high-temperature $ZnCl_2$ activated carbon method a possible way of utilizing lignin biomass residue. In addition, the Zinc residues could be totally removed through the acid wash and water wash which increased the purity of the activated carbon produced.

(3) Electrochemical hydrogenation of acetone using a PEMFC reactor was successfully demonstrated in the present research. The results proved that ECH can be a feasible way of hydrogenating acetone to produce isopropanol in mild conditions. In the experiments, the main product obtained was isopropanol with a selectivity of approximately 90%. A small amount

(about 1%) of diisopropyl ether was also obtained as a byproduct. Temperature had no impact on the isopropanol yield, while humidity brings a positive influence. The mild operation conditions, including low temperature and ambient pressure, are the greatest advantages of the proposed ECH acetone method.

(4) ECH can be a feasible way of hydrogenating furfural in mild conditions (room temperature and atmosphere). The main products include 2-pentanol, 1-pentanol, FA and MTHF, while THFA and MPK were by-products. Temperature negatively impacts the product's yield, while humidity brings a positive influence. Maintaining high current density by applied voltage was a good method to increase the product's yield and accelerate furfural conversion. The mild operation conditions, including room temperature and ambient pressure, are the greatest advantages of the proposed ECH furfural method.

(5) High operating RH and input current density of PEMFC significantly accelerated the degradation of MEAs, while relatively low temperature had a slightly negative influence on the degradation. In sum, the degradation speed of MEAs was proportional to the product's yield rate.

5.2 Recommendations

(1) Relatively high ash content, higher bulb density, oxygen percentage, and relatively lower carbon element, pore volume are the main shortage of UHS-$ZnCl_2$ AC. Especially for the high ash content, it easily causes the corrosion of equipment and blockage of pipes, and also is harmful to the regeneration of AC. Pretreatment is a good option for lignin like UHS before chemical activation, especially to remove Si.

(2) To increase the product yield and rate, the operating conditions for ECH of acetone using a PEMFC reactor including an operating temperature around 65 ℃ and relative high RH above 80% is recommended.

(3) room temperature and relative high RH above 80% are recommended for ECH furfural using a PEMFC reactor.

(4) The effective working life of PEMFC membrane was around 30 hours. After each 1 hour of operating time, a simple method like water wash, acid wash, and air wash is recommended to mitigate the degradation. Reducing the concentration of reactants is another way to mitigate degradation.

(5) To solve the MEA contamination problem, novel non-Pt catalysts need to be developed, such as Pd and Ni-based catalysts. Despite the fact that a wide range of metals can be tested as electrocatalysts at the cathode, for now Pt is still believed to be the strongest capability of hydrogen absorption.

REFERENCES

1. Hidajat, M.J., et al., *Depolymerization of concentrated sulfuric acid hydrolysis lignin to high-yield aromatic monomers in basic sub- and supercritical fluids.* Chemical Engineering Journal, 2017. **317**: p. 9-19.
2. Bridgewater, A.V., *Biomass fast pyrolysis.* Thermal science, 2004. **8**(2): p. 21-50.
3. Lora, J.H. and W.G. Glasser, *Recent industrial applications of lignin: a sustainable alternative to nonrenewable materials.* Journal of Polymers and the Environment, 2002. **10**(1-2): p. 39-48.
4. Soltes, E.J. and T.A. Milne, *Pyrolysis oils from biomass: producing, analyzing, and upgrading*. 2 ed. Vol. 4. 1988: ACS Publications.
5. Daifullah, A. and B. Girgis, *Removal of some substituted phenols by activated carbon obtained from agricultural waste.* Water research, 1998. **32**(4): p. 1169-1177.
6. Gupta, V.K., et al., *Chromium removal from water by activated carbon developed from waste rubber tires.* Environmental Science and Pollution Research, 2013. **20**(3): p. 1261-1268.
7. Lo, S.-F., et al., *Adsorption capacity and removal efficiency of heavy metal ions by Moso and Ma bamboo activated carbons.* Chemical Engineering Research and Design, 2012. **90**(9): p. 1397-1406.
8. Tan, Z., et al., *Gas-phase elemental mercury removal by novel carbon-based sorbents.* Carbon, 2012. **50**(2): p. 362-371.
9. Malik, P., *Dye removal from wastewater using activated carbon developed from sawdust: adsorption equilibrium and kinetics.* Journal of Hazardous Materials, 2004. **113**(1): p. 81-88.
10. Le, H.A., S. Chin, and J. Jurng, *Photocatalytic degradation of methylene blue by a combination of TiO 2-anatase and coconut shell activated carbon.* Powder Technology, 2012. **225**: p. 167-175.
11. Ali, I., M. Asim, and T.A. Khan, *Low cost adsorbents for the removal of organic pollutants from wastewater.* Journal of environmental management, 2012. **113**: p. 170-183.
12. Panwar, N.L., R. Kothari, and V.V. Tyagi, *Thermo chemical conversion of biomass – Eco friendly energy routes.* Renewable and Sustainable Energy Reviews, 2012. **16**(4): p. 1801-1816.
13. Ioannidou, O. and A. Zabaniotou, *Agricultural residues as precursors for activated carbon production—A review.* Renewable and Sustainable Energy Reviews, 2007. **11**(9): p. 1966-2005.
14. Savova, D., et al., *Biomass conversion to carbon adsorbents and gas.* Biomass and Bioenergy, 2001. **21**(2): p. 133-142.
15. Aygün, A., S. Yenisoy-Karakaş, and I. Duman, *Production of granular activated carbon from fruit stones and nutshells and evaluation of their physical, chemical and adsorption properties.* Microporous and Mesoporous Materials, 2003. **66**(2–3): p. 189-195.
16. Cabal, B., et al., *Adsorption of naphthalene from aqueous solution on activated carbons obtained from bean pods.* Journal of Hazardous Materials, 2009. **161**(2): p. 1150-1156.
17. Kula, I., et al., *Adsorption of Cd (II) ions from aqueous solutions using activated carbon prepared from olive stone by ZnCl 2 activation.* Bioresource Technology, 2008. **99**(3): p. 492-501.

18. El-Sheikh, A.H., et al., *Characterization of activated carbon prepared from a single cultivar of Jordanian Olive stones by chemical and physicochemical techniques.* Journal of analytical and Applied Pyrolysis, 2004. **71**(1): p. 151-164.
19. Ahmedna, M., W.E. Marshall, and R.M. Rao, *Production of granular activated carbons from select agricultural by-products and evaluation of their physical, chemical and adsorption properties1.* Bioresource Technology, 2000. **71**(2): p. 113-123.
20. Prahas, D., et al., *Activated carbon from jackfruit peel waste by H3PO4 chemical activation: Pore structure and surface chemistry characterization.* Chemical Engineering Journal, 2008. **140**(1–3): p. 32-42.
21. Adinata, D., W.M.A.W. Daud, and M.K. Aroua, *Preparation and characterization of activated carbon from palm shell by chemical activation with K 2 CO 3.* Bioresource Technology, 2007. **98**(1): p. 145-149.
22. Teng, H., T.-S. Yeh, and L.-Y. Hsu, *Preparation of activated carbon from bituminous coal with phosphoric acid activation.* Carbon, 1998. **36**(9): p. 1387-1395.
23. Martin, M.J., M.D. Balaguer, and M. Rigola, *Feasibility of Activated Carbon Production from Biological Sludge by Chemical Activation with ZnCl2 and H2SO4.* Environmental Technology, 1996. **17**(6): p. 667-671.
24. Kalderis, D., et al., *Production of activated carbon from bagasse and rice husk by a single-stage chemical activation method at low retention times.* Bioresource Technology, 2008. **99**(15): p. 6809-6816.
25. Lillo-Ródenas, M.A., D. Cazorla-Amorós, and A. Linares-Solano, *Understanding chemical reactions between carbons and NaOH and KOH: An insight into the chemical activation mechanism.* Carbon, 2003. **41**(2): p. 267-275.
26. Ji-Lu, Z., *Bio-oil from fast pyrolysis of rice husk: Yields and related properties and improvement of the pyrolysis system.* Journal of analytical and Applied Pyrolysis, 2007. **80**(1): p. 30-35.
27. Gayubo, A., et al., *Pyrolytic lignin removal for the valorization of biomass pyrolysis crude bio‐oil by catalytic transformation.* Journal of chemical technology and biotechnology, 2010. **85**(1): p. 132-144.
28. Xiu, S. and A. Shahbazi, *Bio-oil production and upgrading research: A review.* Renewable and Sustainable Energy Reviews, 2012. **16**(7): p. 4406-4414.
29. Bockris, J., *Electrochemical Processing*, in *Comprehensive Treatise of Electrochemistry*, J.O.M. Bockris, et al., Editors. 2013, Springer Science & Business Media: New York, US. p. 537-616.
30. Cirtiu, C.M., A. Brisach-Wittmeyer, and H. Ménard, *Electrocatalysis over Pd catalysts: A very efficient alternative to catalytic hydrogenation of cyclohexanone.* Journal of Catalysis, 2007. **245**(1): p. 191-197.
31. Amouzegar, K. and O. Savadogo, *Electrocatalytic hydrogenation of phenol on dispersed Pt: reaction mechanism and support effect.* Electrochimica Acta, 1998. **43**(5): p. 503-508.
32. St-Pierre, G., et al., *Rational design of original materials for the electrocatalytic hydrogenation reactions: Concept, preparation, characterization, and theoretical analysis.* Langmuir, 2004. **20**(15): p. 6365-6373.
33. Cirtiu, C.M., et al., *Modification of the surface adsorption properties of alumina-supported Pd catalysts for the electrocatalytic hydrogenation of phenol.* Langmuir, 2006. **22**(14): p. 6414-6421.

34. Song, Y., et al., *Integrated catalytic and electrocatalytic conversion of substituted phenols and diaryl ethers.* Journal of Catalysis, 2016. **344**: p. 263-272.
35. Pintauro, P.N., et al., *Electrochemical Hydrogenation of Soybean Oil with Hydrogen Gas.* Industrial & Engineering Chemistry Research, 2005. **44**(16): p. 6188-6195.
36. Li, Z., et al., *A mild approach for bio-oil stabilization and upgrading: electrocatalytic hydrogenation using ruthenium supported on activated carbon cloth.* Green Chemistry, 2014. **16**(2): p. 844-852.
37. An, W., et al., *The electrochemical hydrogenation of edible oils in a solid polymer electrolyte reactor. II. Hydrogenation selectivity studies.* Journal of the American Oil Chemists' Society, 1999. **76**(2): p. 215-222.
38. An, W., et al., *The electrochemical hydrogenation of edible oils in a solid polymer electrolyte reactor. I. Reactor design and operation.* Journal of the American Oil Chemists' Society, 1998. **75**(8): p. 917-925.
39. Xin, L., et al., *Electricity Storage in Biofuels: Selective Electrocatalytic Reduction of Levulinic Acid to Valeric Acid or γ‐Valerolactone.* ChemSusChem, 2013. **6**(4): p. 674-686.
40. Qiu, Y., et al., *Integrated electrocatalytic processing of levulinic acid and formic acid to produce biofuel intermediate valeric acid.* Green Chemistry, 2014. **16**(3): p. 1305-1315.
41. Nilges, P., et al., *Electrochemistry for biofuel generation: Electrochemical conversion of levulinic acid to octane.* Energy & Environmental Science, 2012. **5**(1): p. 5231-5235.
42. Cyr, A., et al., *Electrocatalytic hydrogenation of lignin models at Raney nickel and palladium-based electrodes.* Canadian Journal of Chemistry, 2000. **78**(3): p. 307-315.
43. Ilikti, H., N. Rekik, and M. Thomalla, *Electrocatalytic hydrogenation of alkyl-substituted phenols in aqueous solutions at a Raney nickel electrode in the presence of a non-micelle-forming cationic surfactant.* Journal of applied electrochemistry, 2004. **34**(2): p. 127-136.
44. Laplante, F., L. Brossard, and H. Ménard, *Considerations about phenol electrohydrogenation on electrodes made with reticulated vitreous carbon cathode.* Canadian Journal of Chemistry, 2003. **81**(3): p. 258-264.
45. Song, Y., et al., *Aqueous phase electrocatalysis and thermal catalysis for the hydrogenation of phenol at mild conditions.* Applied Catalysis B: Environmental, 2016. **182**: p. 236-246.
46. Santana, D.S., et al., *Electrocatalytic hydrogenation of organic compounds using current density gradient and sacrificial anode of nickel.* Tetrahedron Letters, 2003. **44**(25): p. 4725-4727.
47. Singh, N., et al., *Electrocatalytic Hydrogenation of Phenol over Platinum and Rhodium: Unexpected Temperature Effects Resolved.* ACS Catalysis, 2016. **6**(11): p. 7466-7470.
48. Tountian, D., et al., *Effect of support conductivity of catalytic powder on electrocatalytic hydrogenation of phenol.* Journal of applied electrochemistry, 2009. **39**(3): p. 411-419.
49. Ilikti, H., N. Rekik, and M. Thomalla, *Electrocatalytic hydrogenation of phenol in aqueous solutions at a Raney nickel electrode in the presence of cationic surfactants.* Journal of applied electrochemistry, 2002. **32**(6): p. 603-609.
50. Tsyganok, A., et al., *Electrocatalytic hydrogenation of aromatic compounds in ionic liquid solutions over WS2-on-glassy carbon and Raney nickel cathodes.* Fuel, 2012. **93**: p. 415-422.

51. Sáez, A., et al., *Electrocatalytic hydrogenation of acetophenone using a polymer electrolyte membrane electrochemical reactor.* Electrochimica Acta, 2013. **91**: p. 69-74.
52. Dalavoy, T.S., et al., *Mild electrocatalytic hydrogenation of lactic acid to lactaldehyde and propylene glycol.* Journal of Catalysis, 2007. **246**(1): p. 15-28.
53. Lam, C.H., et al., *Electrocatalytic upgrading of model lignin monomers with earth abundant metal electrodes.* Green Chemistry, 2015. **17**(1): p. 601-609.
54. Li, Z., et al., *Aqueous electrocatalytic hydrogenation of furfural using a sacrificial anode.* Electrochimica Acta, 2012. **64**: p. 87-93.
55. Chu, D., et al., *Nano TiO2 film electrode for electrocatalytic reduction of furfural in ionic liquids.* Journal of Nanoparticle Research, 2009. **11**(7): p. 1805.
56. Parpot, P., et al., *Electrochemical investigations of the oxidation–reduction of furfural in aqueous medium: application to electrosynthesis.* Electrochimica Acta, 2004. **49**(3): p. 397-403.
57. Chamoulaud, G., et al., *Biomass conversion II: simultaneous electrosyntheses of furoic acid and furfuryl alcohol on modified graphite felt electrodes.* Electrochimica Acta, 2001. **46**(18): p. 2757-2760.
58. Green, S.K., et al., *The electrocatalytic hydrogenation of furanic compounds in a continuous electrocatalytic membrane reactor.* Green Chemistry, 2013. **15**(7): p. 1869-1879.
59. Nilges, P. and U. Schröder, *Electrochemistry for biofuel generation: production of furans by electrocatalytic hydrogenation of furfurals.* Energy & Environmental Science, 2013. **6**(10): p. 2925-2931.
60. zhao, B., et al., *Electrocatalytic hydrogenation of furfural to furfuryl alcohol using platinum supported on activated carbon fibers.* Electrochimica Acta, 2014. **135**: p. 139-146.
61. Lai, S.C. and M.T. Koper, *Electro-oxidation of ethanol and acetaldehyde on platinum single-crystal electrodes.* Faraday discussions, 2009. **140**: p. 399-416.
62. Huang, B., et al., *Highly selective electrochemical hydrogenation of acetylene to ethylene at Ag and Cu cathodes.* Electrochemistry Communications, 2013. **34**: p. 90-93.
63. Kwon, Y. and M. Koper, *Electrocatalytic hydrogenation and deoxygenation of glucose on solid metal electrodes.* ChemSusChem, 2013. **6**(3): p. 455-462.
64. Moutet, J.-C., *Electrocatalytic hydrogenation on hydrogen-active electrodes. A review.* Organic preparations and procedures international, 1992. **24**(3): p. 309-325.
65. Mahdavi, B., J.M. Chapuzet, and J. Lessard, *The electrocatalytic hydrogenation of phenanthrene at Raney nickel electrodes: the effect of periodic current control.* Electrochimica Acta, 1993. **38**(10): p. 1377-1380.
66. Li, Z., et al., *Mild electrocatalytic hydrogenation and hydrodeoxygenation of bio-oil derived phenolic compounds using ruthenium supported on activated carbon cloth.* Green Chemistry, 2012. **14**(9): p. 2540-2549.
67. Lipkowski, J. and P.N. Ross, *Electrocatalysis*. 1th ed. Vol. 3. 1998, New York, US: John Wiley&Sons. 75-290.
68. Robin, D., et al., *The electrocatalytic hydrogenation of fused poly cyclic aromatic compounds at Raney nickel electrodes: the influence of catalyst activation and electrolysis conditions.* Canadian Journal of Chemistry, 1990. **68**(7): p. 1218-1227.

69. Garraín, D., Y. Lechón, and C. de la Rúa, *Polymer electrolyte membrane fuel cells (PEMFC) in automotive applications: environmental relevance of the manufacturing stage.* Smart Grid and Renewable Energy, 2011. **2**(2): p. 68.
70. Montiel, V., et al., *Use of MEA technology in the synthesis of pharmaceutical compounds: The electrosynthesis of N-acetyl-l-cysteine.* Electrochemistry Communications, 2010. **12**(1): p. 118-121.
71. Wang, Y., et al., *A review of polymer electrolyte membrane fuel cells: Technology, applications, and needs on fundamental research.* Applied Energy, 2011. **88**(4): p. 981-1007.
72. Green, S.K., et al., *Electrocatalytic Reduction of Acetone in a Proton‐Exchange‐Membrane Reactor: A Model Reaction for the Electrocatalytic Reduction of Biomass.* ChemSusChem, 2012. **5**(12): p. 2410-2420.
73. Demiral, İ., A. Eryazıcı, and S. Şensöz, *Bio-oil production from pyrolysis of corncob (Zea mays L.).* Biomass and Bioenergy, 2012. **36**: p. 43-49.
74. Mullen, C.A., et al., *Bio-oil and bio-char production from corn cobs and stover by fast pyrolysis.* Biomass and Bioenergy, 2010. **34**(1): p. 67-74.
75. Biswas, B., et al., *Pyrolysis of agricultural biomass residues: Comparative study of corn cob, wheat straw, rice straw and rice husk.* Bioresource Technology, 2017. **237**: p. 57-63.
76. Shah, A., et al., *Physicochemical properties of bio-oil and biochar produced by fast pyrolysis of stored single-pass corn stover and cobs.* Bioresource Technology, 2012. **125**: p. 348-352.
77. Leng, F., et al., *Characterization of pyrolytic lignins with different activities obtained from bio-oil.* Chinese Journal of Chemical Engineering, 2017. **25**(3): p. 324-329.
78. Wang, S., et al., *Pyrolysis behaviors of four lignin polymers isolated from the same pine wood.* Bioresource Technology, 2015. **182**: p. 120-127.
79. Bai, X., et al., *Formation of phenolic oligomers during fast pyrolysis of lignin.* Fuel, 2014. **128**: p. 170-179.
80. Yin, R., et al., *Characterization of bio-oil and bio-char obtained from sweet sorghum bagasse fast pyrolysis with fractional condensers.* Fuel, 2013. **112**: p. 96-104.
81. Lehmann, J., J. Gaunt, and M. Rondon, *Bio-char sequestration in terrestrial ecosystems–a review.* Mitigation and adaptation strategies for global change, 2006. **11**(2): p. 403-427.
82. McHenry, M.P., *Agricultural bio-char production, renewable energy generation and farm carbon sequestration in Western Australia: Certainty, uncertainty and risk.* Agriculture, Ecosystems & Environment, 2009. **129**(1-3): p. 1-7.
83. Leng, L., et al., *Bio-char derived from sewage sludge by liquefaction: characterization and application for dye adsorption.* Applied Surface Science, 2015. **346**: p. 223-231.
84. Liu, P., et al., *Modification of bio-char derived from fast pyrolysis of biomass and its application in removal of tetracycline from aqueous solution.* Bioresource Technology, 2012. **121**: p. 235-240.
85. Choi, I.S., et al., *Bioethanol production from mandarin (Citrus unshiu) peel waste using popping pretreatment.* Applied Energy, 2013. **102**(0): p. 204-210.
86. Dwivedi, P., J.R.R. Alavalapati, and P. Lal, *Cellulosic ethanol production in the United States: Conversion technologies, current production status, economics, and emerging developments.* Energy for Sustainable Development, 2009. **13**(3): p. 174-182.
87. Sissine, F. *Energy Independence and Security Act of 2007: a summary of major provisions*. 2007. NewYork: DTIC Document.

88. Popov, S., et al., *Bio-oil via catalytic liquefaction of unhydrolyzed solids in aqueous medium.* Biofuels, 2014. **5**(4): p. 431-446.
89. Balan, V., D. Chiaramonti, and S. Kumar, *Review of US and EU initiatives toward development, demonstration, and commercialization of lignocellulosic biofuels.* Biofuels, Bioproducts and Biorefining, 2013. **7**(6): p. 732-759.
90. Teymouri, F., et al., *Optimization of the ammonia fiber explosion (AFEX) treatment parameters for enzymatic hydrolysis of corn stover.* Bioresource Technology, 2005. **96**(18): p. 2014-2018.
91. Li, B.-Z., et al., *Process optimization to convert forage and sweet sorghum bagasse to ethanol based on ammonia fiber expansion (AFEX) pretreatment.* Bioresource Technology, 2010. **101**(4): p. 1285-1292.
92. Mosier, N., et al., *Features of promising technologies for pretreatment of lignocellulosic biomass.* Bioresource Technology, 2005. **96**(6): p. 673-686.
93. Oliveira, L.C., et al., *Preparation of activated carbons from coffee husks utilizing FeCl 3 and ZnCl 2 as activating agents.* Journal of Hazardous Materials, 2009. **165**(1): p. 87-94.
94. Macedo, J.S., et al., *Biomorphic activated porous carbons with complex microstructures from lignocellulosic residues.* Microporous and Mesoporous Materials, 2008. **107**(3): p. 276-285.
95. Pereira, R.G., et al., *Preparation of activated carbons from cocoa shells and siriguela seeds using H 3 PO 4 and ZnCL 2 as activating agents for BSA and α-lactalbumin adsorption.* Fuel Processing Technology, 2014. **126**: p. 476-486.
96. Deng, H., et al., *Preparation and characterization of activated carbon from cotton stalk by microwave assisted chemical activation—application in methylene blue adsorption from aqueous solution.* Journal of Hazardous Materials, 2009. **166**(2): p. 1514-1521.
97. Danish, M., et al., *Effect of acidic activating agents on surface area and surface functional groups of activated carbons produced from Acacia mangium wood.* Journal of analytical and Applied Pyrolysis, 2013. **104**: p. 418-425.
98. *World Health Organization. Guide to local production: WHO-recommended handrub formulations.* 2011. 1123-1156
99. *Ceresana Inc., Market Study Solvents* 4th. ed. 2012. 10.
100. Alt, C., *Ullmann's encyclopedia of industrial chemistry*. 1th ed. 2006, New York, US: Wiley-VCH. 2345-2351.
101. Onoue, Y., et al., *Isopropyl Alcohol by Direct Hydration of Propylene.* Bulletin of The Japan Petroleum Institute, 1973. **15**(1): p. 50-55.
102. John E. Logsdon and R.A. Loke, *Isopropyl Alcohol*, in *Kirk-Othmer encyclopedia of chemical technology*, John E. Logsdon and R.A. Loke, Editors. 2000, Wiley-VCH: New York, US. p. 98-100.
103. Yurieva, T.M., et al., *Mechanisms for hydrogenation of acetone to isopropanol and of carbon oxides to methanol over copper-containing oxide catalysts.* Journal of Molecular Catalysis A: Chemical, 1996. **113**(3): p. 455-468.
104. Zhang, X., U. Pasaogullari, and T. Molter, *Influence of ammonia on membrane-electrode assemblies in polymer electrolyte fuel cells.* International Journal of Hydrogen Energy, 2009. **34**(22): p. 9188-9194.
105. *Florida Solar Energy Center, Test Protocol for Cell Performance Tests Performed Under DOE*. 2009. p.19-20.

106. Dadda, B., et al., *Heat and mass transfer influence on potential variation in a PEMFC membrane.* International Journal of Hydrogen Energy, 2014. **39**(27): p. 15238-15245.
107. Zong, Y., B. Zhou, and A. Sobiesiak, *Water and thermal management in a single PEM fuel cell with non-uniform stack temperature.* Journal of Power Sources, 2006. **161**(1): p. 143-159.
108. Berg, L., *Separation of acetone from isopropanol-water mixtures by extractive distillation*. 1999: United States
109. Jian, Q.-f., G.-q. Ma, and X.-l. Qiu, *Influences of gas relative humidity on the temperature of membrane in PEMFC with interdigitated flow field.* Renewable Energy, 2014. **62**: p. 129-136.
110. Anantaraman, A. and C. Gardner, *Studies on ion-exchange membranes. Part 1. Effect of humidity on the conductivity of Nafion®.* Journal of Electroanalytical Chemistry, 1996. **414**(2): p. 115-120.
111. Sumner, J., et al., *Proton conductivity in Nafion® 117 and in a novel bis [(perfluoroalkyl) sulfonyl] imide ionomer membrane.* Journal of the Electrochemical Society, 1998. **145**(1): p. 107-110.
112. Sone, Y., P. Ekdunge, and D. Simonsson, *Proton conductivity of Nafion 117 as measured by a four‐electrode AC impedance method.* Journal of the Electrochemical Society, 1996. **143**(4): p. 1254-1259.
113. Yuan, W., et al., *Model prediction of effects of operating parameters on proton exchange membrane fuel cell performance.* Renewable Energy, 2010. **35**(3): p. 656-666.
114. Wong, K., et al., *A theoretical study of inlet relative humidity control in PEM fuel cell.* International Journal of Hydrogen Energy, 2011. **36**(18): p. 11871-11885.
115. Lee, C.-I. and H.-S. Chu, *Effects of cathode humidification on the gas–liquid interface location in a PEM fuel cell.* Journal of Power Sources, 2006. **161**(2): p. 949-956.
116. Guvelioglu, G.H. and H.G. Stenger, *Flow rate and humidification effects on a PEM fuel cell performance and operation.* Journal of Power Sources, 2007. **163**(2): p. 882-891.
117. Zhang, J., et al., *PEM fuel cell relative humidity (RH) and its effect on performance at high temperatures.* Electrochimica Acta, 2008. **53**: p. 5315-5321.
118. Jeon, D.H., et al., *The effect of relative humidity of the cathode on the performance and the uniformity of PEM fuel cells.* International Journal of Hydrogen Energy, 2011. **36**(19): p. 12499-12511.
119. Ikeda, T., et al., *MRI Investigation of Water Transport Mechanism in a Membrane Under Elevated Temperature Condition With Relative Humidity and Current Density Variation.* ECS Transactions, 2008. **16**(2): p. 1035-1040.
120. Misran, E., et al., *Water transport characteristics of a PEM fuel cell at various operating pressures and temperatures.* International Journal of Hydrogen Energy, 2013. **38**(22): p. 9401-9408.
121. Knights, S.D., et al., *Aging mechanisms and lifetime of PEFC and DMFC.* Journal of Power Sources, 2004. **127**(1-2): p. 127-134.
122. Abe, T., et al., *Study of PEFCs by AC Impedance, Current Interrupt, and Dew Point Measurements I. Effect of Humidity in Oxygen Gas.* Journal of the Electrochemical Society, 2004. **151**(1): p. A101-A105.
123. Saleh, M.M., et al., *Exploring the effects of symmetrical and asymmetrical relative humidity on the performance of H2/air PEM fuel cell at different temperatures.* Journal of Power Sources, 2007. **164**(2): p. 503-509.

124. Xu, H., et al., *Effect of elevated temperature and reduced relative humidity on ORR kinetics for PEM fuel cells.* Journal of the Electrochemical Society, 2005. **152**(9): p. A1828-A1836.
125. Uribe, F.A., T.E. Springer, and S. Gottesfeld, *A Microelectrode Study of Oxygen Reduction at the Platinum/Recast‐Nafion Film Interface.* Journal of the Electrochemical Society, 1992. **139**(3): p. 765-773.
126. Jang, J.-H., et al., *Humidity of reactant fuel on the cell performance of PEM fuel cell with baffle-blocked flow field designs.* Journal of Power Sources, 2006. **159**(1): p. 468-477.
127. Broka, K. and P. Ekdunge, *Oxygen and hydrogen permeation properties and water uptake of Nafion® 117 membrane and recast film for PEM fuel cell.* Journal of applied electrochemistry, 1997. **27**(2): p. 117-123.
128. Murillo, L.E. and J.G. Chen, *Adsorption and reaction of propanal, 2-propenol and 1-propanol on Ni/Pt (111) bimetallic surfaces.* Surface Science, 2008. **602**(14): p. 2412-2420.
129. Takalloo, P.K., E.S. Nia, and M. Ghazikhani, *Numerical and experimental investigation on effects of inlet humidity and fuel flow rate and oxidant on the performance on polymer fuel cell.* Energy Conversion and Management, 2016. **114**: p. 290-302.
130. Jiang, R., H.R. Kunz, and J.M. Fenton, *Investigation of membrane property and fuel cell behavior with sulfonated poly (ether ether ketone) electrolyte: temperature and relative humidity effects.* Journal of Power Sources, 2005. **150**: p. 120-128.
131. Xu, H., H.R. Kunz, and J.M. Fenton, *Analysis of proton exchange membrane fuel cell polarization losses at elevated temperature 120 C and reduced relative humidity.* Electrochimica Acta, 2007. **52**(11): p. 3525-3533.
132. Jiang, R., H.R. Kunz, and J.M. Fenton, *Influence of temperature and relative humidity on performance and CO tolerance of PEM fuel cells with Nafion®–Teflon®–Zr (HPO4) 2 higher temperature composite membranes.* Electrochimica Acta, 2006. **51**(26): p. 5596-5605.
133. Zhang, J., et al., *PEM fuel cell relative humidity (RH) and its effect on performance at high temperatures.* Electrochimica Acta, 2008. **53**(16): p. 5315-5321.
134. Wang, X., et al., *An experimental overview of the effects of hydrogen impurities on polymer electrolyte membrane fuel cell performance.* International Journal of Hydrogen Energy, 2014. **39**(34): p. 19701-19713.
135. Cheng, X., et al., *A review of PEM hydrogen fuel cell contamination: Impacts, mechanisms, and mitigation.* Journal of Power Sources, 2007. **165**(2): p. 739-756.
136. Benziger, J. and J. Nehlsen, *A polymer electrolyte hydrogen pump hydrogenation reactor.* Industrial & Engineering Chemistry Research, 2010. **49**(21): p. 11052-11060.
137. Lundin, M.D. and M.J. McCready, *High pressure anode operation of direct methanol fuel cells for carbon dioxide management.* Journal of Power Sources, 2011. **196**(13): p. 5583-5590.
138. Scholta, J., et al., *Development and performance of a 10kW PEMFC stack.* Journal of Power Sources, 2004. **127**(1): p. 206-212.
139. Cleghorn, S., et al., *A polymer electrolyte fuel cell life test: 3 years of continuous operation.* Journal of Power Sources, 2006. **158**(1): p. 446-454.
140. St-Pierre, J., et al., *Relationships between water management, contamination and lifetime degradation in PEFC.* Journal of New Materials for Electrochemical Systems, 2000. **3**(2): p. 99-106.

141. Satyapal, S. *Hydrogen & Fuel Cells Program Overview*. in *Annual Merit Review and Peer Evaluation Meeting*. 2011. Arlington,US: DOCI
142. Wipke, K., et al. *VII. 1 Controlled Hydrogen Fleet and Infrastructure Analysis*. in *DOE Annual Merit Review and Peer Evaluation Meeting*. 2012. Washington, DC, US.
143. Wu, J., et al., *A review of PEM fuel cell durability: Degradation mechanisms and mitigation strategies.* Journal of Power Sources, 2008. **184**(1): p. 104-119.
144. Ferreira, P., et al., *Instability of Pt／C electrocatalysts in proton exchange membrane fuel cells a mechanistic investigation.* Journal of the Electrochemical Society, 2005. **152**(11): p. A2256-A2271.
145. Xie, J., et al., *Microstructural changes of membrane electrode assemblies during PEFC durability testing at high humidity conditions.* Journal of the Electrochemical Society, 2005. **152**(5): p. A1011-A1020.
146. Antolini, E., *Formation, microstructural characteristics and stability of carbon supported platinum catalysts for low temperature fuel cells.* Journal of materials science, 2003. **38**(14): p. 2995-3005.
147. Murugan, A. and A.S. Brown, *Review of purity analysis methods for performing quality assurance of fuel cell hydrogen.* International Journal of Hydrogen Energy, 2015. **40**(11): p. 4219-4233.
148. St-Pierre, J., M. Angelo, and Y. Zhai, *Focusing research by developing performance related selection criteria for PEMFC contaminants.* ECS Transactions, 2011. **41**(1): p. 279-286.
149. St-Pierre, J., Y. Zhai, and M.S. Angelo, *Effect of selected airborne contaminants on PEMFC performance.* Journal of the Electrochemical Society, 2014. **161**(3): p. F280-F290.
150. Fukuzumi, S., Y.M. Lee, and W. Nam, *Mechanisms of Two‐Electron versus Four‐Electron Reduction of Dioxygen Catalyzed by Earth‐Abundant Metal Complexes.* ChemCatChem, 2018. **10**(1): p. 9-28.
151. Chen, Y., C. Hwang, and C. Liaw, *One-step synthesis of methyl isobutyl ketone from acetone with calcined Mg/Al hydrotalcite-supported palladium or nickel catalysts.* Applied Catalysis A: General, 1998. **169**(2): p. 207-214.
152. Nikolopoulos, A., B.-L. Jang, and J. Spivey, *Acetone condensation and selective hydrogenation to MIBK on Pd and Pt hydrotalcite-derived MgAl mixed oxide catalysts.* Applied Catalysis A: General, 2005. **296**(1): p. 128-136.
153. Montané, D., et al., *High-temperature dilute-acid hydrolysis of olive stones for furfural production.* Biomass and Bioenergy, 2002. **22**(4): p. 295-304.
154. Win, D.T., *Furfural-gold from garbage.* Au J Technol, 2005. **8**: p. 185-190.
155. Dutta, S., et al., *Advances in conversion of hemicellulosic biomass to furfural and upgrading to biofuels.* Catalysis Science & Technology, 2012. **2**(10): p. 2025-2036.
156. Binder, J.B., et al., *Synthesis of furfural from xylose and xylan.* ChemSusChem, 2010. **3**(11): p. 1268-1272.
157. Corma, A., S. Iborra, and A. Velty, *Chemical routes for the transformation of biomass into chemicals.* Chemical reviews, 2007. **107**(6): p. 2411-2502.
158. Kijeński, J., et al., *Platinum deposited on monolayer supports in selective hydrogenation of furfural to furfuryl alcohol.* Applied Catalysis A: General, 2002. **233**(1-2): p. 171-182.
159. Rao, R.S., R.T.K. Baker, and M.A. Vannice, *Furfural hydrogenation over carbon‐supported copper.* Catalysis Letters, 1999. **60**(1-2): p. 51-57.

160. Lange, J.P., et al., *Furfural—a promising platform for lignocellulosic biofuels.* ChemSusChem, 2012. **5**(1): p. 150-166.
161. Vargas Hernández, D., et al., *Furfuryl alcohol from furfural hydrogenation over copper supported on SBA-15 silica catalysts.* Journal of Molecular Catalysis A: Chemical, 2014. **383**: p. 106-113.
162. Zheng, H.Y., et al., *Towards understanding the reaction pathway in vapour phase hydrogenation of furfural to 2-methylfuran.* Journal of Molecular Catalysis A: Chemical, 2006. **246**(1-2): p. 18-23.
163. Srivastava, S., G. Jadeja, and J. Parikh, *Copper-cobalt catalyzed liquid phase hydrogenation of furfural to 2-methylfuran: An optimization, kinetics and reaction mechanism study.* Chemical Engineering Research and Design, 2018. **132**: p. 313-324.
164. Panagiotopoulou, P., N. Martin, and D.G. Vlachos, *Liquid ‐Phase Catalytic Transfer Hydrogenation of Furfural over Homogeneous Lewis Acid ‐Ru/C Catalysts.* ChemSusChem, 2015. **8**(12): p. 2046-2054.
165. Merlo, A.B., et al., *Bimetallic PtSn catalyst for the selective hydrogenation of furfural to furfuryl alcohol in liquid-phase.* Catalysis Communications, 2009. **10**(13): p. 1665-1669.
166. Nagaraja, B., et al., *Vapor phase selective hydrogenation of furfural to furfuryl alcohol over Cu–MgO coprecipitated catalysts.* Journal of Molecular Catalysis A: Chemical, 2007. **265**(1-2): p. 90-97.
167. CHU, D.-B., et al., *Heterogeneous Electrocatalytic Reduction of Furfural on Nanocrystalline TiO 2-CNT Complex Film Electrode in DMF Solution.* Acta Physico-Chimica Sinca, 2006. **22**(03): p. 373-377.
168. Chen, X., et al., *Liquid phase hydrogenation of furfural to furfuryl alcohol over Mo-doped Co-B amorphous alloy catalysts.* Applied Catalysis A: General, 2002. **233**(1-2): p. 13-20.
169. Yang, J., et al., *Effects of calcination temperature on performance of Cu–Zn–Al catalyst for synthesizing γ-butyrolactone and 2-methylfuran through the coupling of dehydrogenation and hydrogenation.* Catalysis Communications, 2004. **5**(9): p. 505-510.
170. Zheng, H.-Y., et al., *Synthesis of g-butyrolactone and 2-methylfuran through the coupling of dehydrogenation and hydrogenation over copper-chromite catalyst.* Reaction Kinetics and Catalysis Letters, 2004. **82**(2): p. 263-269.
171. Zhu, Y.-L., et al., *A new strategy for the efficient synthesis of 2-methylfuran and γ-butyrolactone.* New Journal of Chemistry, 2003. **27**(2): p. 208-210.
172. Mariscal, R., et al., *Furfural: a renewable and versatile platform molecule for the synthesis of chemicals and fuels.* Energy & Environmental Science, 2016. **9**(4): p. 1144-1189.
173. Li, L., et al., *Combustion and emission characteristics of diesel engine fueled with diesel/biodiesel/pentanol fuel blends.* Fuel, 2015. **156**: p. 211-218.
174. Campos-Fernandez, J., et al., *Performance tests of a diesel engine fueled with pentanol/diesel fuel blends.* Fuel, 2013. **107**: p. 866-872.
175. Wei, L., C. Cheung, and Z. Huang, *Effect of n-pentanol addition on the combustion, performance and emission characteristics of a direct-injection diesel engine.* Energy, 2014. **70**: p. 172-180.
176. Saravanan, S., *Effect of exhaust gas recirculation (EGR) on performance and emissions of a constant speed DI diesel engine fueled with pentanol/diesel blends.* Fuel, 2015. **160**: p. 217-226.

177. Vaidya, P.D. and V.V. Mahajani, *Kinetics of liquid-phase hydrogenation of furfuraldehyde to furfuryl alcohol over a Pt/C catalyst.* Industrial & Engineering Chemistry Research, 2003. **42**(17): p. 3881-3885.
178. Kaufmann, W. and R. Adams, *The use of platinum oxide as a catalyst in the reduction of organic compounds. IV. reduction of furfural and its derivatives.* Journal of the American Chemical Society, 1923. **45**(12): p. 3029-3044.
179. Marinelli, T., et al., *Furfural—Hydrogen Reactions, Manipulation of Actmty and Selectmty of The Catalyst.* Studies in surface science and catalysis, 1993. **78**: p. 195-202.
180. An, W., et al., *The electrochemical hydrogenation of edible oils in a solid polymer electrolyte reactor. II. Hydrogenation selectivity studies.* Journal of the American Oil Chemists' Society, 1999. **76**(2): p. 215-222.
181. Holton, O.T. and J.W. Stevenson, *The role of platinum in proton exchange membrane fuel cells.* Platinum Metals Review, 2013. **57**(4): p. 259-271.
182. Zhang, J., *PEM fuel cell electrocatalysts and catalyst layers: fundamentals and applications*. 2 ed. Vol. 31. 2008, Canada: Springer Science & Business Media. p.861-990.
183. West, R.M., et al., *Liquid alkanes with targeted molecular weights from biomass - derived carbohydrates.* ChemSusChem: Chemistry & Sustainability Energy & Materials, 2008. **1**(5): p. 417-424.
184. Chen, M., Q. Guo, and Y. Fu, *Electrocatalytic hydrogenation of furfural to furfuryl alcohol using platinum supported on activated carbon fibers.* Electrochimica Acta, 2014. **135**: p. 139-146.
185. Macías-Pérez, M.C., et al., *SO2 retention on CaO/activated carbon sorbents. Part I: Importance of calcium loading and dispersion.* Fuel, 2007. **86**(5-6): p. 677-683.
186. Nowicki, P., H. Wachowska, and R. Pietrzak, *Active carbons prepared by chemical activation of plum stones and their application in removal of NO2.* Journal of Hazardous Materials, 2010. **181**(1-3): p. 1088-1094.
187. Elsayed, Y., et al., *Desulfurization of air at high and low H2S concentrations.* Chemical Engineering Journal, 2009. **155**(3): p. 594-602.
188. Tsai, W.T., C.Y. Chang, and S.L. Lee, *Preparation and characterization of activated carbons from corn cob.* Carbon, 1997. **35**(8): p. 1198-1200.
189. Stavropoulos, G.G. and A.A. Zabaniotou, *Production and characterization of activated carbons from olive-seed waste residue.* Microporous and Mesoporous Materials, 2005. **82**(1-2): p. 79-85.
190. Ahmedna, M., et al., *The use of nutshell carbons in drinking water filters for removal of trace metals.* Water research, 2004. **38**(4): p. 1062-1068.
191. Sudaryanto, Y., et al., *High surface area activated carbon prepared from cassava peel by chemical activation.* Bioresource Technology, 2006. **97**(5): p. 734-739.

APPENDIXES

Table 7. Summary of biomass feedstock chemical activation for ACs production

Feed stock	Temp.(^{o}C)	Reaction Time(min)	Activation chemicals	Surface area(m^2/g)	Ref.
Wood	850	60	H_3PO_4	1708	[185]
Plum stones	500	60	KOH	2174~3228	[186]
Coconut shell	800	-	Strong base	931	[187]
Corn cob	500	30~240	$ZnCl_2$	400~1410	[188]
Olive-seed	800	60	KOH	1339	[189]
Pecan shell	--	-	H_3PO_4	682	[190]
Cassava peel	750	180	KOH	1378	[191]
Bean pods	700	60	K_2CO_3	1580	[16]
Apricot stone shells	800	120	$ZnCl_2$	783	[15]
Almond shell	800	120	$ZnCl_2$	736	
Hazelnut shell	800	120	$ZnCl_2$	793	
Walnut shell	800	120	$ZnCl_2$	774	
olive stones	850	120	-	677	[18]
olive stones	650	120	$ZnCl_2$	790	[17]
Pecan Shell	450	60	-	>800	[19]
Jackfruit peel	500	30	H_3PO_4	907~1260	[20]
Rice husk	700	30	$ZnCl_2$	750	[24]
Bagsse	700	30	$ZnCl_2$	674	
Palm shell	800	120	K_2CO_3	1170	[21]

Table 8. Brief of the current techniques used for upgrading bio-oil

Upgrading methods	Treatment condition /requirement	Reaction mechanism /process	Technique feasibility	
			Pros.	Cons.
Hydrotreating /hydrofining	Mild condition(~500°C/low pressure),chemical need:H_2/CO, catalyst(e.g.,CoMo,HDS,NiMO,HZSM-5)	Hydrogenation without simultaneous cracking(eliminating N, O and S as NH_3, H_2O, and H_2S)	The cheaper route commercialized already	High coking(8~25%) and poor quality of fuels obtained
Hydrocracking/hydrogenolysis /catalytic cracking	Severe condition(>350ºC, 100~1000Psi), a chemical needed: H_2/CO or H_2 donor solvents, catalyst(e.g., Ni/Al_2O_3-TiO_2)	Hydrogenation with simultaneous cracking	Makes large quantities of light products	Need complicated equipment, excess cost, catalyst deactivation, reactor clogging
Sub-/super-critical fluid	Mild conditions, organic solvents needed such as alcohol, acetone, ethyl acetate, glycerol	Promotes the reaction by its unique transport properties: gas-like diffusivity and liquid-like density, thus dissolved materials not soluble in either the liquid or gaseous phase of the solvent	Higher oil yield, better fuel quality(lower oxygen content, lower viscosity	Solvent is expensive
Solvent addition(direct add solvent or esterification of the oil with alcohol and acid catalysts)	The mild condition, polar solvents needed such as water, methanol, ethanol, and furfural	Reduces oil viscosity by three mechanisms(1)physical dilution(2)molecular dilution or by changing the oil microstructure(3)chemical reactions like esterification and acetalization	The most practical approach(simplicity, the low cost of some solvents and their beneficial effects on the oil properties)	Mechanisms involved in adding solvent are not quite understood yet
Emulsification/emulsions	Mild conditions need surfactant(e.g., CANMET)	Combines with diesel directly. Bio-oil is miscible with the aid of surfactants	Simple, less corrosive	Requires high energy of production
Steam reforming	High temperature(800-900°C) need catalyst(e.g,.Ni)	Catalytic steam reforming +water-gas shift	Produces H_2 as a clean energy resource	Complicated, requires steady dependable, fully developed reactors
Chemical extraction from the bio-oil	Mild condition	Solvent extraction, distillation, or chemical modification	Extract valuable chemicals	Low-cost separation and refining techniques still needed

Table 9. Operating parameters of UHS chemical activation experiments

Exp. No	Temp.(^{o}C)	Heating ratio (^{o}C/Min)	Reaction Time(min)	Impregnation Ratio	Activation Chemical	Preparation method
1	500	40	60	0.175	$ZnCl_2$	
2	500	47	60	0.175	$ZnCl_2$	
3	500	11.8	75	0.175	$ZnCl_2$	Mix and Filtration
4	500	9.5	90	0.175	$ZnCl_2$	
5	500	7.75	90	0.09	$ZnCl_2$	
4	500	7.1	90	2	$ZnCl_2$	
5	500	125	90	2	$ZnCl_2$	
6	500	52.6	90	2	$ZnCl_2$	Co-precipitation
7	500	66.6	60	2	$ZnCl_2$	
8	500	62.5	60	1	$ZnCl_2$	
9	500	62.5	60	1.5	$ZnCl_2$	
10	600	56.1	60	2	$ZnCl_2$	
11	500	62.5	60	2.5	$ZnCl_2$	
12	550	55	60	2	$ZnCl_2$	
13	450	60	60	2	$ZnCl_2$	
14	400	61.5	60	2	$ZnCl_2$	
15	500	58.8	60	3	$ZnCl_2$	
16	500	62.5	60	2	$ZnCl_2$	
17	500	7.1	90	2	$ZnCl_2$	
18	500	125	90	2	$ZnCl_2$	
19	500	55.5	60	1.5	$ZnCl_2$	
20	500	55.5	60	2.5	$ZnCl_2$	
20	500	31	60	1.7	H_3PO_4	
21	500	52.8	60	1.7	H_3PO_4	Co-precipitation
22	600	52.1	90	8	H_3PO_4	

Table 10. Operating parameters of the acetone ECH experiments

Exp. No	Anode Temp. (^oC)	Reaction Temp. (^oC)	Relative Humidity (%)	Membrane Used Times	Voltage supply (V)	Average current Density ($mA.cm^2$)	H_2 Utilization (%)	Current Efficiency (%)	Total Efficiency (%)	Products Volume Percentage (%)	
										Propanol (V%)	Isopropyl (V%)
1	60	65	80	1	0.02	52	4.5	59.66	2.68	12.70	1.04
2	60	65	80	2	0.02	38	3.29	57.59	1.89	13.84	0.94
3	60	65	80	3	0.02	36	3.11	50.76	1.58	13.34	1.1
4	60	65	80	4	0.02	30	1.78	40.75	0.73	12.89	1.3
5	60	65	80	1	0.02	44	3.87	53.69	2.08	12.30	1.35
6	60	65	80	2	0.02	44	3.80	49.96	1.90	11.60	1.64
7	60	65	80	3	0.02	36	3.11	48.54	1.51	16.30	1.45
8	60	65	80	4	0.02	30	2.05	41.25	0.97	15.98	0.8
9	60	65	80	5	0.01	26	2.25	42.54	0.96	15.87	0
10	60	65	80	6	0.15	18	1.56	37.30	0.58	16.96	0
11	55	64	66	1	0.02	24	2.07	45.12	0.93	8.71	1.43
12	56	65	66	2	0.02	20	1.73	41.18	0.71	7.80	0.85
13	50	65	49	3	0.02	16	1.38	43.83	0.61	5.84	0.8
14	52	67	50	4	0.02	16	1.39	43.17	0.60	5.86	0.72
15	44	65	36	5	0.02	10	0.86	41.79	0.36	4.91	0.64
16	63	65	91	6	0.02	32	2.77	54.70	1.51	16.06	1.46
17	61	65	82	7	0.02	20	2.25	47.69	1.07	15.10	0.1
18	60	65	81	8	0.02	18	3.11	43.96	1.37	13.55	0.1
19	75	80	81	1	0.02	68	5.88	18.46	1.09	14.29	1.36
20	68	73	81	2	0.02	56	4.84	19.89	0.96	10.39	1.04
21	60	65	80	3	0.02	45	3.57	27.60	0.98	13.03	0.98
22	53	57	83	4	0.02	32	2.64	28.14	0.74	10.48	0.55
23	46	50	82	5	0.02	20	1.73	29.20	0.51	28.82	0.1
24	63	65	91	6	0.02	18	2.42	50.68	1.23	16.08	0.1

H_2 flow rate was 0.25 ml/min; acetone flow rate was 6 ml/hour.

Table 11. Operating parameters of the furfural ECH experiments

Exp. No	Anode Temp. (°C)	Reaction Temp. (°C)	RH (%)	Membrane Used Times	Vol. Supply (V)	Current Density (mA.cm^2)	H_2 Utilization (%)	Current Efficiency (%)	Total Efficiency (%)	Products Concentration (ppm)					
										FA	THFA	MTHF	1-Pentanol	MPK	2-Pentanol
1	60	65	80	1	-	200	24.95	0.78	0.19	106.01	1.10	177.60	467.62	23.54	644.60
2	60	65	80	2	-	160	19.96	0.71	0.14	88.41	0.89	183.16	279.95	24.71	469.37
3	60	65	80	3	-	120	14.97	0.84	0.13	84.61	0.74	190.37	226.86	31.93	406.82
4	60	65	80	4	-	80	9.98	0.91	0.09	68.78	0.77	146.14	162.71	16.87	288.48
5	60	65	80	5	-	40	4.99	1.81	0.09	74.23	0.88	166.53	146.36	23.28	273.88
6	60	65	80	6	-	20	2.50	3.43	0.09	85.82	0.10	188.21	129.53	22.12	240.66
7	65	65	100	1	0.02	-	3.11	1.84	0.06	28.74	0.57	115.05	109.44	18.63	148.10
8	60	65	80	2	0.02	-	3.24	1.60	0.05	28.73	0.57	113.56	89.80	20.86	130.67
9	55	65	63	3	0.02	-	2.69	5.55	0.04	28.72	0.56	111.69	65.91	23.09	108.71
10	50	65	50	4	0.02	-	0.41	17.30	0.04	37.12	0.55	98.04	59.68	30.97	99.86
11-1	45	65	38	5	0.02	-	0.58	16.33	0.09	78.98	0	191.86	124.62	67.19	267.98
11-2	45	65	38	5	0.02	-	0.07	30.83	0.02	21.88	0	47.86	28.50	26.86	47.95
11-3	45	65	38	5	0.02	-	0.02	85.27	0.01	20.77	0.1	31.05	25.40	16.75	21.19
12-1	46	50	80	1	0.02	-	5.69	11.03	0.63	512.92	2.91	1201.89	1484.68	83.77	1437.46
12-2	46	50	80	1	0.02	-	1.90	12.24	0.14	131.52	1.78	174.22	344.76	24.45	273.61
13-1	54	58	80	2	0.02	-	3.75	7.53	0.28	182.16	2.67	597.13	515.68	82.52	695.03
13-2	54	58	80	2	0.02	-	1.41	6.27	0.09	84.76	1.69	166.02	145.97	31.12	170.67
14-1	68	73	80	3	0.02	-	2.42	4.12	0.10	55.85	1.07	160.54	113.00	64.35	253.45
14-2	68	73	80	3	0.02	-	1.06	3.51	0.04	25.75	0.8	45.19	29.78	24.03	54.05
15-1	75	80	80	4	0.02	-	1.43	2.60	0.04	31.72	0.5	53.45	32.82	42.90	79.40
15-2	75	80	80	4	0.02	-	0.65	2.20	0.01	25.84	0.2	15.34	2	11.12	17.09

16-1	60	65	80	5	-	-	16.73	0.12	0.02	566.25	2.00	287.02	431.00	47.68	265.73
16-2	60	65	80	5	-	-	13.00	0.07	0.01	364.69	1.04	175.65	214.64	41.37	174.89
16-3	60	65	80	5	-	-	10.8	0.03	0.01	87.25	0.38	101.63	86.21	21.81	68.45

For experiment 15, 14, 13 and 12, H_2 flow rate was 0.25 ml/min, others were 0.15 ml/min; acetone solution flow rate was 0.2 ml/min.

VITA

Chen Li cxxli001@odu.edu

PROFESSIONAL PROFILE

A compassionate, results-driven, and performance-oriented Ph. D graduate in Environmental Engineering with a sound academic background and teaching experience in the field of biomass, water/wastewater treatment, treatment plant design and electrochemistry. Perfect understanding of working with mainstream and diverse student populations and developing and implementing various curricula based on state and federal educational standards and requirements. An effective and resourceful motivator, team-builder, and facilitator with exceptional communication and presentation skills possessing an innate ability to perform accurate student assessments and conceptualize and employ individualized education plans. Proven experience in utilizing electrochemical method to investigate bio-oil upgrading problems, with focus on biomass composition analysis, biomass hydrolysis, electrolysis and organic compound hydrogenation.

EDUCATION

OLD DOMINION UNIVERSITY Sept. 2012 – Present
Ph.D. Candidate in Environmental Engineering
GPA:3.92/4.00. Advisor: Sandeep Kumar
Thesis: Value-added Products from Lignin and Biomass Derivative.

UNIVERSITY OF SCIENCE TECHNOLOGY& BEIJING Sept. 2007 – Jan. 2010
Master Degree in Environmental Engineering
GPA:3.22/4.00. Advisor: Chunbao Sun
Thesis: Experiment Research of Supercritical Water Oxidation of the Tobias Acid Production Wastewater.

ZHENGZHOU UNIVERSITY, Zhengzhou, China Sept. 2002 – May 2006
Bachelor Degree in Environmental Science
GPA:3.05/4.00.
Project: Biomass Gasification Products Identified by Infrared Spectroscopy Method.

PUBILICATION

1. Chen Li and Sandeep Kumar, Preparation of Activated Carbon from Un-hydrolyzed Biomass Residue by $ZnCl_2$ Activation and Their Use on Methylene Blue Adsorption. *Biomass Conversion and Biorefinery,* vol. 6, pp.407-419, 2016.

2. Chen Li, Ashanti M. Sallee, Xiaoyu Zhang and Sandeep Kumar, Electrochemical Hydrogenation of Acetone to Produce Isopropanol Using a Polymer Electrolyte Membrane Reactor. *Energies*, 2018, 11(10): 2691.

3. Chen Li, Xiaoyu Zhang and Sandeep Kumar, Electrochemical Hydrogenation of Furfural Using a Polymer Electrolyte Membrane Reactor. *Journal of Renewable and Sustainable Energy*. (Submitted).

4. Sunbao Sun and Chen Li, et al. Treatment of Wastewater from Tobias Acid Production with supercritical water oxidation. *Journal of University of Science and Technology Beijing*, vol.10, pp.1097-1101, 2012.

5. Li Qing and Chen Li, et al. The Research of Ozone Oxidation Treatment and Reuse of the Tails Wastewater from Tibet Jiama Polymetallic Sulphide Ore Flotation, *Chinese Mining Industry*, vol.7, pp.53, 2009.